Elucidating the Influence of Surface Treatments, Material Functionalization, and Additives on Adhesion at Buried Interfaces

by

John S. Andre

A dissertation submitted in partial fulfillment
of the requirements for the degree of
Doctor of Philosophy
(Chemistry)
in The University of Michigan
2022

Doctoral Committee:

Professor Zhan Chen, Chair
Professor Charles McCrory
Professor Roseanne Sension
Professor Anish Tuteja

John S. Andre
joandre@umich.edu
ORCID iD: 0000-0003-0033-7677

DEDICATION

This thesis is dedicated to my loving wife Adrianna for her unwavering support and for always encouraging me to accomplish my goals. I love you so much!

ACKNOWLEDGMENTS

I want to extend a heartfelt thanks to my mentor and advisor, Professor Zhan Chen. I cold emailed him one day in the fall of 2015 while visiting the University of Michigan his research interested me and I was just becoming familiar with the techniques used in his lab. He answered my email, had a meeting with me, and gave me a lab tour. The following summer I came back to Michigan to participate in the NSF REU program in Dr. Chen's lab and the summer after that I came to his lab to kick-off my graduate studies. By this time, I was learning so much about adhesion and different methods to study them from him and his lab members. In his lab I learned to think like a scientist and solve problems like a researcher. Dr. Chen gave me a great opportunity that I will be forever thankful for.

I also want to acknowledge Professor Roseanne Sension, I rotated in her lab during my first-year of graduate school, I learned a lot about lasers during this time. She was also one of my professors that year for Statistical Mechanics. I really appreciate her for being on my dissertation committee. Professor Charles McCrory was also one of my professors during my second-year for Materials Chemistry. His enthusiasm for teaching is unforgettable and I am grateful to have him on my thesis committee. Professor Anish Tuteja's group does research I am truly interested in, and I am happy to have him on my committee. I knew he would have good insight into the adhesion work I am thankful for his input.

Much of this work I could not have done alone and was possible with the mentorship and contributions from Nathan Ulrich and Bolin Li. Bolin helped collect data and do the analysis for

much of Chapter 4, I am very grateful to his contribution to my thesis and the number of things he taught me as a post-doctoral researcher while in the Chen Lab. I received guidance and help on the research presented from several collaborators and undergraduate students as well.

The Chen lab has always been a good place for me, and I appreciate all the members new and old. Other lab members who have had an impact are: Xingquan Zou, Josh Jasensky, Minyu Xiao, Chengcheng Zhang, Tieyi Lu, Ralph Crisci, Ting Lin, Wen Guo, Yuchen Wu, Jinpeng Gao, Shuqing Zhang, and Najae Escoffery. Our newer post-docs Rubel Kahn and Danny Rossi have been great to work with as well. Our lab has had a number of visiting scholars that all deserve some recognition, but I would like to give Ruiying Guo, Tatsuki Abe, and Haiye Wang a shout out for being good friends during their time in Ann Arbor.

I would also like to acknowledge my collaborators at Dow Chemical, they provided many more samples than the following chapters contain and so much scientific insight throughout my PhD. I appreciate Carol Mohler, Xiaoyun Chen, Chris Tucker, Brian Walther, Rajesh Paradkar, Ray Drumright, Eric Greyson, Joe Grant, Eric Wasserman, and Scott Backer.

I want to acknowledge some of the great friends I have met along the way: Nhat and Lizzy, Nick and Rachel, and Elvin have been some of the greatest parts of being in Michigan. Games nights with Adrianna, Elvin, Ralph, and Nhat are some of my fondest memories. Finally, I want to thank my family: Adrianna for supporting me these years and our kid Cameron for being a welcome addition as I bring this chapter to a close and open a new one. I want to thank Trevor for being my friend since we were kids. Forust and Kelsey have always been great friends and down to game.

John Andre

3/17/2022

TABLE OF CONTENTS

LIST OF FIGURES

LIST OF TABLES

ABSTRACT

Adhesion is important to a variety of applications and for a number of industries. Adhesion occurs at buried interfaces and is mediated by interfacial structure. It is difficult to probe buried interfacial structure in situ nondestructively. In this thesis, sum frequency generation (SFG) vibrational spectroscopy was applied to study molecular structures of buried interfaces to understand molecular mechanisms of polymer adhesion at buried interfaces in situ. In addition to the studies of enhancing adhesion of polymer adhesives to substrates, research on a reversible adhesive for polymer recycling and sustainability was also conducted.

Soldering flux treatment on copper is an important procedure to ensure bonding of interconnects in an electronic device but can disrupt adhesion of packaging polymers. Chapter 2 reports SFG studies on the effect of model and commercial flux on polymer adhesion. It was found that with surface treatments of the flux treated copper leads to disordered polymer at the buried copper/polymer interfaces, increasing the adhesion.

Chemical reactions occurring at the buried interface between two polymers in situ were studied in Chapters 3 and 4. First, the buried ethylene vinyl alcohol (EVOH)/maleic anhydride (MAH) grafted polyethylene (MAHgEO) interface was studied, showing that interfacial chemical reactions occurred, greatly enhancing the adhesion. The chemical reactions can greatly increase adhesion between nylon and MAHgEO was also observed, evidenced by the disappearance of the reactants and appearance of reaction products in the SFG spectra. SFG experiments were also

performed to follow the reaction kinetics and measure the activation energy of the interfacial reaction.

Chapter 5 studied the influence of an amino silane adhesion promoter on the interfacial structure and adhesion of butyl acrylate/methylmethacrylate copolymers (BAMMAs) incorporated with methyl acrylic acid (MAA) to silica. SFG results elucidated the mechanisms of adhesion enhancement by the adhesion promoter, showing: (1) ionic bonds formed between the tail amine group and acid functionality of BAMMA, (2) migration of more ester C=O groups to the interface with order, and (3) disordered or reduced levels of CH groups at the interface.

A self-assembled monolayer (SAM) for debonding adhesives on demand was developed in Chapter 6. The SAM was applied to a silica surface and characterized with SFG and x-ray photoelectron spectroscopy (XPS). Once the SAM was fully prepared, the UV sensitivity was also tested with SFG. Before debonding the UV sensitive group on the SAM, adhesives were applied resulting in an adhesive interface that can be selectively broken. Adhesion tests were performed on silica/adhesive and silica/SAM/adhesive samples before and after UV irradiation exposure, which showed that the debonding could reduce the adhesion strength.

SFG has been developed into a powerful tool to characterize interfaces but most of the SFG research has focused on simple model systems. This research demonstrated that SFG can be applied to study many complex polymer interfaces of commercial materials, adding an important technique to the toolbox used to study “real-life” interfaces important to industry. This research showed that for commercial flux, packaging polymers, and polymer resins that disordering, covalent bond formation, and ionic bond formation at buried interfaces could greatly enhance adhesion. This study also reported an easy way to create reversible adhesives, important for

recycling. The methods developed in this thesis are generally applicable to study important interfaces of many polymer systems in the future.

Chapter 1: Introduction

1.1 Goals and motivation

Adhesion of polymer materials to a variety of substrates is vital to many industries and applications from food packaging to electronics. Understanding the mechanisms of adhesive materials is important to develop new products and expand applications of already mature chemistry. The goal of this thesis research was to study adhesive interfaces involving complex material formulations that are important for a variety of industrial applications. The first research project was to examine the effects of surface treatments in electronic packaging. The next topic was to investigate[1-16] chemical reactions between polymer layers in multilayer films typically used in food packaging.[17-24] Finally the addition of adhesion promoters was studied in water-based polymer coatings to understand their interfacial behavior to improve adhesion of paint to glass substrates.[25-28] Along with studies on methods to enhance adhesion through surface treatments, chemical reactions, and additives in a formulation, this research also demonstrated a proof-of-principle self-assembled monolayer (SAM) capable of selectively debonding a polymer adhesive interface. Debonding adhesives from a substrate is important feature of many adhered interfaces and a number of methods have been devised for a variety of applications where recycling the composite materials is difficult.[29-35] All together this thesis presents interfacial studies on molecular adhesion mechanisms involving complex/multicomponent materials. The

methodologies adopted/developed in this research can be generally applicable to study other complicated polymer-based formulations. In this work sum frequency generation (SFG) vibrational spectroscopy was the primary tool used to study adhesive interfaces involving surface treatment, interfacial reactions, and additives to describe the behavior of interfacial molecular structures of adhesive polymers on various substrates. SFG is an ideal metrology to gain molecular level information form the types of interfaces discussed above because SFG can probe many types of buried interfaces without contributions from the bulk material being studied.[36-62] More details on SFG, instrumentation, and the methodologies used are described below.

Interfaces of interest in this research include polymers on metal, polymer/polymer interactions and polymer materials deposited on glass. One important goal of this thesis research was to use methods developed in our Lab previously to study materials used in real-life applications, to move the developed analytical methodology from model systems to systems currently being developed in industry to solve adhesion problems in the applications discussed above.

There are four specific aims in this thesis research, alluded to above. Aim 1 was to study flux molecules and surface treatments to remove or neutralize them on metal surfaces to enhance adhesion of polymer packaging materials. Aim 2 was to investigate interfacial reactions occurring between maleic anhydride functionalized polyolefins (polyethylene) with ethylene vinyl alcohol (EVOH) and nylon that increase polymer/polymer adhesion. Aim 3 was to gain better understanding of amino silane additives on the interfacial structures of water-based acrylic polymer interfaces with silica substrates. Finally, aim 4 was to demonstrate that a SAM containing a photocleavable bond could be used to reduce adhesion between a glass substrate and polymeric materials.

1.2 Adhesion at buried interfaces

Adhesion is a multidisciplinary research topic that has been studied for decades. The chemistry of adhesion has been published in a variety of scientific journals and there are entire conferences dedicated to adhesion science and engineering. Although there is a mountain of research on the topic, there are many unanswered questions and hypotheses that have yet to be elucidated fully. Prior to the 1980s there were few methods available to study polymer adhesives without breaking the interface and inferring mechanisms for the resulting surfaces.[63-65] SFG has been an important tool to study adhesive interfaces for a number of years now. Along with limited analytical methodologies to study adhesion, there are a variety of mechanisms proposed by which two materials can be adhered together, providing important knowledge on improving adhesion in many systems.

The different modes of adhesion that are widely accepted include interfacial mechanical coupling, interfacial molecular interactions, and thermodynamic equilibrium mechanisms.[66-68] Mechanical coupling is similar to how Velcro works, where the adhesive goes into the rough parts of a surface and anchors to the material, thus increasing the adhesion strength. The main debate with this theory of adhesion is that adhesion to a rough surface may be due to the increased surface area and not due to anchoring of the material, therefore other mechanisms may be behind the adhesive strength and since more area has these other interactions higher adhesion strength can be achieved.[67] Molecular interactions consists of intermolecular forces that increase the interaction between the adhesive material and the substrate resulting in higher adhesion strength at the interface. This theory includes covalent bonds, ionic bonds, hydrogen bonds, metallic bonds, dipole-dipole interactions, and van der Waals forces. All these molecular interactions require close and good contact between the substrates. Thermodynamic adhesion mechanisms are thought to

only require an equilibrium process at the interface where the free energy of the surface is minimized, through this energy minimization the interaction between the layers can result in adhesion. This theory also applies to surfaces that are resistant to materials adhering to their surface.[69-70] From the thermodynamic theory of adhesion contact angle and surface tension analysis can be related to the potential adhesion strength of a surface.[61, 69-72] In real systems though, performing contact angle and surface tension analysis may be impractical and the observed results may be determined by other factors such as surface roughness leading to errors in the adhesion determination.

Within the modes of adhesion outlined in detail above there is still considerable debate about which force is the driving force determining adhesion strength between two materials.[67] More than one or all kinds of interactions may have some influence on the observed adhesion between two materials, further complicating the picture. In this research, interfacial molecular interactions were examined. In the first project, I studied the effect of surface treatments of metal on adhesion. The surface treatment changed the chemical composition (molecular interaction) and morphology (mechanical bonding) of the metal resulting in higher adhesion strength between the adhesive polymer and the metal substrate. The results of this research indicated that the enhancement of adhesion is molecular in nature based on the real-world system studied. In the following projects, I focused on investigating interfacial reactions between polymer materials to probe the molecular interaction mechanism of adhesion, which showed that interfacial chemical reactions could greatly increase adhesion strength. I also studied effect of additives on interfacial structure in a polymer formulation to examine interfacial molecular interactions and how adhesion promoters could be used to facilitate greater molecular compatibilization between dissimilar materials. In the above research projects, SFG was the primary analytical tool used to probe

molecular structures and interactions at buried interfaces. The last project which will be presented below was to study the debonding mechanism of a SAM to examine how changing interfacial interactions (e.g., interfacial chemical bonding) can disrupt adhesion with a combination of analytical techniques including SFG.

1.3 Sum frequency generation (SFG) vibrational spectroscopy

In this thesis research, SFG was extensively used to study surfaces and buried interfaces. A brief introduction to SFG will be presented below although the theoretical background, mathematical framework, and experimental parameters have been published widely in both research papers and textbooks.[63-65, 73-83] SFG is a valuable analytical technique for *in situ* adhesion studies because it is an optical tool to probe buried interfaces and surfaces with submonolayer sensitivity noninvasively. SFG is an optical process that can occurs at an interface that is accessible by visible and infrared light. Since adhesion is inherently an interfacial phenomenon, SFG is well suited to answer many questions regarding important mechanisms addressed in this thesis. Previously this technique was been used to study a number of polymer interfaces including those of polymer coatings, food packaging materials, semiconducting polymers, underfills in electronics, etc. In this thesis SFG was used to study many industrially relevant systems involving surface treatments, chemical reactions between polymer layers, the influence of additives on polymer interfacial structures, and the influence of UV irradiation on interfacial structures and properties. A schematic of a typical SFG experiment setup and an energy level diagram of the process is shown in **Figure 1.1**. Since a variety of SFG sample geometries were used in this research, more experimental details will be provided in individual chapters regarding the sample being studied.

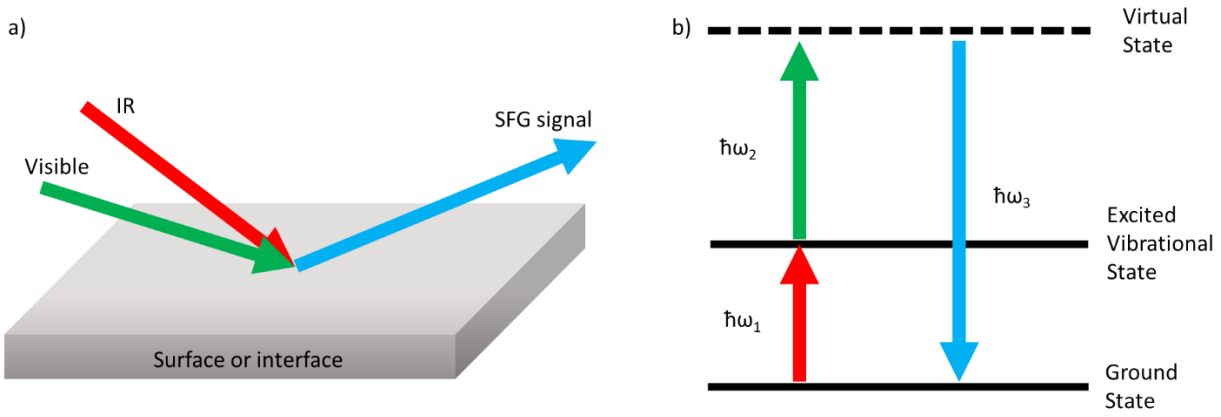

Figure 1.1 A schematic of a SFG experiment for illustration in panel a). Panel b) shows an energy level diagram depicting the input IR and visible beam energy and the output SFG signal generated from this process.

SFG is a second-order nonlinear optical process. Under the electronic dipole approximation, the selection rule of SFG indicates that SFG signal can only be generated from a medium with no inversion symmetry, which leads to SFG being surface and interface specific for many materials. Information provided by SFG is similar to FTIR or Raman spectroscopy, but the signal arises from the surface or interface, providing the major advantage of SFG. For surface/interface specificity, an SFG experiment probes the second-order non-linear optical susceptibility ($\chi^{(2)}$) of a given material which is non-zero only when inversion symmetry is broken. This can be shown with the following tensor property for a second order nonlinear optical process:

$$\chi^{(2)}(r) = -\chi^{(2)}(-r) \qquad (1)$$

The above tensor changes sign under inversion. Since $\chi^{(2)}$ is constant after inversion operation in bulk material that has inversion symmetry, the only possible solution for $\chi^{(2)}$ in bulk is that $\chi^{(2)} = 0$. This is not the case at an interface where inversion symmetry is broken, therefore a SFG process is allowed. Polymers studied in this thesis work have inversion symmetry in the bulk and the SFG signals are generated from the surface or interface in the experiments. The SFG signal measured

is proportional to the intensities of the input visible and infrared beams (I_{vis} and I_{IR}, respectively) and the square of $\chi^{(2)}$:[80]

$$I_{SFG} \propto |\chi^{(2)}|^2 I_{vis} I_{IR} \quad (2)$$

When a surface or interface vibrational mode is on-resonance with the input IR frequency the SFG signal intensity is greatly enhanced. The SFG signal can be plotted with respect to the IR wavenumber to generate a vibrational spectrum from the probed interface. The relationship between the IR frequency and the SFG intensity can be shown to have a Lorentzian line shape:[83]

$$I_{\mathrm{SFG}} = |A_{\mathrm{NR}} + \sum_q \frac{A_q}{\omega_2 - \omega_q + \mathrm{i}\Gamma_q}| \quad (3)$$

In equation 3, A_{NR} is the nonresonant contribution to the SFG signal, A_q is the amplitude of a resonate peak, ω_q is the vibrational mode wavenumber, ω_2 is the input IR beam frequency and Γ_q is the resonate peak width or damping coefficient. The signal obtained from experiments can be fit with these parameters to perform further quantitative analysis. $\chi^{(2)}$ is a tensor that is defined in the lab fixed coordinate system, which allows for the different tensor components to be found by making measurements with different polarization combinations of the input and output beams.[80]

When SFG is collected from some interfaces or surfaces, a high non-resonate signal is possible. This usually occurs at highly charged interface and interfaces involving metals due to the high degree of polarizability of a metal substrate.[83] This scenario is relevant to the material presented in Chapter 2, where the effect of surface treatments on copper substrates and copper/polymer interfaces was studied. More discussion on this can be found in section 1.5 and Chapter 2 related to selectively probing the polymer/metal selectively using the ppp polarization combination.

In this thesis research, a picosecond SFG system was used (EKSPLA) and the details of this type of instrument have been published extensively.[60, 84-88] For SFG experiment, a fixed

frequency 532 nm beam and a tunable frequency IR beam are overlapped spatially and temporally at the substrate/solution interface where a third beam, the SFG beam, is generated.

1.4 SFG instrumentation

For the SFG experiments, a Nd:YAG laser (EKSPLA PL2251, Lithuania) generated a picosecond fundamental output laser pulse with a wavelength of 1064 nm, which was split into two portions. One portion was frequency doubled to generate a fixed frequency, 532 nm (visible) beam (EKSPLA H500). The remaining 1064 nm energy and part of the 532 nm energy were used to generate the frequency tunable infrared (IR) input beam through optical parametric generation/amplification (OPG/OPA) and a difference frequency generation (DFG) process (EKSPLA PG501/DFG1P). The various components of the SFG system discussed are shown in **Figure 1.2**. Visible and IR beams were incident at the buried interfaces studied at 65° and 60° versus the surface normal, respectively. The overlap region for these two beams was about 0.5 mm in diameter and the energies of the visible and IR pulses were approximately 30 μJ and 120 μJ, respectively for the hydroxyl O-H stretching frequency region (3000-3800 cm^{-1}). The carbonyl C=O stretching frequency region (1550-1950 cm^{-1}) beam energies were 30 μJ for the visible beam and 40 uJ for the IR beam at the sample interface. These energies are specific for the instrument used for this research and can vary from instrument to instrument. Spatially and temporally overlapped visible and IR beams at a surface or a buried interface generated a third output SFG beam. The SFG beam intensity was detected by a monochromator/PMT as a function of the IR frequency (wavenumber, cm^{-1}), producing a vibrational spectrum.

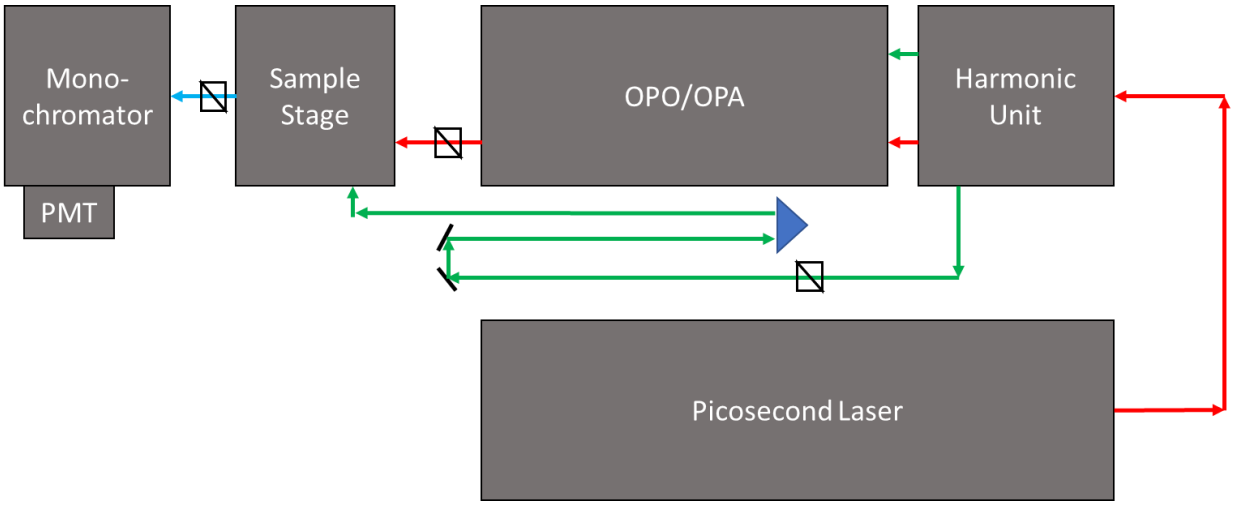

Figure 1.2 Diagram of the EKSPLA SFG system used in this thesis research. The red line indicates near- and mid-IR beams (near-IR is 1064 nm and the mid-IR from the OPO/OPA is the tunable IR used for experiments), the green line indicates the visible beam, and the blue line is the SFG beam. Black boxes indicate polarization control, the blue triangle indicates a delay line for the visible beam.

1.5 Analysis of buried polymer interfaces with SFG

To produce a vibrational spectrum, the SFG signal intensity is plotted with respect to the input IR beam frequency, allowing a vibrational spectrum to be obtained, as discussed above. Peak centers in the SFG spectrum allow for identification of functional groups present at a surface or an interface. The intensity of the SFG peaks with respect to the polarization combinations (s-polarized SFG signal, s-polarized input visible beam, p-polarized input IR beam or ssp and ppp in this thesis) allows for quantitative information, such as orientation, orientation distribution, and surface coverage of the functional groups probed, to be obtained.[73, 89] Quantitative SFG data analysis has been extensively published previously. This thesis research does not involve quantitative SFG data analysis, therefore such detailed data analysis is not discussed or in the following chapters.

Several different sample geometries were used for SFG data collection in this thesis research, as shown in **Figure 1.3**. **Figure 1.3 (a)** shows the sample geometry used to probe a polymer/metal interface. More details about such a sample geometry will be discussed in Chapter

2. Here a short explanation to justify the polymer/metal interface signal is given below. With the sample geometry shown in **Figure 1.3 (a)**, both the substrate/polymer interface and the polymer/metal interface can generate SFG signal. To ensure that SFG signal was generated from the polymer/metal interface, the polymer layer between the metal and the substrate was made to be very thin to avoid attenuation of the IR beam, which needs to reach the polymer/metal interface to generate SFG signal. Typically, SFG signal collected from polymer/metal interfaces were collected in the ppp polarization, which has been found to be dominated by the polymer/metal interface.[62] The substrate with the polymer was then placed in contact with the metal surface and the polymer is cured, a depiction of this type of sample is shown in **Figure 1.3 (a)**.

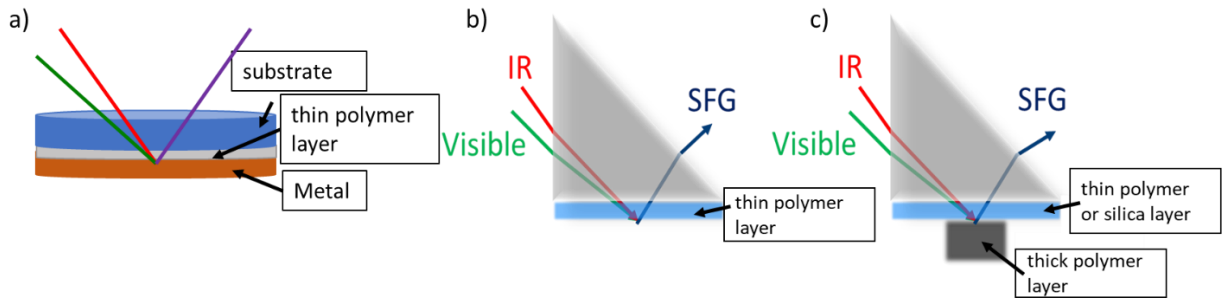

Figure 1.3 Depiction of the different SFG geometries used in this research. A polymer/metal interface can be probed in (a). A thin polymer layer in panel (b) allows for polymer/air interface to be studied. A sample like the one shown in (c) allows for polymer/polymer or polymer/silica interfaces to be studied without interference from the polymer/air interface.

SFG experiments can be used to probe polymer surfaces or buried polymer/polymer interface as shown in **Figure 1.3 (b)** and **(c)**.[90] The SFG signals collected using the sample geometry shown in **Figure 1.3 (b)** may have contributions from both the polymer/air and polymer/substrate interface. Typically, the polymer/air interface signal was dominate because of the larger Fresnel coefficients of this interface and more ordered polymer structure of this interface. With a proper film thickness, the Fresnel coefficient of the polymer/substrate interface can be minimized, then it is reasonable to ignore the signal contribution from the polymer/substrate interface. To probe a buried interface

of a polymer adhesive on a polymer substrate, the sample geometry shown in **Figure 1.3 (c)** was used. First, a thin polymer layer was applied to the substrate then a thicker polymer layer was placed into contact with the thin layer creating a buried polymer/polymer interface. SFG signals could then be obtained from the polymer/polymer interface without contribution from the thick polymer/air interface in the spectrum (because the IR beam could not reach the polymer/air interface). Similar to the polymer/air study above, here it was also important to make sure that the thin polymer layer did not have strong interference signal from the substrate/polymer interface. Typically this can be checked by varying the layer thickness and checking the interfacial signal with the SFG instrument.[46-47] Even if SFG signals from the polymer/substrate interface cannot be ignored, their contribution can be deconvoluted from the polymer film thickness dependent SFG study. A similar sample geometry to that shown in **Figure 1.3 (c)** (without the presence of a think polymer layer) could be applied to study substrate/polymer interfaces (e.g., silica/polymer and calcium fluoride/polymer interfaces), where the polymer in contact with a substrate was sufficiently thick to block the IR beam to reach the polymer/air interface - this type of sample was used in Chapter 5 to study silica/polymer interfaces.

To measure the polymer thin film thickness accurately, ellipsometry was used, which is addressed further in Chapter 3.

1.6 Presented research

This thesis examines four types of adhesive interfaces in the following chapters. (1) SFG was used to examine the effects of surface treatments of copper on structures of buried polymer interfaces. (2) Interfacial reactions between polymers at buried interfaces were investigated by SFG. (3) The role of additives added to aqueous polymer formulations was examined at

silica/polymer interfaces. (4) A method to selectively debond an adhesive interface with a SAM was developed.

In more detail: Chapter 2 presents research on solder flux and the washing influence on copper surfaces and the resulting adhesion properties to an epoxy-based adhesive using SFG to examine buried interfacial structures. This work focused on using SFG and adhesion testing methods to study effects of surface treatments at polymer/metal interfaces. The aim was to study the role of flux removal by washing and heat treatment on adhesion of epoxy to copper. In conclusion surface treatment of the flux on copper caused disordering of the epoxy polymer at the copper interface and results in increased adhesion to the copper.

In Chapters 3 and 4 interfacial polymer/polymer reactions were studied with SFG. The primary research presented focused on EVOH (Chapter 3) and nylon (Chapter 4) interfacial chemical reactions with maleic anhydride grafted polyethylene to enhance adhesion between polymer layers. The application for this project was to understand adhesion mechanisms in multilayer polymer films containing dissimilar polymer layers. SFG was used to determine changes in reactive groups and observe the appearance of bonding groups formed at polymer/polymer buried interfaces. This research provides insight into fundamental molecular interactions important to understanding how to improve high performance polymer materials.

The focus of Chapter 5 was to study an amino silane adhesion promoter additive's influence on dry emulsion polymer structures, used in paint formulations, at glass interfaces. This chapter also reported the influence of polymer composition on resulting interfacial structures with and without the adhesion promoter. This project aims to use SFG to elucidate the interfacial influence of silane adhesion promoters and polymer composition on water-borne acrylic polymer interactions with glass. It was found that the adhesion promoter and polymer composition lead to

a large number of hydrogen bonding groups at the interface which can influence the amount of water left behind at the buried interface after the emulsion dries. It was also found that an ionic pair forms between the amino group of the adhesion promoter and the carboxylic acid groups of one of the polymer monomers, leading to the strong interfacial adhesion.

Chapter 6 shows a proof-of-principle photocleavable SAM which could be used to reduce adhesion between polymer adhesives and substrates after UV irradiation. The SAM preparation process was carefully characterized with SFG, and XPS. SFG was also used to study buried polymer adhesive/substrate (with SAM) interfaces before and after UV irradiation. Two polymer adhesives, an epoxy adhesive and a silicone adhesive were studied. In conclusion, this research showed the successful SAM preparation and about 1/3 adhesion loss after UV irradiation.

To summarize, this work shows the principles of molecular bonding in a variety of adhesive systems important to several applications. It demonstrates that SFG can elucidate molecular mechanisms of polymer adhesion in situ. Along with showing fundamental principles of polymer adhesion, the samples studied in each chapter are multicomponent formulations used in industry and the results show the efficacy of SFG along with other analytical techniques to elucidate adhesion mechanisms in complicated formulations. A better understanding of using SFG to study real industry materials was gained in this research and mechanisms for adhesion that were hypothesized were uncovered using the technique.

1.7 References

1. Sun, M.; Zhu, S.; Zhang, C.; Olah, A.; Baer, E.; Schiraldi, D. A., HDPE/EVOH Multilayered, High Barrier Films for Flexible Organic Photovoltaic Device Packaging. *ACS Applied Polymer Materials* **2019,** *1* (2), 259-266.
2. Sang, J.; Hirahara, H.; Aisawa, S.; Kang, Z.; Mori, K., Direct Bonding of Polypropylene to Aluminum Using Molecular Connection and the Interface Nanoscale Properties. *ACS Applied Polymer Materials* **2019,** *1* (9), 2450-2459.
3. Rana, S.; Sindhu, P.; Ballav, N., Perspective on the Interfacial Reduction Reaction. *Langmuir* **2019,** *35* (30), 9647-9659.

4. Pletincx, S.; Fockaert, L. L. I.; Mol, J. M. C.; Hauffman, T.; Terryn, H., Probing the formation and degradation of chemical interactions from model molecule/metal oxide to buried polymer/metal oxide interfaces. *npj Materials Degradation* **2019,** *3* (1).
5. De Keersmaecker, M.; Reynolds, J. R., Simple Interface Modification of Electroactive Polymer Film Electrodes. *ACS Appl Mater Interfaces* **2019**.
6. Chen, Y.; Ginga, N. J.; LePage, W. S.; Kazyak, E.; Gayle, A. J.; Wang, J.; Rodriguez, R. E.; Thouless, M. D.; Dasgupta, N. P., Enhanced Interfacial Toughness of Thermoplastic-Epoxy Interfaces Using ALD Surface Treatments. *ACS Appl Mater Interfaces* **2019,** *11* (46), 43573-43580.
7. Urata, S.; Yoshino, H.; Ono, M.; Miyasaka, S.; Ando, R.; Hayashi, Y., Adhesion between Copper and Amorphous Silica: A Reactive Molecular Dynamics Study. *The Journal of Physical Chemistry C* **2018,** *122* (49), 28204-28214.
8. Pletincx, S.; Abrahami, S.; Mol, J. M. C.; Hauffman, T.; Terryn, H., Advanced (in situ) surface of organic coating/metal oxide interactions for corrosion protection of passivated metals. In *Encyclopedia of Interfacial Chemistry*, Wandelt, K., Ed. Elsevier: Amsterdam, 2018; pp 1-17.
9. Díez-Pascual, A.; Luceño Sánchez, J.; Peña Capilla, R.; García Díaz, P., Recent Developments in Graphene/Polymer Nanocomposites for Application in Polymer Solar Cells. *Polymers* **2018,** *10* (2).
10. Bouhamed, A.; Kia, A. M.; Naifar, S.; Dzhagan, V.; Müller, C.; Zahn, D. R. T.; Choura, S.; Kanoun, O., Tuning the adhesion between polyimide substrate and MWCNTs/epoxy nanocomposite by surface treatment. *Appl. Surf. Sci.* **2017,** *422*, 420-429.
11. Wang, B.; Huang, M.; Tao, L.; Lee, S. H.; Jang, A. R.; Li, B. W.; Shin, H. S.; Akinwande, D.; Ruoff, R. S., Support-Free Transfer of Ultrasmooth Graphene Films Facilitated by Self-Assembled Monolayers for Electronic Devices and Patterns. *ACS Nano* **2016,** *10* (1), 1404-1410.
12. Kornain, Z.; Jalar, A.; Rasid, R.; Abdullah, S., Comparative study of phenolic-based and amine-based underfill materials in flip chip plastic ball grid array package. *J. Electron. Packag.* **2010,** *132* (4), 041012.
13. Niklaus, F.; Stemme, G.; Lu, J. Q.; Gutmann, R. J., Adhesive wafer bonding. *J. Appl. Phys.* **2006,** *99* (3), 031101.
14. Zhang, Z.; Wong, C. P., Recent advances in flip-chip underfill: Materials, process, and reliability. *IEEE Trans. Adv. Packag.* **2004,** *27* (3), 515-524.
15. Zhang, J., Fatigue crack propagation behavior of underfill materials in microelectronic packaging. *Mat. Sci. Eng. A* **2001,** *314*, 194–200.
16. Wong, C. P., Recent advances in hermetic equivalent flip-chip hybrid IC packaging of microelectronics. *Mat. Chem. Phys.* **1995,** *42*, 25-30.
17. Feng, J.; Li, Z.; Olah, A.; Baer, E., High oxygen barrier multilayer EVOH/LDPE film/foam. *Journal of Applied Polymer Science* **2018,** *135* (26).
18. Jantanasakulwong, K.; Leksawasdi, N.; Seesuriyachan, P.; Wongsuriyasak, S.; Techapun, C.; Ougizawa, T., Reactive blending of thermoplastic starch and polyethylene-graft-maleic anhydride with chitosan as compatibilizer. *Carbohydr Polym* **2016,** *153*, 89-95.
19. Ge, C.; Fortuna, C.; Lei, K.; Lu, L.-X., Neat EVOH and EVOH/LDPE blend centered three-layer co-extruded blown film without tie layers. *Food Packaging and Shelf Life* **2016,** *8*, 33-40.

20. Ge, C.; Lei, K.; Aldi, R., Barrier, mechanical, and thermal properties of the three-layered co-extruded blown polyethylene/ethylene–vinyl alcohol/low density polyethylene film without tie layers. *Journal of Thermoplastic Composite Materials* **2015,** *30* (6), 794-807.
21. Hong, S. I.; Kim, K. B.; Lee, Y.; Cho, S. Y.; Ko, J. A.; Hong, S. K.; Park, H. J., Surface modification of ethylene-vinyl alcohol copolymer treated with plasma source ion implantation. *J. Appl. Polym. Sci.* **2009,** *113* (5), 2988-2996.
22. Ait-Kadi, A.; Bousmina, M.; Yousefi, A. A.; Mighri, F., High performance structured polymer barrier films obtained from compatibilized polypropylene/ethylene vinyl alcohol blends. *Polymer Engineering & Science* **2007,** *47* (7), 1114-1121.
23. Lasagabaster, A.; Abad, M. J.; Barral, L.; Ares, A., FTIR study on the nature of water sorbed in polypropylene (PP)/ethylene alcohol vinyl (EVOH) films. *European Polymer Journal* **2006,** *42* (11), 3121-3132.
24. Severinia, F.; Pegoraroa, M.; Yuana, L.; Riccab, G.; Fanti, N., Free radical grafting of maleic anhydride in vapour phase on polypropylene film. *Polymer* **1999,** *40*, 7059–7064.
25. Zhang, X.; Carter, M. C. D.; Belowich, M. E.; Wan, G.; Crimmins, M.; Laughlin, K. B.; Even, R. C.; Kalantar, T. H., Catechol-Functionalized Latex Polymers Display Improved Adhesion to Low-Surface-Energy Thermoplastic Polyolefin Substrates. *ACS Applied Polymer Materials* **2019,** *1* (6), 1317-1325.
26. Giraud, L.; Nadarajah, R.; Matar, Y.; Bazin, G.; Sun, J.; Zhu, X. X.; Giasson, S., Amino-functionalized monolayers covalently grafted to silica-based substrates as a robust primer anchorage in aqueous media. *Applied Surface Science* **2016,** *370*, 476-485.
27. Ludwig, I. Drying, Film Formation and Open Time of Aqueous Polymer Dispersions. University of Karlsruhe, Germany, 2008.
28. Steward, P. A.; Hearna, J.; Wilkinsonb, M. C., An overview of polymer latex film formation and properties. *Advances in Colloid and Interface Science* **2000,** *86*, 195-267.
29. Oh, Y.; Park, J.; Park, J.-J.; Jeong, S.; Kim, H., Dual cross-linked, polymer thermosets: Modular design, reversible transformation, and triggered debonding. *Chem. Mater.* **2020,** *32* (15), 6384-6391.
30. Bandl, C.; Kern, W.; Schlögl, S., Adhesives for "debonding-on-demand": Triggered release mechanisms and typical applications. *Int. J. Adhes. Adhes.* **2020,** *99*, 102585.
31. Zeng, X.; Mathews, J. A.; Li, J., Urban Mining of E-Waste is Becoming More Cost-Effective Than Virgin Mining. *Environ Sci Technol* **2018,** *52* (8), 4835-4841.
32. Kaiser, K.; Schmid, M.; Schlummer, M., Recycling of polymer-based multilayer packaging: A review. *Recycling* **2017,** *3* (1), 1-26.
33. Ayer, M. A.; Simon, Y. C.; Weder, C., Azo-containing polymers with degradation on-demand feature. *Macromolecules* **2016,** *49* (8), 2917-2927.
34. Heinzmann, C.; Coulibaly, S.; Roulin, A.; Fiore, G. L.; Weder, C., Light-induced bonding and debonding with supramolecular adhesives. *ACS Appl. Mater. Interfaces* **2014,** *6* (7), 4713-4719.
35. Siracusa, V.; Rocculi, P.; Romani, S.; Rosa, M. D., Biodegradable polymers for food packaging: a review. *Trends in Food Science & Technology* **2008,** *19* (12), 634-643.
36. Li, B.; Zhang, S.; Andre, J. S.; Chen, Z., Relaxation behavior of polymer thin films: Effects of free surface, buried interface, and geometrical confinement. *Prog. Polym. Sci.* **2021,** *120*.

37. Zhang, S.; Andre, J. S.; Hsu, L.; Toolis, A.; Esarey, S. L.; Li, B.; Chen, Z., Nondestructive in situ detection of chemical reactions at the buried interface between polyurethane and isocyanate-based primer. *Macromolecules* **2020,** *53* (22), 10189-10197.
38. Lin, T.; Wu, Y.; Santos, E.; Chen, X.; Ahn, D.; Mohler, C.; Chen, Z., Molecular insights into adhesion at a buried silica-filled silicone/polyethylene terephthalate interface. *Langmuir* **2020,** *36* (49), 15128-15140.
39. 39. Li, B.; Andre, J. S.; Chen, X.; Walther, B.; Paradkar, R.; Feng, C.; Tucker, C.; Mohler, C.; Chen, Z., Probing molecular behavior of carbonyl groups at buried nylon/polyolefin interfaces in situ. *Langmuir* **2020,** *36* (38), 11349-11357.
40. Fockaert, L.-L. I.; Ganzinga-Jurg, D.; Versluis, J.; Boelen, B.; Bakker, H. J.; Terryn, H.; Mol, J. M. C., Studying Chemisorption at Metal–Polymer Interfaces by Complementary Use of Attenuated Total Reflection–Fourier Transform Infrared Spectroscopy (ATR-FTIR) in the Kretschmann Geometry and Visible–Infrared Sum-Frequency Generation Spectroscopy (SFG). *The Journal of Physical Chemistry C* **2020,** *124* (13), 7127-7138.
41. Watts, K. E.; Blackburn, T. J.; Pemberton, J. E., Optical Spectroscopy of Surfaces, Interfaces, and Thin Films: A Status Report. *Anal Chem* **2019,** *91* (7), 4235-4265.
42. Sensui, K.; Tarui, T.; Miyamae, T.; Sato, C., Evidence of chemical-bond formation at the interface between an epoxy polymer and an isocyanate primer. *Chem Commun* **2019,** *55* (98), 14833-14836.
43. Zuo, B.; Inutsuka, M.; Kawaguchi, D.; Wang, X.; Tanaka, K., Conformational Relaxation of Poly(styrene-co-butadiene) Chains at Substrate Interface in Spin-Coated and Solvent-Cast Films. *Macromolecules* **2018,** *51* (6), 2180-2186.
44. Yamamoto, K.; Kawaguchi, D.; Sasahara, K.; Inutsuka, M.; Yamamoto, S.; Uchida, K.; Mita, K.; Ogawa, H.; Takenaka, M.; Tanaka, K., Aggregation States of Poly(4-methylpentene-1) at a Solid Interface. *Polymer Journal* **2018,** *51* (2), 247-255.
45. Hong, Y.; Li, Y.; Wang, F.; Zuo, B.; Wang, X.; Zhang, L.; Kawaguchi, D.; Tanaka, K., Enhanced thermal stability of polystyrene by interfacial noncovalent interactions. *Macromolecules* **2018,** *51* (15), 5620-5627.
46. Ulrich, N. W.; Li, X.; Myers, J. N.; Williamson, J.; Lu, X.; Chen, Z., Distinct Molecular Structures of Edge and Middle Positions of Plasma Treated Covered Polymer Film Surfaces Relevant in the Microelectronics Industry. *IEEE Transactions on Components, Packaging and Manufacturing Technology* **2017,** *7* (8), 1377-1390.
47. Ulrich, N. W.; Andre, J.; Williamson, J.; Lee, K. W.; Chen, Z., Plasma treatment effect on polymer buried interfacial structure and property. *Phys. Chem. Chem. Phys.* **2017,** *19* (19), 12144-12155.
48. Lu, X.; Zhang, C.; Ulrich, N.; Xiao, M.; Ma, Y. H.; Chen, Z., Studying polymer surfaces and interfaces with sum frequency generation vibrational spectroscopy. *Anal. Chem.* **2017,** *89* (1), 466-489.
49. Ulrich, N. W.; Myers, J. N.; Chen, Z., Characterization of polymer/epoxy buried interfaces with silane adhesion promoters before and after hygrothermal aging for the elucidation of molecular level details relevant to adhesion. *RSC Advances* **2015,** *5* (128), 105622-105631.
50. Myers, J. N.; Zhang, X.; Xiu, Y.; Wei, Y.; Williamson, J. M.; Lee, K.-W.; Chen, Z., Nondestructive characterization of molecular structures at buried copper/epoxy interfaces and their relationship to locus of failure analysis. *IEEE Trans. Adv. Packag.* **2015,** *5* (10), 1432-1440.

51. Myers, J. N.; Zhang, X.; Bielefeld, J. D.; Chen, Z., Plasma Treatment Effects on Molecular Structures at Dense and Porous Low-k SiCOH Film Surfaces and Buried Interfaces. *The Journal of Physical Chemistry C* **2015,** *119* (39), 22514-22525.
52. Myers, J. N.; Chen, Z., Surface plasma treatment effects on the molecular structure at polyimide/air and buried polyimide/epoxy interfaces. *Chin. Chem. Lett.* **2015,** *26* (4), 449-454.
53. Zhang, C.; Myers, J. N.; Chen, Z., Molecular behavior at buried epoxy/poly(ethylene terephthalate) interface. *Langmuir* **2014,** *30* (42), 12541-50.
54. Ye, S.; Tong, Y.; Ge, A.; Qiao, L.; Davies, P. B., Interfacial structure of soft matter probed by SFG spectroscopy. *Chem Rec* **2014,** *14* (5), 791-805.
55. Zhang, C.; Hankett, J.; Chen, Z., Molecular level understanding of adhesion mechanisms at the epoxy/polymer interfaces. *ACS Appl. Mater. Interfaces* **2012,** *4* (7), 3730-7.
56. Loch, C. L.; Ahn, D.; Chen, Z., Sum frequency generation vibrational spectroscopic studies on a silane adhesion-promoting mixture at a polymer interface. *J. Phys. Chem. B* **2006,** *110*, 914-918.
57. Schultz, Z. D.; Biggin, M. E.; White, J. O.; Gewirth, A. A., Infrared-Visible Sum Frequency Generation Investigation of Cu Corrosion Inhibition with Benzotriazole. *Analytical Chemistry* **2004,** *76*, 604-609.
58. Harp, G. P.; Rangwalla, H.; Yeganeh, M. S.; Dhinojwala, A., Infrared-Visible Sum Frequency Generation Spectroscopic Study of Molecular Orientation at Polystyrene/Comb-Polymer Interfaces. *J Am Chem Soc* **2003,** *125* (37), 11283-11290.
59. Harp, G. P.; Gautam, K. S.; Dhinojwala, A., Probing Polymer/polyer interfaces. *Journal of the American Chemical Society Communications* **2002,** *124*, 7908-7909.
60. Chen, C.; Wang, J.; Even, M. A.; Chen, Z., Sum frequency generation vibrational spectroscopy studies on "buried" polymer/polymer interfaces. *Macromolecules* **2002,** *35*, 8093-8097.
61. Gracias, D. H.; Chen, Z.; Shen, Y. R.; Somorjai, G. A., Molecular characterization of polymer and polymer blend surfaces. Combined sum frequency generation surface vibrational spectroscopy and scanning force microscopy studies. *Acc. Chem. Res.* **1999,** *32*, 930-940.
62. Lu, X.; Xue, G.; Wang, X.; Han, J.; Han, X.; Hankett, J.; Li, D.; Chen, Z., Directly probing molecular ordering at the buried polymer/metal interface 2: Using P-polarized input beams. *Macromolecules* **2012,** *45* (15), 6087-6094.
63. Hirose, C.; Akamatsu, N.; Domen, K., Formulas for the analysis of surface sum-frequency generation spectrum by CH stretching modes of methyl and methylene groups. *J. Chem. Phys.* **1992,** *96* (2), 997-1003.
64. Superfine, R.; Huang, J. Y.; Shen, Y. R., Phase measurement for surface infrared-visible sum-frequency generation. *Opt. Lett.* **1990,** *15* (22), 1276-1278.
65. Shen, Y. R., Optical second harmonic generation at interfaces. *Annu. Rev. Phys. Chem.* **1989,** *40* (1), 327–350.
66. Gong, L.; Xiang, L.; Zhang, J.; Chen, J.; Zeng, H., Fundamentals and advances in the adhesion of polymer surfaces and thin films. *Langmuir* **2019,** *35* (48), 15914-15936.
67. Awajaa, F.; Gilbertb, M.; Kellya, G.; Foxa, B.; Pigram, P. J., Adhesion of polymers. *Prog Polym Sci* **2009,** *34* (9), 948–968.
68. Plueddemann, E. P., Adhesion Through Silane Coupling Agents. *The Journal of Adhesion* **2008,** *2* (3), 184-201.

69. Merian, T.; Goddard, J. M., Advances in nonfouling materials: perspectives for the food industry. *J Agric Food Chem* **2012,** *60* (12), 2943-57.
70. Chevallier, P.; Turgeon, S.; Sarra-Bournet, C.; Turcotte, R.; Laroche, G., Characterization of multilayer anti-fog coatings. *ACS Appl Mater Interfaces* **2011,** *3* (3), 750-8.
71. Miyama, M.; Yang, Y.; Yasuda, T.; Okuno, T.; Yasuda, H. K., Static and Dynamic Contact Angles of Water on Polymeric Surfaces. *Langmuir* **1997,** *13*, 5494-5503.
72. Villalpando-Olmos, J.; Sanchez-Valdes, S.; Yanez-Flores, I. G., Performance of polyethyIene/ethyIene-vinyI alcohol copolymer/polyethylene multilayer films using maleated polyethylene blends. *Polymer Engineering and Science* **1999,** *39* (9), 1597-1603.
73. Shen, Y. R., *Fundamentials of Sum-Frequency Generation Spectroscopy*. Cambridge University Press: Cambridge, 2016.
74. Shen, Y. R., Basic theory of surface sum-frequency generation. *J. Phys. Chem. C* **2012,** *116* (29), 15505-15509.
75. Geiger, F. M., Second harmonic generation, sum frequency generation, and chi(3): dissecting environmental interfaces with a nonlinear optical Swiss Army knife. *Annu Rev Phys Chem* **2009,** *60*, 61-83.
76. Boyd, R. W., *Nonlinear Optics*. 3rd ed.; Academic Press: 2008; p 640.
77. Lagutchev, A.; Hambir, S. A.; Dlott, D. D., Nonresonant background suppression in broadband vibrational sum-frequency generation spectroscopy. *J. Phys. Chem. C Lett.* **2007,** *111*, 13645-13647.
78. Perry, A.; Neipert, C.; Space, B.; Moore, P. B., Theoretical Modeling of Interface Specific Vibrational Spectroscopy: Methods and Applications to Aqueous Interfaces. *Chem. Rev.* **2006,** *106* (4), 1234-1258.
79. Moad, A. J.; Simpson, G. J., A unified treatment of selection rules and symmetry relations for sum-frequency and second harmonic spectroscopies. *J. Phys. Chem. B* **2004,** *108*, 3548-3562.
80. Zhuang, X.; Miranda, P. B.; Kim, D.; Shen, Y. R., Mapping molecular orientation and conformation at interfaces by surface nonlinear optics. *Physical Review B* **1999,** *59* (19), 12632-12640.
81. Richter, L. J.; Petralli-Mallow, T. P.; Stephenson, J. C., Vibrationally resolved sum-frequency generation with broad-bandwidth infrared pulses. *Optics Letters* **1998,** *23* (20), 1594-1596.
82. Guyot-Sionnest, P., Coherent processes at surfaces: Free-induction decay and photon echo of the Si-H stretching vibration for H/Si(111). *Phys Rev Lett* **1991,** *66* (11), 1489-1492.
83. Lambert, A. G.; Davies, P. B.; Neivandt, D. J., Implementing the theory of sum frequency generation vibrational spectroscopy: A tutorial review. *Appl. Spectrosc. Rev.* **2005,** *40* (2), 103-145.
84. Lu, X.; Li, B.; Zhu, P.; Xue, G.; Li, D., Illustrating consistency of different experimental approaches to probe the buried polymer/metal interface using sum frequency generation vibrational spectroscopy. *Soft Matter* **2014,** *10* (29), 5390-7.
85. Zhang, C.; Chen, Z., Quantitative molecular level understanding of ethoxysilane at poly(dimethylsiloxane)/polymer interfaces. *Langmuir* **2013,** *29* (2), 610-619.
86. Fang, Y.; Li, B.; Yu, J.; Zhou, J.; Xu, X.; Shao, W.; Lu, X., Probing surface and interfacial molecular structures of a rubbery adhesion promoter using sum frequency generation vibrational spectroscopy. *Surface Science* **2013,** *615*, 26-32.

87. Lu, X.; Clarke, M. L.; Li, D.; Wang, X.; Xue, G.; Chen, Z., A Sum Frequency Generation Vibrational Study of the Interference Effect in Poly(n-butyl methacrylate) Thin Films Sandwiched between Silica and Water. *The Journal of Physical Chemistry C* **2011,** *115* (28), 13759-13767.
88. Chen, Z., Investigating buried polymer interfaces using sum frequency generation vibrational spectroscopy. *Prog. Polym. Sci.* **2010,** *35* (11), 1376-1402.
89. Simpson, G. J., *Nonlinear Optical Polarization Analysis in Chemistry and Biology*. Cambridge University Press: Cambridge, 2017.
90. Zhang, C.; Myers, J.; Chen, Z., Elucidation of molecular structures at buried polymer interfaces and biological interfaces using sum frequency generation vibrational spectroscopy. *Soft Matter* **2013,** *9*, 4738-4761.

Chapter 2: Interfacial Behavior of Flux Residues and Its Impact on Copper/Underfill Adhesion in Microelectronic Packaging

Material covered in this chapter was published in the *Journal of Electronic Packaging* **2021,** *143,* 011004.

2.1 Introduction

Integrated circuit (IC) and flip-chip on lead frame (FCOL) devices have revolutionized the micro-electronics industry. In these devices, replacing wire bonds with solder bumps has allowed industry to keep up with Moore's Law and make smaller, more capable devices. Advances in this technology have led to devices with increased density of transistors per chip. Underfill (UF) materials are introduced as packaging for many common electronic devices, specifically IC and FCOL devices to improve and strengthen various interfaces, leading to improved device reliability.[1-5] UF materials commonly contain bisphenol derivative epoxy adhesives due to many advantageous properties of the material such as its high strength and short curing times, and general applicability.[4] Adhesion of epoxies to many types of substrates (composite materials, metals, and polymers), along with different types of surface treatments have been extensively studied and is important for the application of epoxy-based adhesives in industry.[6-14]

Electronic chips or dies are typically attached to lead frames through copper posts. In processing the connection of copper post to the lead frame, flux materials are added to prepare the copper posts for soldering [15, 16]. Usually the flux material used is a proprietary blend of water, organic compounds, salts, and carboxylic acids or amines [15, 16]. The purpose of the flux is to remove organic solderability preservatives and oxides from the copper surface allowing better wettability and electrical contact to the solder joint.[17-20] A potential problem arises when, after the soldering process, flux residues are left behind on exposed surfaces before addition of UF. Residual flux materials can cause UF voids, poor UF adhesion to die and substrate, and/or solder bridging between the copper posts, negatively impacting the device performance.[17-20] Therefore, to improve the device performance and reliability, it is necessary to investigate flux residue behavior and related interfacial effects.

Various effects of flux materials and their underlined mechanisms in soldering have been previously investigated.[15, 21-24] For example, it was found that a model flux, adipic acid, a free acid, in solution, binds surface copper oxides, forms a salt, and is moved away from the solder contact in a cleaning step. [22-24 22-2422-24] This theory of fluxing is very general due to the different in processes conditions and flux materials used in practice. In many real applications, flux residues typically remain at buried solid/solid interfaces.[15, 21] Although excellent research on flux residues has been performed, *in situ* investigation of interfacial behavior of flux residues at buried solid/solid interface was rare, due to the lack of appropriate analytical tools to probe buried interfaces *in situ*. Previously, the Chen group successfully applied a nonlinear optical laser technique, sum frequency generation (SFG) vibrational spectroscopy, to elucidate the molecular behavior of a model flux, glutaric acid, at silica/UF and copper/UF buried interfaces *in situ* where SFG results were correlated to the adhesion of the UF to copper surface.[25] This work lead to

broader understanding on how flux residues could be removed from surfaces, how the residue changed the buried cupper/UF interface, and how adhesion strength varies after the removal of flux residues. The research reported in this chapter generalized the approach developed in our previous study by examining more different model fluxes and a commercial flux used in real microelectronic fabrication. Previous work also studied locus failure on different copper/UF systems, which analyzed the broken interface with SEM, EDX, and XPS.[26] These *ex situ* measurements were not performed in the present study as they are applied to the exposed surfaces after adhesion failure.

Here, SFG was used to probe flux behavior at the copper surface and buried copper/UF interfaces and correlate these findings to adhesion strength between the copper and UF materials. Adipic acid and phenylacetic acid were used as model fluxes. Kester 979 no-clean flux, a commercial flux, was also studied due to its industrial relevance. Bisphenol A diglycidyl ether (BADGE), an epoxide containing molecule and diaminodiphenylmethane (DDM), the curing agent, were cured and used as the model UF material. The molecular structures of the above materials are shown in **Figure 2.1**. In this study, adipic acid was chosen because of the different chain length of adipic acid vs previously studied glutaric acid. Phenylacetic acid's aromatic functionality and asymmetry helps to give a more general understanding on the role of organic acids used in real flux formulations.

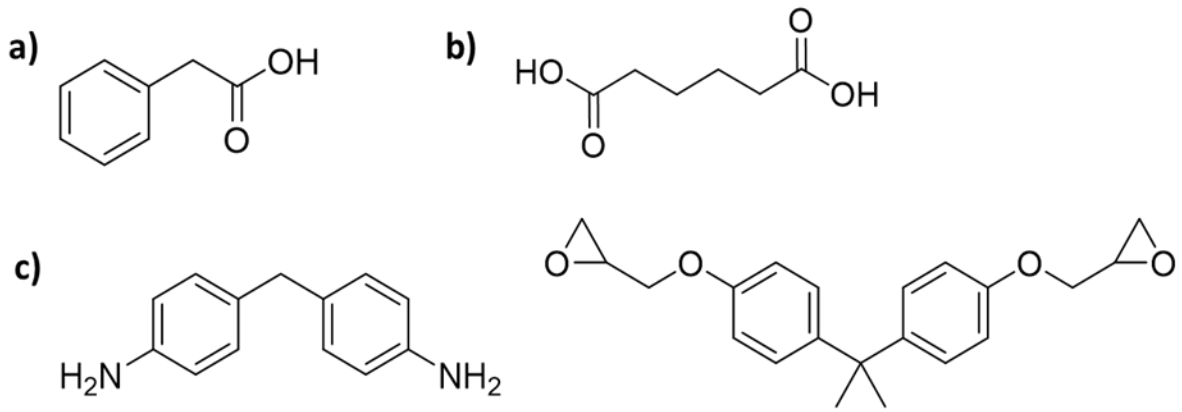

Figure 2.1 Model fluxes studied are a) phenylacetic acid and b) adipic acid. The model UF is prepared using c) DDM (left) and BADGE (right).

To correlate the SFG results to adhesion, lap shear adhesion testing was also performed. As will be presented below, our research showed the following: (1) Flux residues can disrupt adhesion when not treated properly (lacking either removal by washing or neutralization with heat treatments). (2) Proper treatment (washing or heating) of the residue changed the buried interface between copper and UF. (3) UF structure at an interface affected the strength of adhesion. We believe that this study generalizes the previous findings on structure-function relationships of flux residues at buried interfaces, which should substantially impact the research and application of flux in packaging of microelectronics.

2.2 Materials and methods

2.2.1 Materials

Bisphenol A diglycidyl ether (BADGE), 4,4'-diamino-diphenylmethane (DDM), and model fluxes including adipic acid and phenylacetic acid were obtained from Sigma-Aldrich (St. Louis, MO). Aqueous solutions composed of model fluxes (2% wt.) were used for all experiments. Kester 979 no-rinse flux was purchased from Allied Electronics & Automation (Fort Worth, TX) and used as received. Calcium fluoride windows and prisms for SFG studies were bought from

Altos Photonics (Bozeman, MT). Calcium fluoride substrates were cleaned with toluene, water, then air plasma for 3 minutes in a PE-25-JW plasma oven (Plasma Etch,) before use. Copper surfaces used in SFG measurements were prepared by depositing 100 nm of copper onto a 4-inch silicon wafer via electron-beam evaporation (Cook Vacuum Products) then used as prepared. Thin films of fluxes were prepared by spin-casting (Speedline Technologies P-6000) 2% wt. flux solutions onto optical substrates (calcium fluoride prisms, copper surfaces) at 2000 RPM for 30 seconds. For the washed samples, flux treated copper substrates were submerged in a stirred 500 mL warm deionized water (70 °C) bath for 4 hours. Heat treated no-clean flux samples were not washed, but heated in a convection oven at 150 °C for a short period of time (<30 seconds) before epoxy deposition.

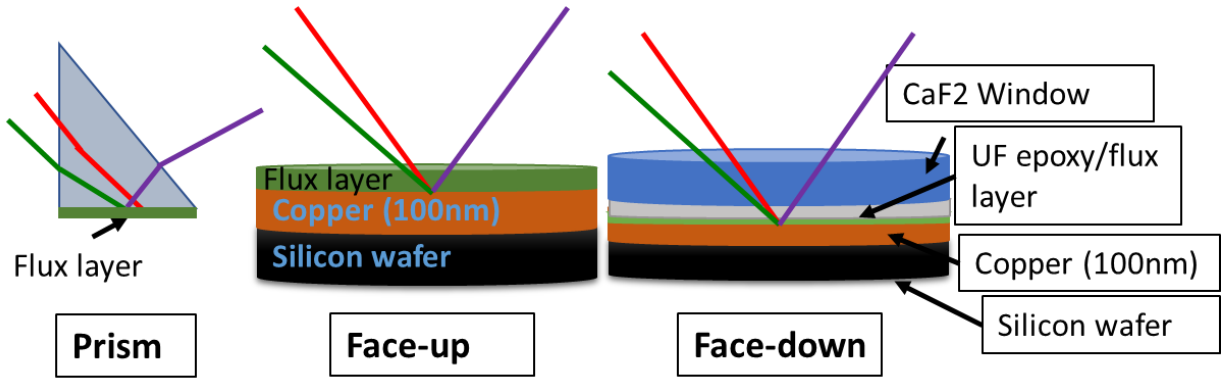

Figure 2.2 SFG sample geometries used for this study. Prism and face-up geometries provide spectra of surfaces after flux treatments. Face-down geometry allows for studying the epoxy/copper interface with/without flux and after the flux has been washed.

The BADGE and DDM epoxy UF was prepared in a 2:1 stoichiometric ratio, respectively and heated to make a homogeneous mixture. The UF mixture was then diluted in toluene to a concentration of ~60 g/L. Epoxy thin films were prepared by spin-casting a mixture of BADGE and DDM in toluene (UF solution) for 30 seconds at 2000 rpm onto calcium fluoride substrates, resulting in a film thickness of around 200 nm. After coating the windows with the UF solution,

samples were degassed at room temperature and atmospheric pressure for an hour to remove residual solvent. Copper substrates (control, flux treated, flux treated with wash, no-clean flux untreated, and no-clean flux heat treated) were then contacted with the UF and cured in an oven for 1 hour at 50°C, 45 minutes at 75°C, and 30 minutes at 110°C. Copper substrates were adhered to the calcium fluoride windows by the UF after the curing cycle, suitable for SFG experiments. **Figure 2.2** shows SFG geometries used in this experiment.

2.2.2 Methods

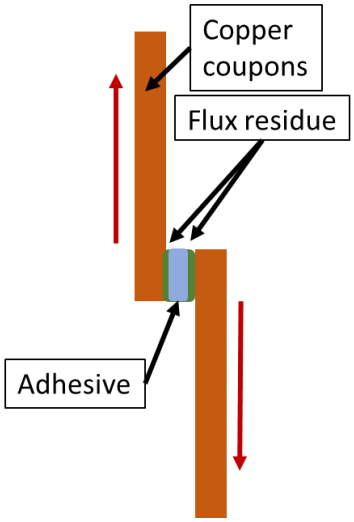

Figure 2.3 Geometry used for lap shear adhesion testing. Copper coupons were adhered with the UF material and pulled until contact between a coupon and the UF is broken.

SFG sample geometries used in this study are shown in **Figure 2.2**. Prism sample geometry was used to collect flux SFG signal without the non-resonate contribution from the metal surface. Experiments involving copper used both the face-up and face-down geometries shown. Face-up geometry has reflection of the beams directly from the copper surface. In the face-down geometry, the laser beams pass through an optical substrate (calcium fluoride window) to the buried interface and SFG signal was reflected from the copper/UF buried interface. In this study, face-down geometry was used to study buried interfaces between copper and UF. Face-up geometry was used

to study flux residues on copper surfaces without UF present, as shown in **Figure 2.2**. Other SFG details are covered in Chapter 1.

Grazing incidence X-ray diffraction (GIXRD) experiments were performed to gain understanding on the flux role in oxide removal from the copper surface. A Rigaku Ultima IV X-Ray Diffractometer (Tokyo, Japan), with a 2.2 kW Cu K-α radiation source, was used in this study. GIXRD is widely used as a surface characterization technique in materials science. In GIXRD, X-rays are incident at small angles allowing the technique to be more surface sensitive [27], measuring only a few nanometers into the copper bulk. GIXRD provided insight into the changes in the copper surface structure before and after contact with flux. Copper samples for GIXRD were prepared in the same fashion as the SFG samples.

Adhesion lap shear testing was performed under standard conditions based on the ASTM D3163 method, with an Instron 5544 (Norwood, MA). Copper coupons for lap shear were obtained from "onlinemetals.com" and used as received. Copper coupons were 25 mm wide and around 80 mm long. Lap shear samples had overlap area of 25 mm x 5 mm between the copper coupons, which were orientated 180° relative to each other. Flux solutions were applied to copper coupons, as described above. The UF was prepared with BADGE and DDM in a 2:1 stochiometric ratio, same as the SFG experiments. Coupons were adhered in a lap geometry, shown in **Figure 2.3**, and the UF was cured. The thickness of the cured UF was about 1mm. When the coupon separated from the UF, a sudden drop in tensile load was observed, the maximum shear before the drop divided by the overlap area is reported as the adhesion strength (N/m^2) for the system. Results for adhesion tests are averaged from ten or more samples.

2.3 Results

2.3.1 SFG results on model fluxes on surfaces

Before examining flux residues on copper or at buried interfaces with UF, SFG spectra were collected from the two model flux samples prepared from flux solutions on calcium fluoride prisms (**Figure 2.4)**. This was done to identify the characteristic peaks of the flux molecules unperturbed by the non-resonate contribution to SFG signal from the copper (high background signal in **Figure 2.5**, more discussion on this effect later). The flux materials on calcium fluoride have SFG peaks characteristic to each organic acid. For example, adipic acid has methylene symmetric and antisymmetric stretching peaks at around 2860 cm^{-1} and 2925 cm^{-1} respectively, while phenylacetic acid has a dominating peak from the aromatic ring C-H stretching around 3070 cm^{-1}. These data indicate that the fluxes are well ordered at the calcium fluoride/air interface.

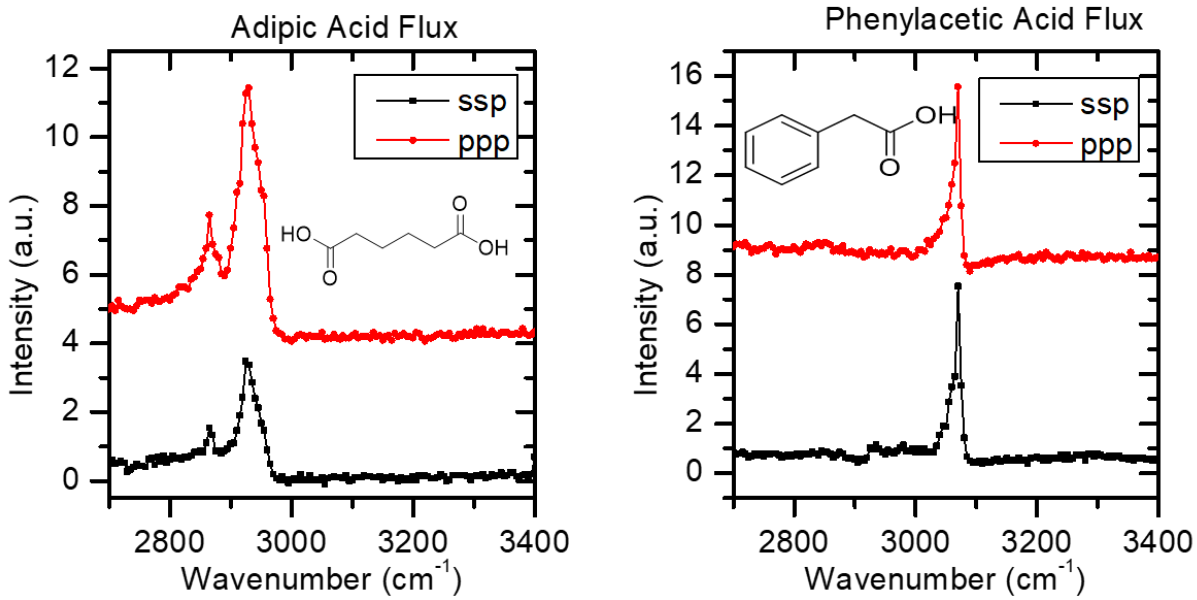

Figure 2.4 SFG spectra of fluxes from calcium fluoride surface. Spectra on the left are from the adipic acid/calcium fluoride surface, on the right are from the phenylacetic acid/calcium fluoride surface.

Figure 2.5 shows SFG spectra collected from the flux treated copper surfaces in air before (top) and after washing (bottom). The unique peaks of the model fluxes which were detected on calcium fluoride are present but due to interactions between the flux SFG signals and strong non-

resonant background SFG signal from metal (copper), very different spectral features (negative or half negative/half positive) were observed. No SFG resonant signals could be detected after washing, showing that flux molecules could be removed from the copper surfaces.

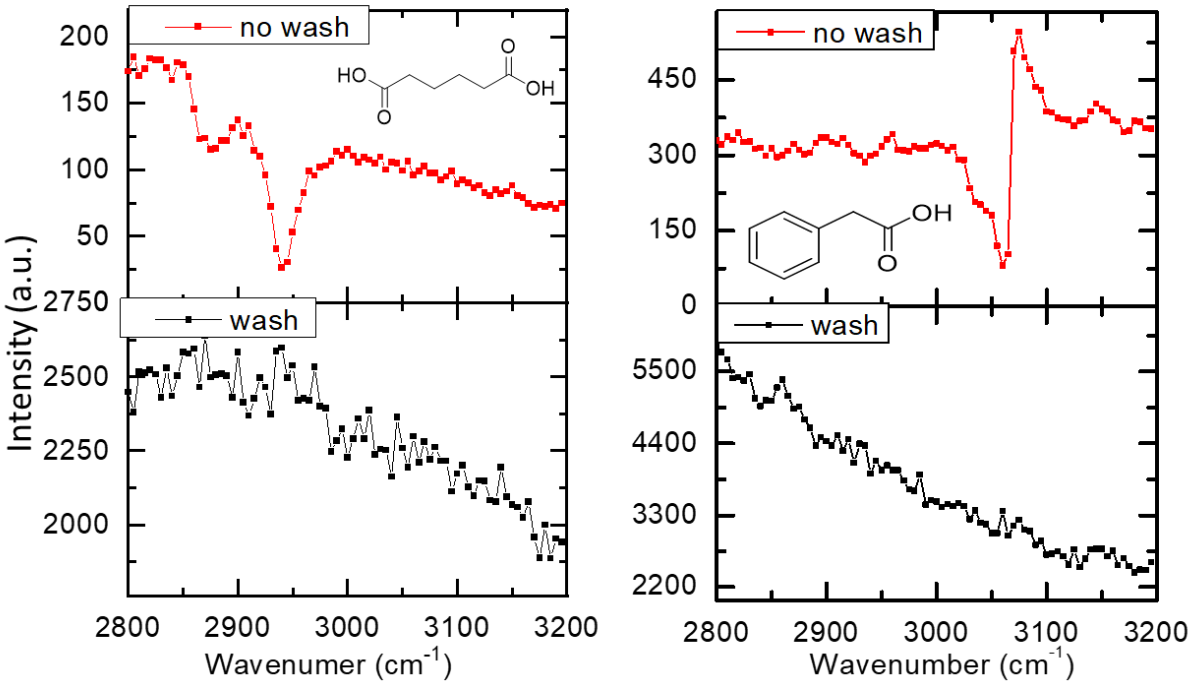

Figure 2.5 SFG spectra of fluxes from copper surfaces with no wash (red) and after washing the fluxes (black). Spectra were collected in ppp polarization.

2.3.2 XRD results from copper surfaces

Grazing incidence X-ray diffraction experiments were performed on copper samples prepared by CVD on a silicon wafer before addition of flux to the copper surface and after flux treatment/water washing. The GIXRD spectra in **Figure 2.6** showed characteristic copper peaks at 43.5°, 50.7°, and 74.3° for all the three samples: copper before flux treatment and copper after adipic acid or phenylacetic acid treatment/water washing. The untreated copper spectrum contained additional peaks at 52.4° and 56.0°, contributed by the copper oxide formed on the untreated copper surface [24, 27-30]. The two oxide peaks disappeared after flux treatment and water

washing, indicating that the copper oxides were removed from the copper surface by flux treatment/water washing. Copper peak intensities were similar for untreated and flux treated samples. This is reasonable since these peaks are mainly contributed from the copper bulk where no oxides have formed.

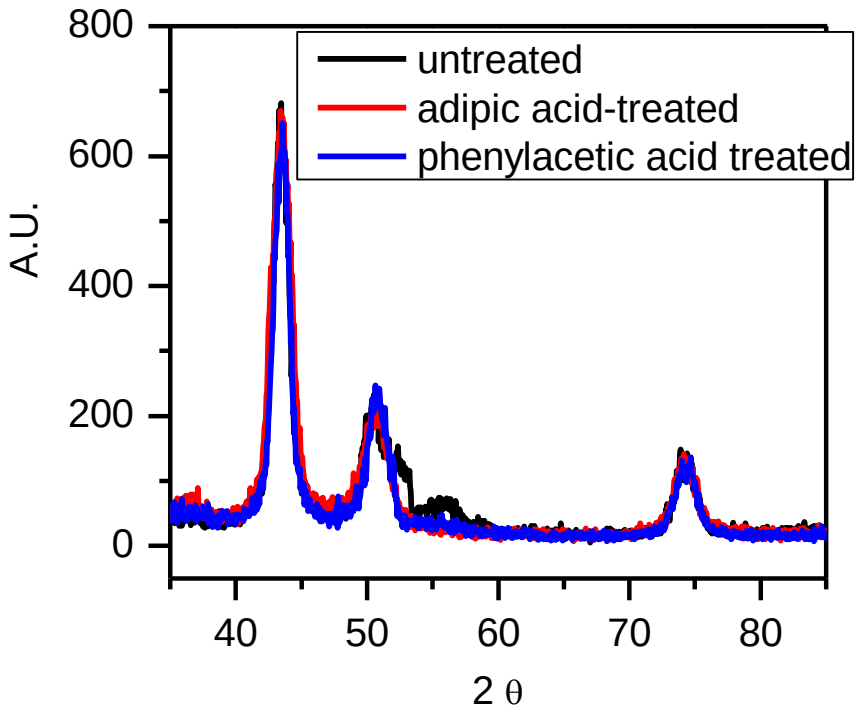

Figure 2.6 XRD spectra from untreated and washed flux treated copper surfaces.

2.3.3 SFG results of model fluxes at buried interfaces

SFG ppp spectra collected from a polymer film on a metal surface are dominated by signals contributed from the buried polymer/metal interface. [31-34] SFG spectrum (**Figure 2.7**) was collected from the control sample, the copper (without flux treatment)/UF interface, using the window face-up geometry. SFG signals observed in this spectrum are centered at 2860 cm^{-1} (CH_2 ss), 2920 cm^{-1} (CH_2 as), and 2950 cm^{-1} (CH_3 Fermi), all contributed from the UF (because no flux was applied yet). With no flux the UF can still order at the buried copper/UF interface.

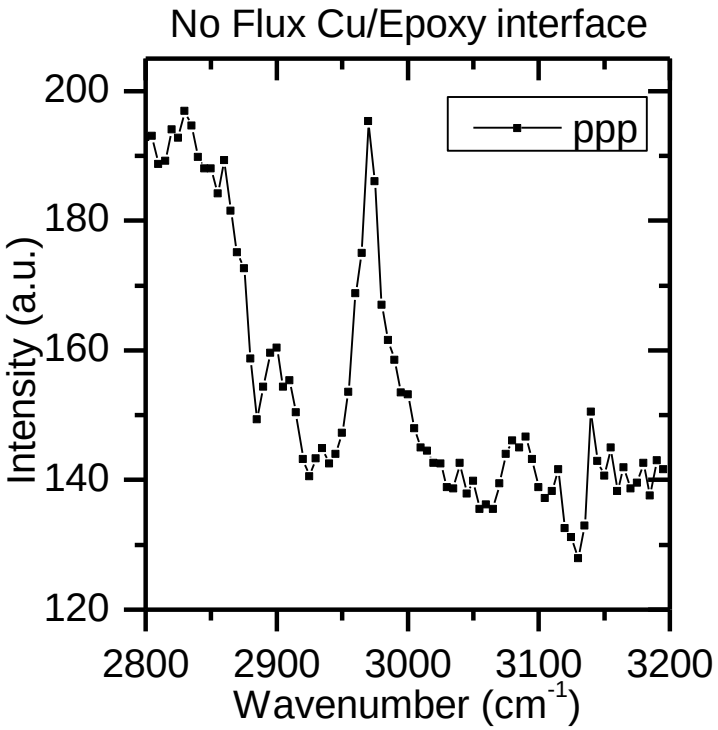

Figure 2.7 SFG spectra from the copper/UF buried interface. The copper was not treated with flux.

SFG spectra were then collected from the copper/UF interfaces with copper first treated by flux with or without washing (**Figure 2.8)**. For copper surfaces treated by adipic acid or phenylacetic without washing, SFG spectra were similar to each other and also similar to that collected from the control copper/UF interface (without flux treatment on the copper surface). Therefore, we believe that for all the three cases, copper without flux treatment or with treatment by adipic acid or phenylacetic acid before washing, the SFG spectra collected from the copper/UF interfaces are dominated by signals contributed from the UF material. The three spectra were not identical, showing that flux may have some minor contributions to the SFG signals or flux may induce some small changes in the UF molecules at the interfaces. After washing the flux on copper, SFG signals detected from the UF and flux materials at the buried copper/UF interfaces greatly diminished in both cases, with adipic acid or phenylacetic acid treatment on copper. This suggests

that washing the copper surface alone after the flux treatment could greatly alter the buried interface and indicates that under this situation the copper/UF interface is disordered.

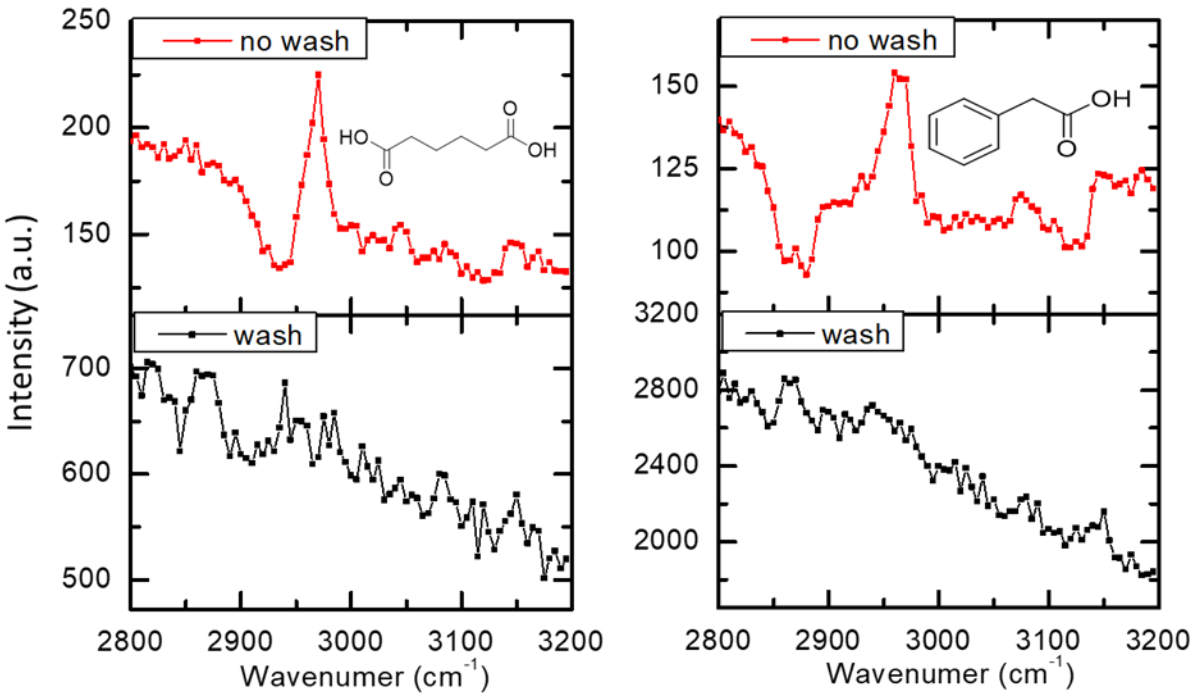

Figure 2.8 SFG spectra from the copper/UF buried interface. Copper surfaces were treated with flux. Spectra from adipic acid treated surface are shown on the left and spectra from phenylacetic acid treated surface are shown on the right.

2.3.4 SFG results on commercial flux materials at the copper/UF interface

With regular flux treatment, washing process was needed to remove the flux residue on metal surface. Adipic acid and phenylacetic acid studied above were used as models for such flux molecules and therefore the washing effects were observed. Recently no-clean fluxes were developed [1, 15, 21]; they are not removed by washing but rather by heating. Here we also applied SFG to study no-clean flux. The no-clean flux chosen for this study, Kester-959, was applied to the copper surface, by spin casting a small amount onto the copper surface. Samples were then treated with high temperatures for short periods (30s) of time to remove volatile molecules and

complete the flux interaction with the metal surface, simulating steps in wave-soldering conditions. Before carrying our SFG experiments, we observed with the naked eyes that flux residues remained on the copper surface before and after heat treatment. After the treatment, the flux left on the surface was slightly different in appearance than before heat was applied.

SFG spectra were collected from the copper/UF interfaces with the treatment of no-clean flux on copper before and after heating (**Figure 2.9**). These spectra are similar to those collected from the copper/UF interfaces with copper treated by model fluxes studied above before and after washing. Before heat treatment, the SFG signal appeared to be dominated by UF. After heat treatment, the UF signal decreased and the spectrum became very noisy, indicating that the copper/UF interface was disordered. SFG signals from the copper/UF interface with the copper treated with no-clean flux before heating was slightly different from buried interface with copper treated with the model systems before washing. This may indicate that signals contain minor contributions from no-clean flux.

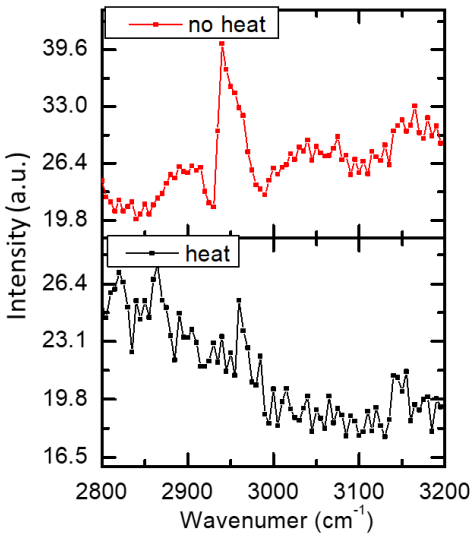

Figure 2.9 SFG spectra collected from the copper/UF interface. Kester-959 no clean flux was left untreated (top). The copper/UF interface after the no-clean flux was treated has no characteristic peaks but was dominated by the non-resonate signal from the copper surface (bottom).

2.3.5 Discussion of SFG results

Copper is a common metal used in microelectronics and adding flux to the copper surface before soldering and packaging is a ubiquitous processing step in microelectronic fabrication. Interactions between flux and copper are chemical in nature, where the flux molecules react with the copper surface leading to the removal of surface oxides. Treating copper with flux alters the copper surface enough to change the interaction of copper and UF. One feature of note in the washed versus the unwashed flux samples was that the SFG non-resonate background, which was present due to the high degree of polarizability of metal surface electrons, increased after flux treatment and washing. This result is reasonable, as flux chemically reacts with the copper surface and byproducts of this interaction are removed by washing, exposing the metal copper surface, leading to stronger SFG non-resonant signal compared to that from the metal oxide before flux treatment and washing. This could also be confirmed by the GIXRD results presented above.

In the control sample, with no flux added, the UF ordered at the copper interface. After adding flux to the copper surface, the UF still ordered at the copper interface and the copper/UF interface was relatively unchanged. Once the flux was washed, the UF no longer ordered at the copper/UF interface. The removal of flux at the buried copper/UF interface is important to adhesion in packaging, explained in the following section.

It is difficult to determine and assign SFG peaks in the no-clean flux case accurately because the composition of the no-clean flux is unknown and may be quite complex. We believe that the composition of the no-clean flux must be very different from the two model fluxes investigated above. Even so, many of the same features were observed with the no-clean flux and the model flux samples. Namely, UF dominated the buried copper/UF interface with copper treated with flux before heating or washing, while after treatment, the interfaces became disordered.

Therefore, we believe that the very different flux materials play similar roles at the metal/UF interfaces in electronic device packaging, a counterintuitive hypothesis, demonstrated only with the SFG results from the buried interfaces *in situ*. This research further demonstrated that SFG is a powerful tool to probe flux behavior at buried interfaces *in situ*, regardless of a model flux or commercial flux, with washing or heating treatment (more directly related to industrial process).

2.3.6 Lap shear analysis

To understand the role of flux residues on the interfacial reliability of packaging materials, adhesion testing experiments by lap shear analysis were performed. **Figure 2.10** displays the adhesion testing results for the copper/UF interface without flux treatment, treated with adipic acid, phenyl acetic acid, no-clean flux before and after washing or heating. For all the three flux systems, some general trends could be observed in adhesion strengths at the copper/flux interfaces: (1) The adhesion measured at the copper/UF interface without flux treatment on copper (control sample) was similar to that measured at the buried copper/UF interface with the flux treated copper. The adhesion strengths measured from different copper/UF interfaces with copper treated with different flux molecules including phenylacetic acid, adipic acid, and no-clean flux were similar. (2) After washing or heating the flux treated copper surface, the adhesion at the copper/UF interfaces substantially increased.

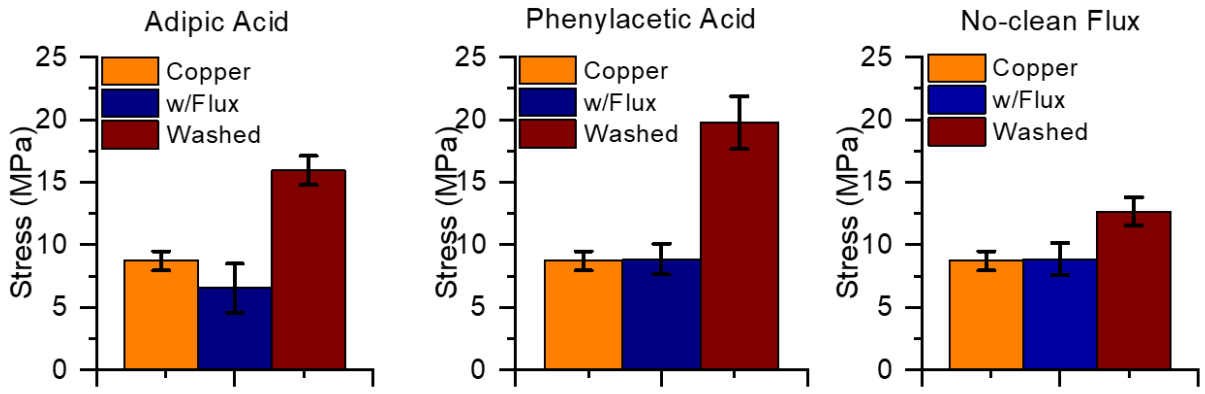

Figure 2.10 Lap shear adhesion test data from adipic and phenylacetic acid model fluxes, and the no-clean flux. "Copper" is the control with no flux added to copper, "w/Flux no wash" are samples with flux at the buried interface, and "w/Flux wash" is with the flux washed away before preparing the buried interface.

Quantitatively, the copper/UF control (without flux treatment on copper) adhesion strength was found to be 8.7±0.8 MPa. For adipic acid treated copper, not washing the flux resulted in an adhesion strength of the copper/UF interface of 6.5±2.0 MPa, washing the flux away resulted in a much stronger adhesion strength of 16.0±1.2 MPa. For phenylacetic acid treated copper, not washing the flux away resulted in an adhesion strength of 8.8±1.2 MPa at the copper/UF interface, while washing the flux away resulted in a much higher adhesion strength of 19.8±2.1 MPa. For no-clean flux treated copper, not heating the sample resulted in an adhesion strength of 8.9±1.3 MPa, heating led to a substantial increase in adhesion – measured to be 12.7±1.1 MPa.

Lap shear adhesion testing results can be well correlated to SFG results above. As we presented above, the SFG spectra collected from the buried interface between copper (without flux treatment) and UF and collected from the buried interfaces between copper treated with different fluxes (including adipic acid, phenylacetic acid, and no-clean flux) and UF were all similar. Therefore, they exhibited similar adhesion. Flux molecules chemically react with the copper. SFG data show that interfacial structures at the copper (without flux)/UF interface and the copper (with

flux)/UF interface are similar, dominated by UF, indicating that UF has similar structure at such interfaces. The adhesion of such interfaces was determined by interfacial UF structure; therefore the adhesion strengths were similar at these interfaces. When we removed the flux molecules from the copper surface, the copper/UF interface showed a very different structure, evidenced by different SFG spectra detected. Such a different structure lead to enhanced adhesion, as we showed above. All the SFG spectra collected from the copper (after flux treatment and washing or heating) did not show distinct peaks, but strong non-resonant signal instead. This indicates that the interfaces were pretty disordered. In the past, we showed that disordered interfaces exhibit stronger adhesion.[35, 36]

2.4 Conclusions

In this study, SFG was used to investigate the interfacial behavior of flux materials *in situ* in real time between copper and UF. Interfacial property of adhesion of the copper/UF interface was measured using lap shear test. It was found that without washing or heating, the buried interfaces between flux treated copper and UF are similar (regardless of the flux type – model flux or commercial flux) and were also similar to that between copper (without flux treatment) and UF. Such interfaces were dominated by ordered epoxy molecules in UF, leading to similar adhesion. With washing or heating of the flux on copper, SFG signals collected from the copper (flux treated and then washed by water or heated)/UF interfaces only showed non-resonant signals from copper, indicating disordered interfaces, leading to much stronger adhesion of these interfaces.

Gaining a general understanding of the role of flux materials at buried interfaces in electronics packaging is important to industry. Fluxes are used ubiquitously when manufacturing electronics and they play a crucial role in packaging these devices, therefore knowledge about their role helps to improve package reliability leading to more robust devices. This study shows clearly

that washing or heating flux treated copper leads to disordered copper/UF interface, resulting in much stronger adhesion. Proper treatment of flux materials is crucial for electronic device durability.

The previous publication[25] showed the *in situ* study of one particular flux, which is important for developing a new method. The research reported in this chapter validates the general use of the method, which is also significant, because it ensures the broader impact of the method. This research studies two model systems, and more importantly, a real flux sample commercially available. Therefore, this research demonstrated the capability to study practical flux samples, which has not been studied previously using SFG. In addition, previously we only studied washing as a removal method for flux, while this chapter examined both washing removal and heating removal (of no-clean flux). This is the first time to study the heating effect on the interfacial structure of no clean flux *in situ* using SFG. Therefore, this research generalizes the SFG methodology to study flux interfacial molecular behavior by studying both model and commercial flux systems with varied removal strategies.

SFG spectroscopy is a powerful analytical tool to study buried interfaces important to electronic and materials engineering. Here SFG results along with lap shear testing successfully provide structure-property relationships of buried solid/solid interfaces in detail. SFG research will continue to be significant due to the few methods that allow for probing of buried solid/solid interfaces *in situ*.

2.5 References

1. Zhang, F.; Li, M.; Chen, W. T.; Chian, K. S., An investigation into the effects of flux residues on properties of underfill materials for flip chip packages. *IEEE Trans. Compon. Packag. Technol.* **2003,** *26* (1), 233-244.
2. Zhang, Z.; Wong, C. P., Recent advances in flip-chip underfill: Materials, process, and reliability. *IEEE Trans. Adv. Packag.* **2004,** *27* (3), 515-524.

3. Doi, H.; Kawano, K.; Yasukawa, A.; Sato, T., Reliability of underfill encapsulated flip-chips with heat spreaders. *J. Electron. Packag.* **1998,** *120*, 322–327.
4. Kornain, Z.; Jalar, A.; Rasid, R.; Abdullah, S., Comparative study of phenolic-based and amine-based underfill materials in flip chip plastic ball grid array package. *J. Electron. Packag.* **2010,** *132* (4), 041012.
5. Rzepka, S.; Korhonen, M. A.; Meusel, E.; Li, C.-Y., The effect of uderfill and underfill delamination on the thermal stress in flip-fhip solder joints. *J. Electron. Packag.* **1998,** *120*, 342-348.
6. Bouhamed, A.; Kia, A. M.; Naifar, S.; Dzhagan, V.; Müller, C.; Zahn, D. R. T.; Choura, S.; Kanoun, O., Tuning the adhesion between polyimide substrate and MWCNTs/epoxy nanocomposite by surface treatment. *Appl. Surf. Sci.* **2017,** *422*, 420-429.
7. Chen, Y.; Wilson, J. A.; Petersen, S. R.; Luong, D.; Sallam, S.; Mao, J.; Wesdemiotis, C.; Becker, M. L., Ring-opening copolymerization of maleic anhydride with functionalepoxides: poly(propylene fumarate) analogues capable of post-polymerization modification. *Angew Chem. Int. Ed. Engl.* **2018,** *57* (39), 12759-12764.
8. Lapique, F.; Redford, K., Curing effects on viscosity and mechanical properties of a commercial epoxy resin adhesive. *Int. J. Adhes. Adhes.* **2002,** *22*, 337–346.
9. Lee, H.-Y.; Kim, S.-R., Pull-out behavior of oxidized copper leadframes from epoxy molding compounds. *J. Adhes. Sci. Technol.* **2002,** *16* (6), 621-651.
10. Parhizkar, N.; Ramezanzadeh, B.; Shahrabi, T., Corrosion protection and adhesion properties of the epoxy coating applied on the steel substrate pre-treated by a sol-gel based silane coating filled with amino and isocyanate silane functionalized graphene oxide nanosheets. *Appl. Surf. Sci.* **2018,** *439*, 45-59.
11. Yuan, X.; Zhu, B.; Cai, X.; Qiao, K.; Zhao, S.; Yu, J., Influence of different surface treatments on the interfacial adhesion of graphene oxide/carbon fiber/epoxy composites. *Appl. Surf. Sci.* **2018,** *458*, 996-1005.
12. Chen, Y.; Ginga, N. J.; LePage, W. S.; Kazyak, E.; Gayle, A. J.; Wang, J.; Rodriguez, R. E.; Thouless, M. D.; Dasgupta, N. P., Enhanced Interfacial Toughness of Thermoplastic-Epoxy Interfaces Using ALD Surface Treatments. *ACS Appl Mater Interfaces* **2019,** *11* (46), 43573-43580.
13. Sensui, K.; Tarui, T.; Miyamae, T.; Sato, C., Evidence of chemical-bond formation at the interface between an epoxy polymer and an isocyanate primer. *Chem Commun (Camb)* **2019,** *55* (98), 14833-14836.
14. YUN, H. K.; CHO, K.; AN, J. H.; PARK, C. E., Adhesion improvement of copper/epoxy joints. *Journal of Materials Science* **1992,** *27*, 5811-5817.
15. Chung, C.-L.; Moon, K.-S.; Wong, C. P., Influence of Flux on Wetting Behavior of Lead-Free Solder Balls during the Infrared-Reflow Process. *J. Electron. Mat.* **2005,** *34* (7), 994-1001.
16. Smith, B. A.; Turbini, L. J., Characterizing the weak organic acids used in low solids fluxes. *J. Electron. Mat.* **1999,** *28* (11), 1299-1306.
17. Tunaboylu, B., Testing of copper pillar bumps for wafer sort. *IEEE Trans. Compon. Packag. Manuf. Technol.* **2012,** *2* (6), 985-993.
18. Zhang, J., Fatigue crack propagation behavior of underfill materials in microelectronic packaging. *Mat. Sci. Eng. A* **2001,** *314*, 194–200.

19. Baldan, A., Adhesively-bonded joints in metallic alloys, polymers and composite materials: Mechanical and environmental durability performance. *Journal of Materials Science* **2004,** *39*, 4729– 4797.
20. Pletincx, S.; Fockaert, L. L. I.; Mol, J. M. C.; Hauffman, T.; Terryn, H., Probing the formation and degradation of chemical interactions from model molecule/metal oxide to buried polymer/metal oxide interfaces. *npj Materials Degradation* **2019,** *3* (1).
21. Verdingovas, V.; Jellesen, M. S.; Ambat, R., Solder flux residues and humidity-related failures in electronics: Relative effects of weak organic acids used in no-clean flux systems. *J. Electron. Mat.* **2015,** *44* (4), 1116-1127.
22. Valley, N. A.; Blower, P. G.; Wood, S. R.; Plath, K. L.; McWilliams, L. E.; Richmond, G. L., Doubling down: delving into the details of diacid adsorption at aqueous surfaces. *J. Phys. Chem. A* **2014,** *118* (26), 4778-89.
23. Qu, G.; Vegunta, S. S. S.; Mai, K.; Weinman, C. J.; Ghosh, T.; Wu, W.; Flake, J. C., Copper oxide removal activity in nonaqueous carboxylic acid solutions. *J. Electrochem. Soc.* **2013,** *160* (4), E49-E53.
24. Cruzan, C. G.; Miley, H. A., Cuprous-cupric oxide films on copper. *J. App. Phys.* **1940,** *11* (10), 631-634.
25. Ulrich, N. W.; Andre, J. S.; Khanna, K.; Wei, Y.; Xiu, Y.; Chen, Z., Nondestructive analysis of buried interfacial behaviors of flux residue and their impact on interfacial mechanical property. *IEEE Trans. Compon. Packag. Manuf. Technol.* **2018,** *8* (6), 982-990.
26. Myers, J. N.; Zhang, X.; Xiu, Y.; Wei, Y.; Williamson, J. M.; Lee, K.-W.; Chen, Z., Nondestructive characterization of molecular structures at buried copper/epoxy interfaces and their relationship to locus of failure analysis. *IEEE Trans. Adv. Packag.* **2015,** *5* (10), 1432-1440.
27. Ofuji, M.; Inaba, K.; Omote, K.; Hoshi, H.; Takanishi, Y.; Ishikawa, K.; Takezoe, H., Grazing incidence in-plane X-ray diffraction study on oriented copper phthalocyanine thin films. *Jpn. J. Appl. Phys.* **2002,** *41* (Part 1, No. 8), 5467-5471.
28. Johan, M. R.; Suan, M. S. M.; Hawari, N. L.; Ching, H. A., Annealing effects on the properties of copper oxide thin films prepared by chemical deposition. *Int. J. Electrochem. Sci.* **2011,** *6*, 6094 - 6104.
29. Nair, M. T. S.; Guerrero, L.; Arenas, O. L.; Nair, P. K., Chemically deposited copper oxide thin films: structural, optical and electrical characteristics. *Appl. Surf. Sci.* **1999,** *150*, 143–151.
30. Ghosh, S.; Avasthi, D. K.; Shah, P.; Ganesan, V.; Gupta, A.; Sarangi, D.; Bhattacharya, R.; Assmann, W., Deposition of thin films of different oxides of copper by RF reactive sputtering and their characterization. *Vacuum* **2000,** *57*, 377-385.
31. Lu, X.; Li, B.; Zhu, P.; Xue, G.; Li, D., Illustrating consistency of different experimental approaches to probe the buried polymer/metal interface using sum frequency generation vibrational spectroscopy. *Soft Matter* **2014,** *10* (29), 5390-7.
32. Lu, X.; Xue, G.; Wang, X.; Han, J.; Han, X.; Hankett, J.; Li, D.; Chen, Z., Directly probing molecular ordering at the buried polymer/metal interface 2: Using P-polarized input beams. *Macromolecules* **2012,** *45* (15), 6087-6094.
33. Lu, X.; Li, D.; Kristalyn, C. B.; Han, J.; Shephard, N.; Rhodes, S.; Xue, G.; Chen, Z., Directly probing molecular ordering at the buried polymer/metal interface. *Macromolecules* **2009,** *42* (22), 9052-9057.

34. Lu, X.; Shephard, N.; Han, J.; Xue, G.; Chen, Z., Probing molecular structures of polymer/metal interfaces by sum frequency generation vibrational spectroscopy. *Macromolecules* **2008,** *41*, 8770-8777.
35. Ulrich, N. W.; Li, X.; Myers, J. N.; Williamson, J.; Lu, X.; Chen, Z., Distinct Molecular Structures of Edge and Middle Positions of Plasma Treated Covered Polymer Film Surfaces Relevant in the Microelectronics Industry. *IEEE Transactions on Components, Packaging and Manufacturing Technology* **2017,** *7* (8), 1377-1390.
36. Ulrich, N. W.; Andre, J.; Williamson, J.; Lee, K. W.; Chen, Z., Plasma treatment effect on polymer buried interfacial structure and property. *Phys. Chem. Chem. Phys.* **2017,** *19* (19), 12144-12155.

Chapter 3: Interfacial Reaction of a Maleic Anhydride Grafted Polyolefins with Ethylene Vinyl Alcohol Copolymer at the Buried Solid/Solid Interface

Material cover in this chapter was published in *Polymer* **2021,** *212,* 123141.

3.1. Introduction

Polymer multilayer films have a great variety of applications and are ubiquitous in daily life. Understanding the molecular structure of interfaces between different layers in such films is important in applications such as designing and producing new high performance barrier packaging.[1-11] Layers in these multilayer films serve as gas barriers, enhance optical properties, and/or provide good puncture resistance. Adhesion of one layer to another is critical to the quality and performance of a multilayer film structure, especially when the layer materials have different chemical compatibilities.[12-14] Typically, immiscible and/or incompatible materials used in multilayer film structures have poor adhesion, due to the low level of interaction between polar and non-polar polymer interfaces.[12, 14]

For example, poly(ethylene vinyl alcohol) (EVOH) which is commonly used as a barrier material in multilayer polymer structures due to its good oxygen barrier properties and high resistance to liquids and various organic solvents[3-6] is highly polar. EVOH is functionalized with

hydroxyl groups that are able to form different types of interactions with other materials in the structure such as hydrogen bonding or covalent bonding to enhance adhesion. Even so, EVOH does not typically have good adhesion to other non-polar polymers in a multilayer film, such as polyethylene. To solve this problem, tie-layers are added between layers in the film. Tie-layers have favorable adhesive interactions with various layers in the multilayer film, such as EVOH and nylon.[15-17] One type of common tie-layer is maleic anhydride (MAH) grafted polyolefins, which have the ability to react with other layers in the structure due to the highly labile anhydride five-membered ring.[14-21] However, reactions occurring between the tie-layer and other materials such as EVOH have not been directly observed at the buried interface, especially at the polymer/polymer buried interface, leading to incomplete knowledge of the mechanism of grafted MAH adhering to EVOH in multilayer films. Enhanced interfacial properties of multilayer polymer structures provide highly desirable applications in multilayer packaging films, flexible organic electronic devices (transistors, LEDs, photovoltaics, etc.) as encapsulants[22], and lithium ion batteries.[23] A fundamental understanding of the molecular basis of adhesion between polymer layers may also provide more knowledge on future interfacial separation for recycling mixed material plastics.[24-25]

In the past we reported the molecular structure of a polyolefin at both nylon and silica interfaces.[14] Here, SFG was applied to examine buried polymer/polymer interfaces to elucidate the interfacial reaction between MAH grafted polymers and EVOH.

3.2 Materials and methods

3.2.1 Materials and sample preparation.

CaF_2 right angle prisms (Altos Photonics, Bozeman MT) were used as substrates for depositing ethylene vinyl alcohol copolymer (EVOH) thin films for SFG studies. Microscope glass

slides (Fisher Scientific, Hampton NH) were used as substrates for depositing EVOH films for adhesion testing. All substrates (prisms and slides) were cleaned prior to sample preparation. First, they were immersed in toluene for 12 hours, followed by rinsing with toluene, ethanol, and ultrapure water (18.2 MΩ cm) three times. The substrates were then dried with nitrogen gas and finally treated with oxygen plasma (PE-50, Plasma Etch Inc., Carson City NV) for three minutes prior to deposition of polymer thin films. The plasma chamber was pumped down to 200 mTorr and the voltage used for the plasma discharge was 20 kV.

The molecular formulas of the two linear low-density ethylene octene co-polymers (LLDPE) studied, provided by the Dow Chemical Company, are shown in **Figure 3.1**. One LLDPE (EO) is a random co-polymer of ethylene and octene (EO); the other EO has the same type of structure but is grafted with 1.1 wt% maleic anhydride (MAH) (MAHgEO). Both EO and MAHgEO polymers were provided in pellet form, having a density of 0.87 g/cm^3. The molecular formula of EVOH is also shown in **Figure 3.1**. The EVOH used in this study was also provided by the Dow Chemical Company in pellet form. EVOH contains ~38 mol% ethylene and has a density of 1.17 g/cm^3.

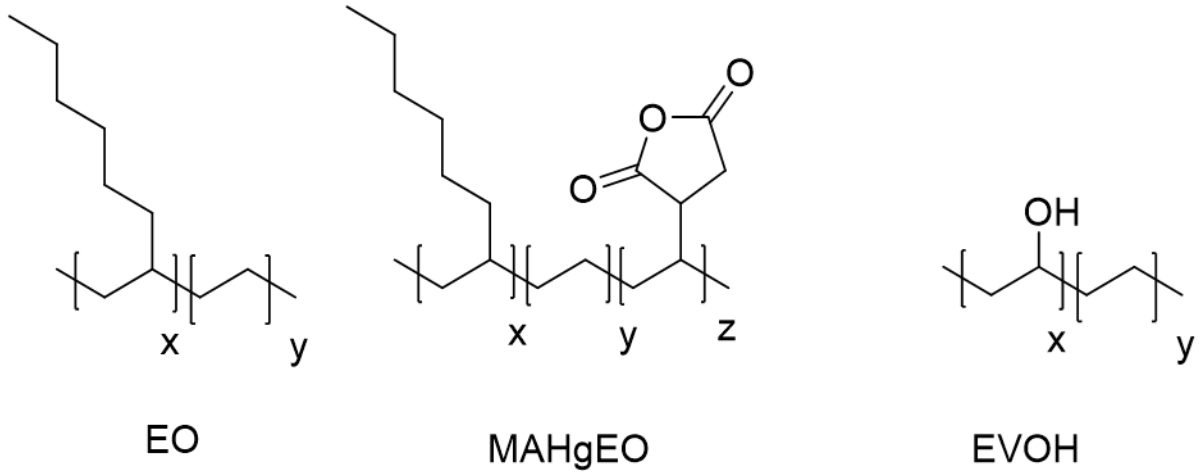

Figure 3.1 Structures of polymers used in this study: EO is a co-polymer of ethylene and octene, MAHgEO is the same co-polymer of ethylene and octene with MAH groups grafted to the

polyethylene backbone. EOVH is an ethylene vinyl alcohol copolymer. The molar ratios of the polymer units are designated as x, y and z units.

EVOH thin films were prepared on substrates by first drying EVOH pellets under vacuum with nitrogen purge at 160 °C for 30 minutes. Once EVOH pellets were dry, 1% (wt/wt) solutions in m-cresol (≥ 98% Food Grade, MilliporeSigma, Burlington MA) were prepared. EVOH was fully dissolved by heating the sealed sample solution on a hot plate at 90 °C for over an hour. The EVOH solution was then spin-cast onto CaF_2 prisms at 2500 rpm for 30 seconds to form thin films using a spin coater (VTC-100, MTI Industries, Richmond CA). The samples were allowed to degas the solvent for 4 hours then annealed at 175 °C for 5 minutes in air prior to the SFG experiments. For SFG studies, buried interfaces of EVOH/EO and EVOH/MAHgEO were prepared by contacting melted EO (or MAHgEO) with EVOH thin films deposited on CaF_2 prisms (sample geometries are shown in **Figure 3.2**). First, EO (or MAHgEO) pellets were dried in a vacuum oven under nitrogen at 160 °C for 30 minutes and heated to ~175 °C on a hotplate for 10 minutes to soften the materials. Once melted, the EVOH films were pressed tightly against the melted EO (or MAHgEO) samples for 1 minute at ~175 °C. Samples were then removed from the hot plate and annealed at 175 °C for 5 minutes in a convection oven under atmospheric conditions. The EVOH/EO and EVOH/MAHgEO samples were then ready for SFG analysis. The melted EO or MAHgEO portion of the prepared sample was thick enough to prevent IR beam from penetrating to the EO/air or MAHgEO/air interfaces.

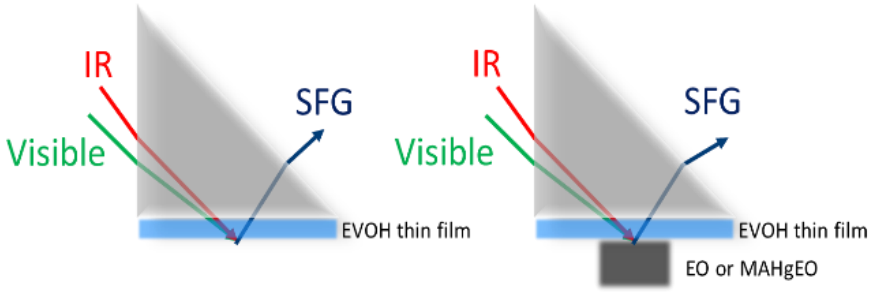

Figure 3.2 SFG sample geometry used for studying EVOH film surface in air (left) and the buried EVOH film interface with EO and MAHgEO polymers (right). The red line represents the IR beam, the green line represents the visible beam, and the blue line represents the resulting SFG beam generated at the surface or interface.

3.2.2 Experimental methods

For thin EVOH films studied for adhesion testing experiments, the films were deposited on microscope glass slides (instead of CaF_2 prisms) using the similar method presented above for preparing samples for SFG studies. Lap shear adhesion testing (Instron 5544, Norwood MA) was done at room temperature, following the ASTM D3163 standard method, to correlate the SFG results from the buried interface to the adhesion of EO and MAHgEO with EVOH. **Figure 3.3** shows the lap shear sample geometry used to study adhesion between EVOH and LLDPEs. At least 10 replicates of each EVOH/EO or EVOH/MAHgEO interface were tested for adhesive failure. EO and MAHgEO adhesion test samples were about 0.25 cm thick and the overlap area of the substrates was about 3.8 cm^2, measured with a ruler. The pull rate of the lap shear test was 1.27 mm/min.

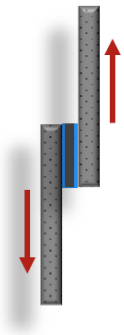

Figure 3.3 Lap shear experiment sample geometry. Light grey is the microscope slide substrate, blue represents the EVOH film, and dark grey represents EO and MAHgEO polymer melts.

3.3 Results and discussion

3.3.1 SFG results: O-H stretching frequency region

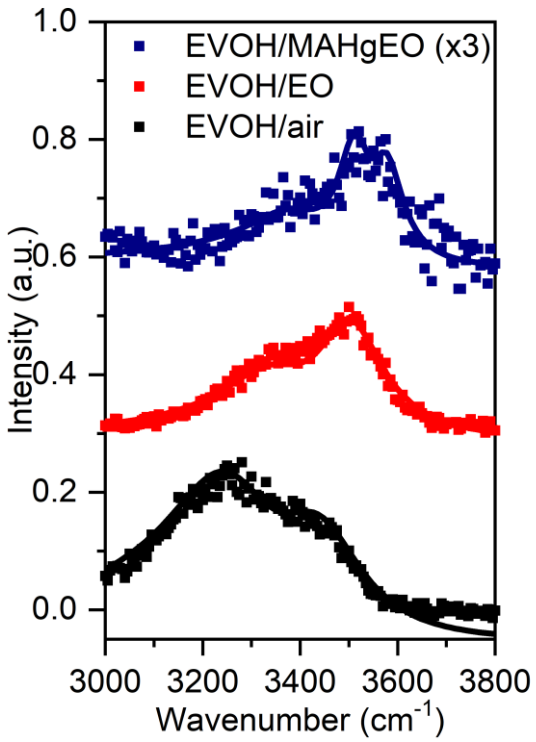

Figure 3.4 SFG spectra of EVOH/air and EVOH/EO, EVOH/MAHgEO buried interfaces. Spectra are offset for clarity. The intensity of the SFG spectrum from the EVOH/MAHgEO interface was multiplied by a factor of three.

The SFG spectrum in the O-H stretching frequency region collected from the EVOH surface in air (EVOH/air) is displayed as the black curve in **Figure 3.4**. The EVOH/air SFG hydroxyl stretching signals contain two prominent peaks, a dominant peak at 3265 cm^{-1} with a shoulder at 3440 cm^{-1}, arising from hydroxyl groups present on the EVOH surface. FTIR spectrum of bulk EVOH show two -OH stretching bands in the range of 3000-3800 cm^{-1}, contributed from the amorphous (weakly hydrogen bonded) and ordered (strongly hydrogen bonded) phases of EVOH.[26] Here we assign the O-H stretching signals detected at 3256 cm^{-1} and 3440 cm^{-1} to contributions from the EVOH strongly and weakly hydrogen bonded surface hydroxyl groups, respectively. It is possible that the two peaks observed for the EVOH/air SFG spectrum could also contain contributions from hydrogen bonding interactions between the EVOH film and a layer of adsorbed water on the surface that is ordered.

SFG ssp spectrum was also collected from the buried EVOH/EO interface, shown as the red curve in **Figure 3.4**. The O-H stretching signal is still present at the EVOH/EO interface, however the band positions and relative intensities are shifted compared to those at the EVOH/air interface. This shift to higher frequencies may be attributed to a more hydrophobic environment at the EVOH/EO buried interface versus the EVOH/air interface, resulting in weaker hydrogen bonding between the EVOH hydroxyl groups. At the high processing temperature (>160 °C) for preparing the buried interfaces, adsorbed water should not be present at the EVOH/EO interface.[27] It is likely that the 3350 cm^{-1} peak is due to O-H stretching from strongly hydrogen bonded region of the EVOH film and the strong peak at 3500 cm^{-1} can be assigned to O-H stretching in more weakly hydrogen bonded region of the EVOH film at the buried polymer/polymer interface.[26] The existence of the -OH stretching bands in the SFG spectra shows that EVOH hydroxyl groups can be ordered at the EVOH/EO interface.

We collected SFG ssp spectrum from the buried interface between EVOH and MAHgEO, which is shown as the blue curve in **Figure 3.4**. It is expected that at the EVOH/MAHgEO interface, grafted MAH groups can react or form strong hydrogen bonds with the hydroxyl groups on EVOH. When covalent bonds are formed, the interfacial EVOH hydroxyl groups will be consumed by the reaction. Therefore, weaker SFG O-H stretching signals from EVOH were expected to be detected from the EVOH/MAHgEO interface than the EVOH/EO interface. In the EVOH/MAHgEO spectrum the 3350 cm^{-1} and 3500 cm^{-1} peaks diminished in intensity compared to the EVOH/EO interface, presumably due to the interfacial reactions between EVOH hydroxyl groups and MAH groups on MAHgEO. There were still weak signals from the hydroxyl groups at 3350 cm^{-1} and 3500 cm^{-1}, which may be due to residual unreacted EVOH hydroxyl groups at the buried interface. There was another peak at 3575 cm^{-1} that could be assigned to the carboxylic acid formed in the reaction of EOVH with MAHgEO or from hydrolyzed MAH as maleic acid hydroxyl groups ordered at the interface.

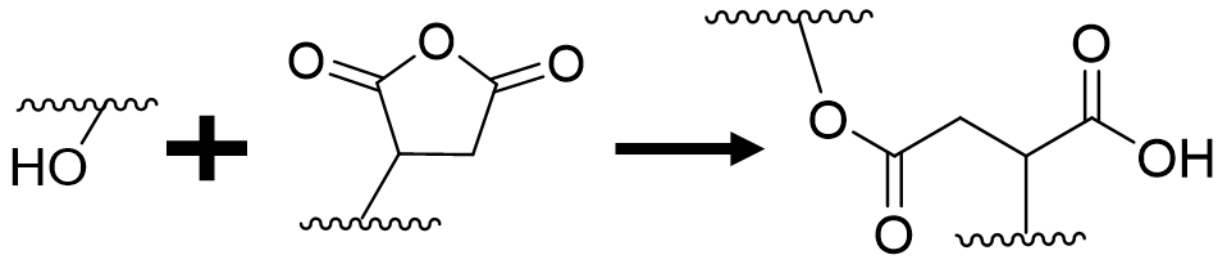

Figure 3.5. Proposed reaction of EVOH hydroxyl group and grafted MAH ethylene-octene co-polymer.

Figure 3.5 shows the proposed reaction between EVOH hydroxyl groups and MAH. The resulting product moieties at the interface would be a carboxylic acid and ester covalent linkages between layers. The reaction of hydroxyl groups with MAH is a well-studied esterification reaction.[15, 28-30] Carboxylic hydroxyl groups from this reaction could be present in the O-H

stretching region of the SFG spectra as well and contribute to the hydroxyl signals observed at the buried EVOH/MAHgEO interface. Carboxylic acid hydroxyl peaks have been shown to appear around 3600 cm^{-1} in a hydrogen bonding environment and the peak position can shift depending on the interfacial environment.[31] Likely the weak SFG signals at 3350 and 3500 cm^{-1} from the EVOH/MAHgEO interface were not because the EVOH hydroxyl groups are lying down or having a random orientation, otherwise weak SFG O-H stretching signal should also be detected from the similar EVOH/EO interface, which was not the case. Therefore, we conclude that a strong interfacial interaction between the MAH group and EVOH occurs, likely a chemical reaction, at the EVOH/MAHgEO interface. Such an interfacial reaction would consume many of the ordered interfacial hydroxyl groups on EVOH, leading to much weaker SFG O-H stretching signals at 3350 and 3500 cm^{-1} from the EVOH/MAHgEO interface and generated the carboxylic acid product which produces signal at 3575 cm^{-1}. [32]

It is worth mentioning that we believe that the CaF_2 substrate/EVOH interface generates minimal O-H SFG signal since the O-H signals are very different at the EVOH/EO and EVOH/MAHgEO interfaces. If the SFG O-H signals were from the CaF_2 substrate/EVOH interface, because no SFG signals could be generated from EO or MAHgEO, the O-H signals from the above two samples should be similar for each case, which is not true. This leads us to believe that the O-H signal was from the polymer/polymer interface.

To summarize the SFG findings for the EVOH/air, EVOH/EO, and EVOH/MAHgEO interfaces, two peaks were observed related to the hydroxyl groups in the EVOH copolymer that are present at the surface or buried interface. For the EVOH/air case, these two peaks were observed at 3256 cm^{-1} and 3440 cm^{-1} and are believed to arise from strongly and weakly hydrogen bonded EVOH hydroxyl groups, respectively. At the buried polymer/polymer interfaces these

peaks are shifted to higher frequencies (3350 cm^{-1} and 3500 cm^{-1}) due to increased hydrophobic interactions. At the EVOH/EO buried interface, there is no MAH present, thus the hydroxyl groups do not react and are ordered at the buried interface, resulting in larger SFG signals. For the EVOH/MAHgEO interface, the EVOH hydroxyl signals were much weaker suggesting the groups have reacted with MAH, producing a product carboxylic acid O-H peak. To further support these results, the SFG signals detected in the carbonyl (C=O) stretching frequency region of each buried interface (EVOH/EO and EVOH/MAHgEO) were also examined.

3.3.2 SFG results: C=O stretching frequency region.

To further characterize the interfacial molecular structures between EVOH and EO as well as MAHgEO, we collected SFG spectra from the buried EVOH/EO interface and EVOH/MAHgEO interface in the carbonyl stretching spectral region (1550-1950 cm^{-1}), as shown in **Figure 3.6**. No discernible SFG signal was detected from the EVOH/EO interface in the C=O stretching frequency region (red line in **Figure 3.6**). This is expected because neither EVOH nor EO contains carbonyl groups.

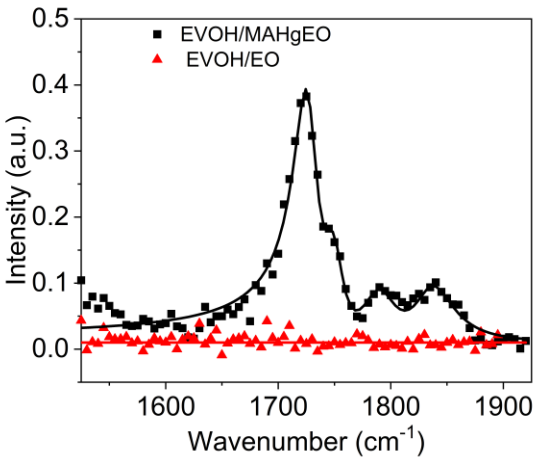

Figure 3.6 SFG spectra (ssp) for the buried EVOH/EO interface (red line). No SFG signal was detected from the EVOH/EO buried interface. Carbonyl signal from the reaction products of EVOH and MAH groups were observed in the SFG spectra of EVOH and MAHgEO (black line).

SFG spectrum collected from the EVOH/MAHgEO interface showed strong C=O stretching signals, displayed in **Figure 3.6** as the black line, which was much different than the EVOH/EO buried interface. The bands were assigned to the MAH-related carboxylic acid and ester moieties that form due to the reaction of EVOH with MAHgEO (shown in **Figure 3.6**). The peak at 1725 cm^{-1} was assigned to the carboxylic acid groups at the buried interface from hydrolyzed MAH groups or formed during the EVOH/MAHgEO interfacial reaction. This peak was also observed in our recent SFG studies on nylon/MAHgEO interface.[67,68] A small peak at ~1750 cm^{-1}, on the shoulder of the large peak centered around ~1725 cm^{-1} can be attributed to the formation of ester carbonyl groups at the buried interface.[33] The different SFG spectral intensities of these two peaks are caused by the different average orientations of the interfacial carboxylic acid and ester carbonyl groups, and different amounts of these functional groups at the interface. Two smaller peaks around 1790 cm^{-1} and 1835 cm^{-1} were also observed in the SFG spectrum and can be attributed to the unreacted MAH groups at the buried EVOH/MAHgEO interface. These results are consistent with the esterification of MAH by hydroxyl functionalities and support the conclusion that an interfacial reaction occurred at the buried EVOH/MAHgEO interface. Although the results suggest an interfacial reaction, the reaction does not appear to be complete since there are MAH groups from MAHgEO observed in the carbonyl stretching SFG spectra frequency region (**Figure 3.6**). The results obtained from the SFG studies in the C=O stretching frequency region are consistent with the SFG results obtained in the O-H stretching frequency region presented above.

It is also worth mentioning that for SFG C=O signals, no C=O signals could be generated from the CaF_2 substrate/EVOH interface because EVOH does not have C=O modes. The C=O

signals could not be generated from the EO/air or MAHgEO/air interfaces because both EO and MAHgEO samples are very thick and the air sides are not flat. Therefore, the C=O signals (if any) should be generated from the buried polymer/polymer interface.

In summary, the molecular structures of the interfaces between EVOH and two LLDPE polymers (EO and MAHgEO) observed are consistent with an interfacial reaction between EVOH and MAHgEO layers. The difference between the EO and MAHgEO polymers is that MAHgEO has grafted reactive MAH groups, while EO does not. EVOH has hydroxyl groups which can react with MAH groups forming a carboxylic acid moiety and an ester linkage. At the EVOH/MAHgEO interface, hydroxyl groups of EVOH can react with the grafted MAH groups on MAHgEO to form covalent ester bonds. Because interfacial covalent bonds can form at the EVOH/MAHgEO interface, this interface should have stronger adhesion than an interface lacking these types of interactions. In contrast, no covalent bonding can occur between EVOH and EO at the EVOH/EO interface because of the absence of grafted MAH groups and other reactive functional groups on EO, and the adhesion between the polymers should be weaker. These results show that SFG is a powerful technique to probe buried interfacial reactions occurring at solid/solid interfaces that are directly related to a material's performance.

3.3.3 Adhesion results.

Our SFG results presented above clearly demonstrated the significant difference of the interfacial interactions between the EVOH/EO and EVOH/MAHgEO interfaces. Such interfacial interaction differences should lead to substantially different interfacial properties. In order to correlate interfacial structure to the adhesion performance, lap shear adhesion testing was performed on the EVOH/EO and EVOH/MAHgEO interfaces. **Figure 3.7** shows that the adhesion strengths measured from the EVOH/EO and EVOH/MAHgEO interfaces were very different. The

adhesion strength of EVOH to MAHgEO was much higher than EVOH to EO. This result is due to the interfacial reaction, chemical bonds were formed, leading to much stronger adhesion. Only non-covalent interactions are expected to occur at the EVOH/EO interface, resulting in a much weaker interface. The adhesion test results also further provide evidence for confirming the occurrence of the interfacial reaction between EVOH and MAHgEO at the buried interface.

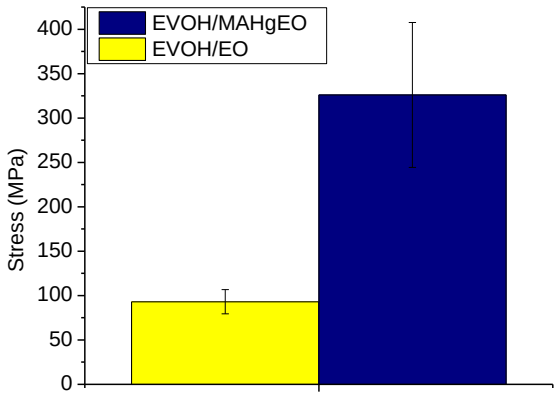

Figure 3.7 Lap shear adhesion data from interfaces between EVOH and EO or MAHgEO. Addition of MAH increases the adhesion strength of MAHgEO to EVOH substantially.

3.4 Conclusions

Different molecular structures at the buried interfaces between EVOH and two LLDPE materials were observed in situ using SFG. At the EVOH/MAHgEO interface, spectral changes in both the -OH and C=O stretching regions were observed that are consistent with interfacial chemical interactions between EVOH hydroxyl groups and MAH groups. In the O-H stretching frequency region, EVOH hydroxyl signal was found on the EVOH surface in air and at the EVOH/EO buried interface, but largely disappeared at the EVOH/MAHgEO buried interface. At the buried EVOH/MAHgEO interface a new peak corresponding to carboxylic acid appeared in the O-H stretching region. In the C=O stretching region, at the EVOH/MAHgEO buried interface,

SFG signals from ester reaction products were observed, along with weak signals contributed from unreacted MAH groups. However, at the EVOH/EO interface, no evidence of covalent bond formation was observed. SFG signal from the EVOH hydroxyl groups was observed from this interface, and no carbonyl signal was detected, because this system does not contain C=O functionality. To further support the spectroscopic evidence for strong interfacial interactions between EVOH and MAHgEO, adhesion strength between EVOH and MAHgEO was measured, which is much greater than that measured between EVOH and EO.

This study shows that the physical interaction dominates the EVOH/EO (a chemically inert polymer) interface while the EVOH/MAHgEO interface has a chemical interaction (based on added MAH functionality to the system) and also possibly a physical interaction (if MAH does not cover the interface entirely). Here we cannot separate the difference between the physical and chemical interactions at the EVOH/MAHgEO interface. According to the adhesion measurements, the adhesion strength induced by the chemical interaction is about two (if the physical interaction is similar at the two interfaces) or three (if the EVOH/MAHgEO interface only has chemical interaction) times larger than that induced by the physical interaction. To understand interfacial interactions more quantitatively, it is necessary to study MAHgEO with various MAH grafting levels in the future.

This result is an important step to uncovering the details of interfacial polymer/polymer reactions significant to a variety of polymer applications that require good adhesion between film materials. SFG provides a direct way to probe molecular structures at buried interfaces in situ, with the ability to probe both the reactants and products at the buried interface of solid materials nondestructively. Further work to understand the temperature dependence and time dependence of

this interfacial reaction would be of great interest to industrial applications involving similar polymer interfaces as well.

3.5 References

1. Villalpando-Olmos, J.; Sanchez-Valdes, S.; Yanez-Flores, I. G., Performance of polyethyIene/ethyIene-vinyI alcohol copolymer/polyethylene multilayer films using maleated polyethylene blends. *Polymer Engineering and Science* **1999,** *39* (9), 1597-1603.
2. Ge, C.; Lei, K.; Aldi, R., Barrier, mechanical, and thermal properties of the three-layered co-extruded blown polyethylene/ethylene–vinyl alcohol/low density polyethylene film without tie layers. *Journal of Thermoplastic Composite Materials* **2015,** *30* (6), 794-807.
3. Maes, C.; Luyten, W.; Herremans, G.; Peeters, R.; Carleer, R.; Buntinx, M., Recent Updates on the Barrier Properties of Ethylene Vinyl Alcohol Copolymer (EVOH): A Review. *Polymer Reviews* **2018,** *58* (2), 209-246.
4. McWatters, R. S.; Rowe, R. K., Barrier permeation properties of EVOH thin-film membranes under aqueous and non-aqueous conditions. *Geotextiles and Geomembranes* **2018,** *46* (4), 529-541.
5. Mokwena, K. K.; Tang, J., Ethylene vinyl alcohol: a review of barrier properties for packaging shelf stable foods. *Crit Rev Food Sci Nutr* **2012,** *52* (7), 640-50.
6. Rahnama, M.; Oromiehie, A.; Ahmadi, S.; Ghasemi, I., Oxygen-barrier films based on low-density polyethylene/ ethylene vinyl alcohol/ polyethylene-grafted maleic anhydride compatibilizer. *Polyolefins Journal* **2017,** *4* (1), 137-147.
7. Salehiyan, R.; Bandyopadhyay, J.; Ray, S. S., Mechanism of Thermal Degradation-Induced Gel Formation in Polyamide 6/Ethylene Vinyl Alcohol Blend Nanocomposites Studied by Time-Resolved Rheology and Hyphenated Thermogravimetric Analyzer Fourier Transform Infrared Spectroscopy Mass Spectroscopy: Synergistic Role of Nanoparticles and Maleic-anhydride-Grafted Polypropylene. *ACS Omega* **2019,** *4* (5), 9569-9582.
8. Feng, J.; Li, Z.; Olah, A.; Baer, E., High oxygen barrier multilayer EVOH/LDPE film/foam. *Journal of Applied Polymer Science* **2018,** *135* (26).
9. Su, H.; Xue, J.; Cai, P.; Li, J.; Guo, S., Structure and oxygen-barrier properties of (linear low-density polyethylene/ethylene-vinyl alcohol copolymer)/linear low-density polyethylene composite films prepared by microlayer coextrusion. *Journal of Applied Polymer Science* **2015,** *132* (27), n/a-n/a.
10. Beuguel, Q.; Guinault, A.; Léger, L.; Restagno, F.; Sollogoub, C.; Miquelard-Garnier, G., Nanorheology with a Conventional Rheometer: Probing the Interfacial Properties in Compatibilized Multinanolayer Polymer Films. *ACS Macro Letters* **2019,** *8* (10), 1309-1315.
11. Ge, C.; Fortuna, C.; Lei, K.; Lu, L.-X., Neat EVOH and EVOH/LDPE blend centered three-layer co-extruded blown film without tie layers. *Food Packaging and Shelf Life* **2016,** *8*, 33-40.
12. Gong, L.; Xiang, L.; Zhang, J.; Chen, J.; Zeng, H., Fundamentals and Advances in the Adhesion of Polymer Surfaces and Thin Films. *Langmuir* **2019,** *35* (48), 15914-15936.
13. Kim, S.; Lee, J.; Kim, H.; Seo, Y. P.; Hong, S. M.; Takahara, A.; Choi, H. J.; Seo, Y., Enhanced interfacial adhesion between an amorphous polymer (polystyrene) and a

semicrystalline polymer [a polyamide (nylon 6)]. *ACS Appl Mater Interfaces* **2011,** *3* (7), 2622-9.
14. Xiao, M.; Mohler, C.; Tucker, C.; Walther, B.; Lu, X.; Chen, Z., Structures and adhesion properties at polyethylene/silica and polyethylene/nylon interfaces. *Langmuir* **2018,** *34* (21), 6194-6204.
15. Aoyagi, J.; Shinohara, I., Esterification of styrene-maleic anhydride copolymer by mixed alcohols. *Journal of Applied Polymer Science* **1972,** *16* (449-460).
16. Jantanasakulwong, K.; Leksawasdi, N.; Seesuriyachan, P.; Wongsuriyasak, S.; Techapun, C.; Ougizawa, T., Reactive blending of thermoplastic starch and polyethylene-graft-maleic anhydride with chitosan as compatibilizer. *Carbohydr Polym* **2016,** *153*, 89-95.
17. Rahnama, M.; Oromiehie, A.; Ahmadi, S.; Ghasemi, I., Investigation of polyethylene-grafted-maleic anhydride presence as a compatibilizer on various properties of nanocomposite films based on polyethylene/ethylene vinyl alcohol/ nanoclay. *Polymers for Advanced Technologies* **2017,** *28* (4), 449-462.
18. Chen, Y.; Wilson, J. A.; Petersen, S. R.; Luong, D.; Sallam, S.; Mao, J.; Wesdemiotis, C.; Becker, M. L., Ring-opening copolymerization of maleic anhydride with functionalepoxides: poly(propylene fumarate) analogues capable of post-polymerization modification. *Angew Chem. Int. Ed. Engl.* **2018,** *57* (39), 12759-12764.
19. Manakhov, A.; Michlíček, M.; Nečas, D.; Polčák, J.; Makhneva, E.; Eliáš, M.; Zajíčková, L., Carboxyl-rich coatings deposited by atmospheric plasma co-polymerization of maleic anhydride and acetylene. *Surface and Coatings Technology* **2016,** *295*, 37-45.
20. Sclavonsa, M.; Franquineta, P.; Carliera, V.; Verfailliea, G.; Fallaisa, I.; Legrasa, R.; Laurentb, M.; Thyrionb, F. C., Quantification of the maleic anhydride grafted onto polypropylene by chemical and viscosimetric titrations, and FTIR spectroscopy. *Polymer* **1999,** *41*, 1989–1999.
21. Severinia, F.; Pegoraroa, M.; Yuana, L.; Riccab, G.; Fanti, N., Free radical grafting of maleic anhydride in vapour phase on polypropylene film. *Polymer* **1999,** *40*, 7059–7064.
22. Sun, M.; Zhu, S.; Zhang, C.; Olah, A.; Baer, E.; Schiraldi, D. A., HDPE/EVOH Multilayered, High Barrier Films for Flexible Organic Photovoltaic Device Packaging. *ACS Applied Polymer Materials* **2019,** *1* (2), 259-266.
23. Ye, C.; Yu, Q.; He, T.; Shen, J.; Li, Y.; Li, J., Physical and Rheological Properties of Maleic Anhydride-Incorporated PVDF: Does MAH Act as a Physical Crosslinking Point for PVDF Molecular Chains? *ACS Omega* **2019,** *4* (29), 21540–21547.
24. Birch, N. P.; Liu, K.; Mun, S. C.; Ghazaryan, G.; Senger, C. T.; Ellison, C. J.; Macosko, C. W.; Peterson, T. H.; Mukhopadhyay, S.; Thurber, C. M., Accelerating the Coupling of Maleated Polyolefins with Polyesters via Tin Compounds. *Macromolecules* **2019,** *52* (21), 8359-8366.
25. Kaiser, K.; Schmid, M.; Schlummer, M., Recycling of Polymer-Based Multilayer Packaging: A Review. *Recycling* **2017,** *3* (1).
26. Foldes, E.; Pukanszky, B., Miscibility-structure-property correlation in blends of ethylene vinyl alcohol copolymer and polyamide 6/66. *J Colloid Interface Sci* **2005,** *283* (1), 79-86.
27. Aucejo, S.; Marco, C.; Gavara, R., Water Effect on the Morphology of EVOH Copolymers. *Journal of Applied Polymer Science* **1999,** *74*, 1201-1206.
28. Bhagiyalakshmi, M.; Shanmugapriya, K.; Palanichamy, M.; Arabindoo, B.; Murugesan, V., Esterification of maleic anhydride with methanol over solid acid catalysts: a novel route for the production of heteroesters. *Applied Catalysis A: General* **2004,** *267* (1-2), 77-86.

29. Kulawska, M.; Sadlowski, J. Z.; Skrzypek, J., Kinetics of the esterification of maleic anhhydride with octyl, decyl or dodecyl alcohol over Dowex catalyst. *React. Kinet. Catal. Lett.* **2005,** *85* (1), 51-56.
30. Siegel, E. F.; Moran, M. K., The esterification rate of dibasic acid anhydrides with primary alcohols at room temperature. *J Am Chem Soc* **1947,** *69*, 1457-1459.
31. Valley, N. A.; Blower, P. G.; Wood, S. R.; Plath, K. L.; McWilliams, L. E.; Richmond, G. L., Doubling down: delving into the details of diacid adsorption at aqueous surfaces. *J. Phys. Chem. A* **2014,** *118* (26), 4778-89.
32. Dreyer, J., Hydrogen-bonded acetic acid dimers: anharmonic coupling and linear infrared spectra studied with density-functional theory. *J Chem Phys* **2005,** *122* (18), 184306
33. Edington, S. C.; Flanagan, J. C.; Baiz, C. R., An Empirical IR Frequency Map for Ester C=O Stretching Vibrations. *J Phys Chem A* **2016,** *120* (22), 3888-96.

Chapter 4: Interfacial Reaction of a Maleic Anhydride Grafted Polyolefins with Nylon at the Buried Solid/Solid Interface

Material in this chapter was published in *Analytical Chemistry* **2020,** *92* (20), 14145-14152.

4.1 Introduction

The work in this research in this chapter was completed by Bolin Li and myself. Bolin collected SFG data, we both performed data analysis and worked on the conclusions from the results together. I also aided in the determination of the activation energy, fitting data and performing the calculations. I want to acknowledge Bolin for taking the lead on much of the research in this chapter and for his assistance producing this chapter and Chapter 3.

In the previous chapter, SFG was applied to probe the interfacial chemical reactions between EVOH and MAHgEO. Besides EVOH, nylon is another widely used material for multilayered films. Films of nylon or polyamide provide critical levels of toughness required in a flexible food package that can ensure the safety of the packaged food. Similar to EVOH, the polar nature of nylon limits its adhesion to non-polar polyolefin films which are the bulk components of the multilayer film. To improve adhesion between these different film layers, “tie-layers” (which usually utilize functional polymers such as polyolefins grafted with maleic anhydride (MAH)), the

same material used to adhere to EVOH, are applied in real applications. Interfacial chemical reactions between MAH-grafted polyolefin and nylon have not been examined and the corresponding molecular adhesion mechanisms are not completely known. In this chapter, the results obtained from SFG studies on the buried nylon/MAHgEO interface will be presented. SFG research elucidated the interfacial chemical reaction mechanisms between nylon and MAHgEO, shedding light on the molecular bonding at the MAHgEO/nylon buried interface and the kinetics of bond formation in situ. SFG results on the interfacial chemical reaction can also be correlated to the adhesion properties at buried polymer interfaces.

4.2 Materials and methods

4.2.1 Materials and sample preparation

The polymers studied in the current research are shown in **Figure 4.1**. Two types of linear low-density polyethylenes (LLDPE), an ethylene-octene (EO) copolymer and an EO copolymer grafted with 1.1% maleic anhydride (MAH) by weight (MAHgEO), were studied. They are the same materials as those studied in the previous chapter. Ultramid C33 nylon-02 (copolyamide PA 6/66) was used in the study. Nylon thin films were prepared by directly spin-coating a nylon/m-cresol solution (5 mg/mL) on the CaF_2 prisms at 2000 rpm for 60 sec. We then heated the EO pellets to 165 °C and MAHgEO pellets to 185 °C, respectively, for 10 min; the partially melted pellets were then tightly pressed against the prepared nylon film on the CaF_2 prism to make the buried nylon/EO or nylon/MAHgEO interfaces. Buried CaF_2/EO interfaces were prepared in a similar fashion but without spin-coating nylon films on CaF_2 prisms. Samples of MAHgEO/nylon for adhesion testing were prepared in the same way as those used for adhesion study on MAHgEO/EVOH in the previous chapter, except that the EVOH film is replaced by a nylon film.

Here glass microscope slides were employed as substrates for making nylon thin films, instead of CaF_2 prisms for SFG studies.

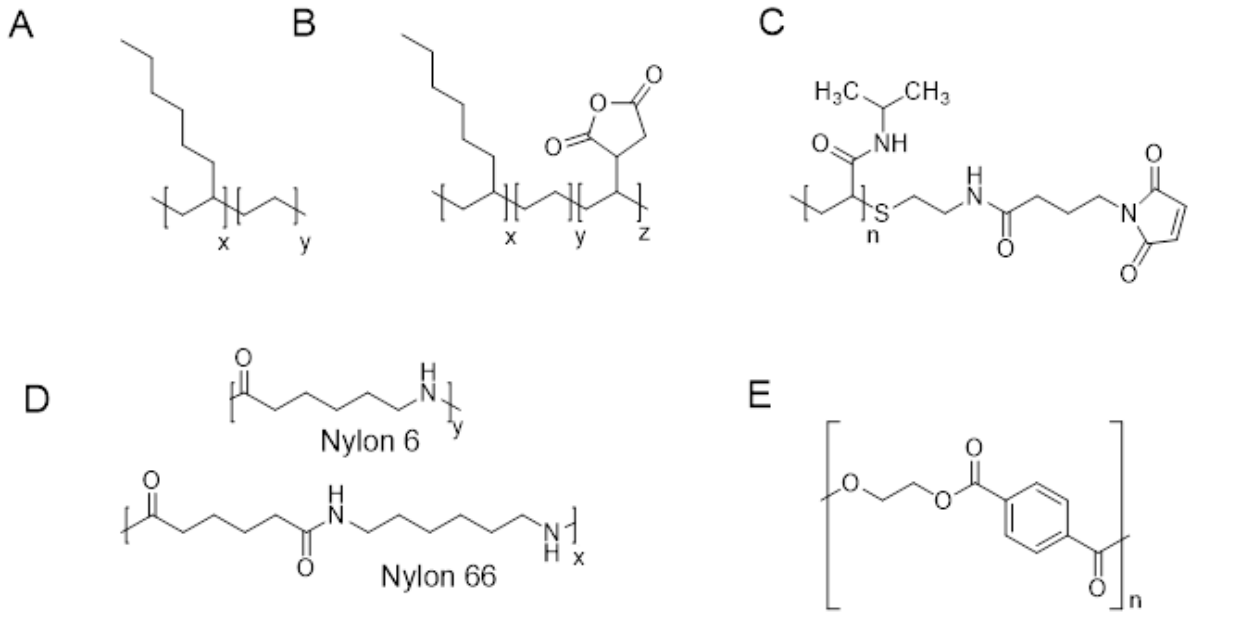

Figure 4.1. Polymers studied in this work. A: ethylene-octene (EO) copolymer; B: MAH grafted ethylene-octene (MAHgEO) copolymer; C: Maleimide-terminated Poly (N-isopropylacrylamide); D: Copolyamide PA 6/66; E: Polyethylene terephthalate (PET). The x, y, and z are the mole ratios of different monomeric units. A and B are random copolymers, same as those used in the previous chapter.

4.2.2 SFG experiment

The same SFG data collection methods as those used in the Chapter 3 were used here. SFG spectra were collected from the nylon surface and buried nylon interfaces with both ssp (s-polarized sum frequency beam, s-polarized visible beam, and p-polarized infrared beam) and ppp polarization combinations.

4.2.3 Adhesion test

The same adhesion testing method as the one introduced in Chapter 3 was used in this study. Lap shear adhesion tests were used for testing adhesiuon, which were preformed on the

Instron 5544 mechanical testing instrument at room temperature using the ASTM D3263 standard method. The EO or MAHgEO polymer was sandwiched between nylon films spin-coated on microscope glass slides instead of CaF_2 prisms. At least 10 replicates of each nylon/EO or nylon/MAHgEO interface were tested. The average adhesion strength per cm^2 with standard deviation was recorded.

4.3 Results and discussion

4.3.1 Nylon-air surface and buried nylon/MAHgEO (or EO) interface: Amine NH stretching region

SFG spectra of the nylon-air surface of spin-coated nylon films on CaF_2 prisms in the amine N-H stretching region (3100-3500 cm^{-1}) are shown in **Figure 4.2 (a)**. The strong and broad band at around 3300 cm^{-1} detected in both ppp and ssp spectra can be assigned to the N-H stretching mode of nylon.[43,44] The presence of this signal suggests that ordered N-H groups on the nylon backbone and/or ordered NH_2 polymer end groups are present at the nylon-air surface or the buried CaF_2/nylon interface. The SFG signal contribution from the nylon-air surface or the buried CaF_2/nylon interface can be varied by changing the nylon film thickness.[45] In our case, a brief (30 s) plasma treatment of the sample greatly reduced or eliminated the 3300 cm^{-1} signal, indicating that this band is due to the N-H stretching mode of the nylon-air surface and is not due to the buried CaF_2/nylon interface or the bulk of nylon film. Our previous IR study showed that the nylon film bulk was not altered by short plasma treatment,[14] therefore the great reduction of the SFG signal is not due to loss of the nylon film, further demonstrating that the original SFG signal comes from the nylon-air surface.

The buried interface between nylon and MAHgEO was also investigated in the amine N-H stretching region using SFG (**Figure 4.2 (b)**). The amine stretching signal detected from the

nylon-air surface near 3300 cm^{-1} was not detected in the SFG spectra of the buried nylon/MAHgEO interface. The absence of this band for the nylon/MAHgEO buried interface can occur for several reasons. First, the orientations of the nylon N-H or NH_2 groups at the nylon-air surface may be different from those at the buried nylon/MAHgEO interface; the NH groups may lie in the plane of the interface or could be randomly oriented at the buried nylon/MAHgEO interface, leading to the absence of SFG amine N-H stretching signals. The interfacial functional group orientation change could also be caused by physical interactions[46,47] (e.g., hydrophobic interactions, interfacial entanglements, interpenetration, adsorption, etc.) between the nylon and the MAHgEO polymer. The second possibility is that the Fresnel coefficients (the reflection and transmission factors of light when it travels through different optical media at a surface or interface) are different at the buried nylon/MAHgEO interface than the nylon-air surface, which may lead to the substantial decrease and even disappearance of the SFG signal. The third possibility is that a chemical reaction (e.g., covalent bond formation) and/or polar interactions[46] (e.g., hydrogen bonding) between nylon NH_2 and/or NH groups and the anhydride functionality occur at the buried interface.

To investigate the possibility of orientation change or Fresnel coefficients decreasing the signal at the buried nylon/MAHgEO interface, the buried interface between nylon and EO was studied as a control experiment. The SFG spectra of the buried nylon/EO interface (**Figure 4.2 (c)**) show the N-H stretching signal around 3270 cm^{-1}, slightly shifted compared to that observed for the nylon-air surface. This might be due to increased average strength of hydrogen bonds of nylon[48,49] at the buried nylon/EO interface compared to that at the nylon/air surface. This band is still very strong even though it has a slightly decreased intensity compared to the nylon-air surface. The functional group orientations and the Fresnel coefficients for nylon N-H and NH_2 groups at

the buried nylon/MAHgEO interface and the buried nylon/EO interface are expected to be similar since MAHgEO and EO should have similar optical constants and physical interactions with nylon. Therefore, interfacial functional group orientation and Fresnel coefficients are not the main reason for the absence of the nylon N-H stretching signal at the buried nylon/MAHgEO interface.

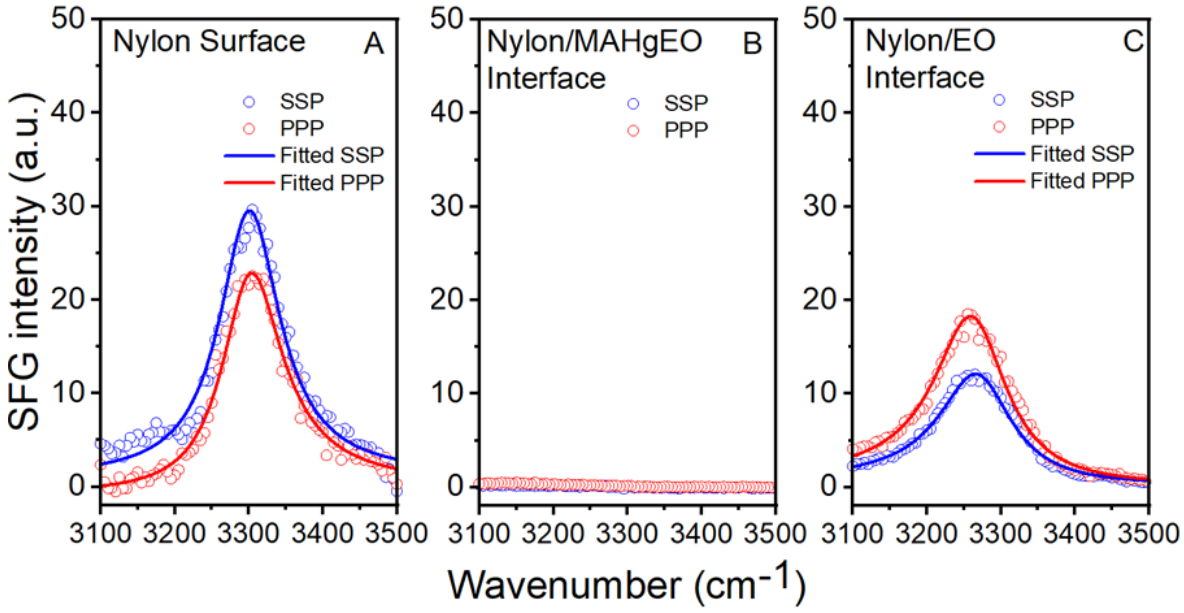

Figure 4.2 SFG ssp and ppp spectra collected in the amine N-H stretching frequency region from: (a) a nylon-air surface, (b) nylon/MAHgEO interface after reaction, and (c) nylon/EO interface. The open circles and solid lines are experimental data and fitting curves, respectively.

Nylon N-H stretching signal intensity ratios of the SFG ssp/ppp spectra are different for the nylon-air surface and the buried nylon/EO interface (see **Figures 4.2 (a) and (c)**), which indicates that nylon N-H or NH_2 groups have different orientations at the nylon-air surface and at the buried nylon/EO interface, but the presence of SFG signal in these cases means the NH groups are not lying in the plane of the interface nor are these groups randomly oriented. The nylon N-H or NH_2 groups at the buried nylon/EO interface appear to tilt more towards the interface than those at the nylon-air surface because SFG ppp spectral intensity is larger than ssp at the buried nylon/EO interface, but smaller on the nylon surface in air.[50] It is worth mentioning that the SFG signals of

water O-H stretching modes are typically centered at ~3200 cm^{-1} (strongly hydrogen bonded), ~3400 cm^{-1} (weakly hydrogen bonded), and ~3700 cm^{-1} (dangling OH), which have different peak positions from the nylon N-H stretching signal centered at ~ 3300 cm^{-1}. Certainly, we could not completely rule out the O-H signal influence on the N-H band, but we believe that the peaks we observed at ~3300 cm^{-1} should be dominated by the N-H stretching contribution.

To study whether the potential contribution of polar interactions or hydrogen bonding interactions can lead to in-plane or random orientation of the nylon N-H and NH_2 groups at the buried nylon/polymer interface, we studied the buried interface between nylon and polar polyethylene terephthalate (PET). The nylon N-H stretching signal was detected, suggesting that polar interactions[51] or hydrogen bonding[52] cannot account for the absence of the nylon N-H stretching signal at the buried nylon/MAHgEO interface. Therefore, most likely the absence of the SFG N-H stretching signal at the nylon/MAHgEO interface was due to an interfacial chemical reaction between nylon and MAHgEO at the buried interface.

Chemical reactions between NH_2 and MAH groups have been extensively reported in literature.[28, 53–58] However, there are few reports of chemical reactions between the amide N-H and MAH groups.[27,59,60] Two mechanisms were proposed previously for the chemical reactions between nylon and MAH groups.[27,59] In the first mechanism, NH_2 end groups of nylon are postulated to directly react with the MAH groups, resulting in the formation of an imide linkage. The amic acid moiety is formed as an intermediate, as shown in **Figure 4.3**.[27] When excess MAH groups are present, a second mechanism may be involved: Nylon amide groups may indirectly react with the excess MAH groups. A chemical reaction may occur when an amide group is hydrolyzed, forming a NH_2 group and a carboxylic acid.[27,59] The NH_2 group formed by hydrolysis of the amide group can react with MAH when most of the original nylon NH_2 end groups have

been consumed. The chemical reaction between a NH_2 group and a MAH group is thought to occur much faster than that between an amide and a MAH group, therefore the NH_2-MAH reaction dominates the overall reaction between nylon and MAH.[59] The reaction between NH_2 and MAH is reported to have up to 99% conversion at 180 °C in 2 min.[61] The overall reaction leads to the consumption of both the interfacial NH_2 end groups and the interfacial amide groups to form imide and carboxylic acid groups. The two reaction mechanisms which have been reported by Van Duin et al.[27] are shown in **Figure 4.4**. The feasibility of the second reaction mechanism was verified by our SFG studies on maleimide-terminated PNIPAM/MAHgEO interface.[65] We conclude that the disappearance of the nylon N-H stretching signal at the nylon/MAHgEO buried interface was due to the interfacial chemical reaction between MAH groups and the nylon end NH_2 groups as well as hydrolyzed nylon amide groups.

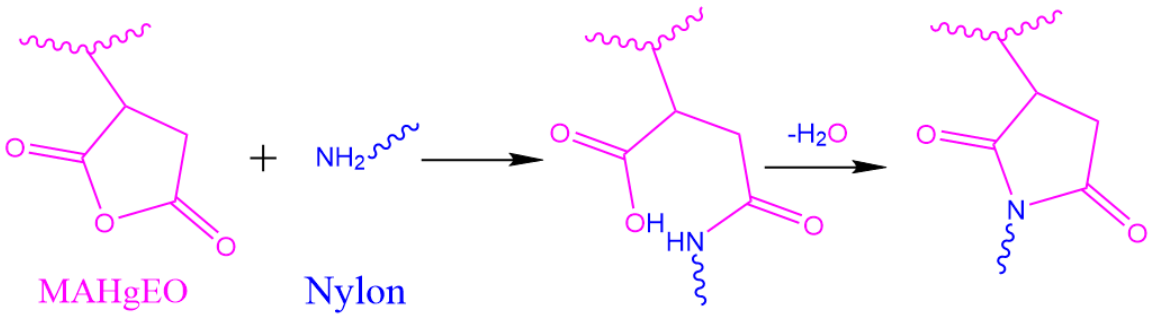

Figure 4.3 The chemical reaction between a nylon NH_2 end group and a MAH group at a buried interface.

The interfacial reaction was too rapid to experimentally observe the time-dependent process at high temperatures using our SFG system. After annealing the nylon/MAHgEO sample at a high temperature, the interfacial reaction had already occurred and no N-H stretching signal could be detected by SFG. To directly probe the buried nylon/MAHgEO interface and monitor the

interfacial reaction process in situ, the interfacial structure of the nylon/MAHgEO buried interface was determined at different temperatures.

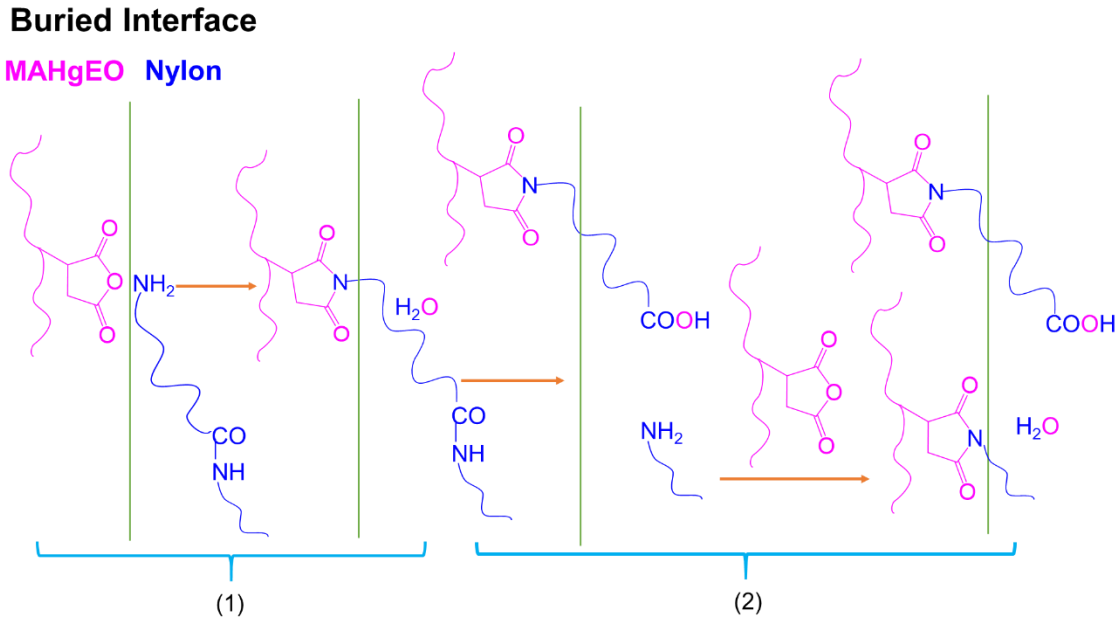

Figure 4.4 Two reaction mechanisms ((1) and (2)) at a buried nylon/MAHgEO interface that result in the formation of imide and carboxylic acid.

The nylon/MAHgEO sample was heated at various temperatures from 80 °C to 160 °C using an SFG sample stage equipped with a hotplate. SFG spectra were collected at each temperature after allowing the sample to equilibrate for 10 minutes. Temperature dependent SFG ssp spectra collected from the buried nylon/MAHgEO interface are shown in **Figure 4.5**, for the amine N-H stretching frequency region. The SFG ssp spectrum collected from the nylon-air surface before contact with the MAHgEO sample at room temperature is also displayed for comparison. The nylon N-H stretching signal at 3300 cm^{-1} decreased in intensity as the temperature increased from 90 °C to 100 °C, and then remained relatively constant between 100 °C and 120 °C, where a weak N-H stretching signal was observed. For temperatures higher than 120 °C, no N-H stretching signal was detected. This suggests that the interfacial reaction between nylon NH_2

(and amide) and MAH groups begins to occur around 90 °C and proceeds rapidly at 120 °C. The nylon NH_2 and amide groups appear to be consumed at the buried nylon/MAHgEO interface by the reaction. Again, it is worth mentioning that the disappearance of the nylon N-H signal is not caused by changes in NH_2 (or amide) group orientation since the N-H stretching signal was detected from nylon at the buried interface with ungrafted EO polymer (nylon/EO) after annealing at 175 °C for 5 min **Figure 4.2 (c)**). This is strong evidence of a direct observation of the interfacial chemical reaction between nylon and MAHgEO, done in situ at the buried interface.

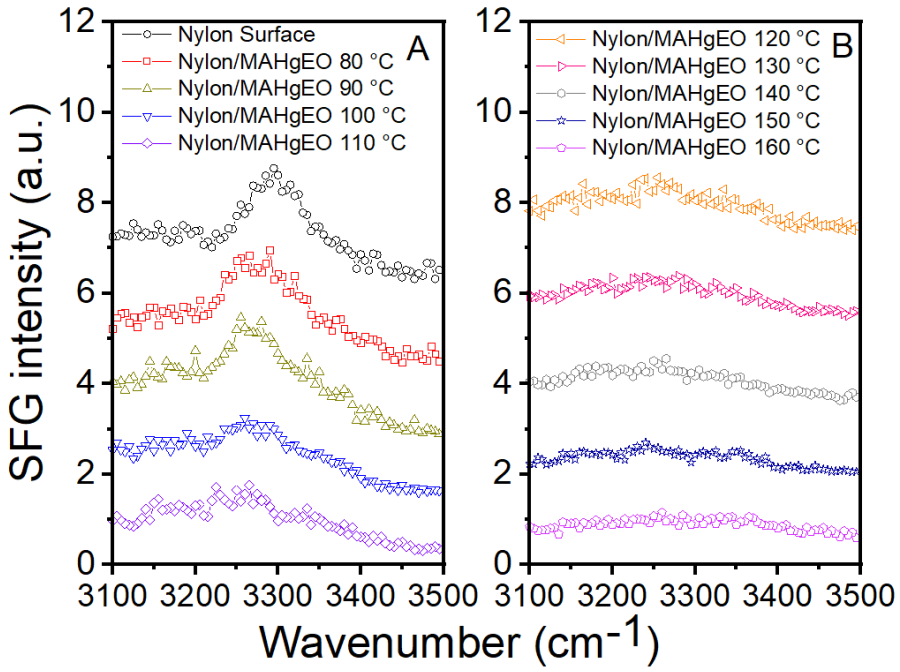

Figure 4.5 SFG ssp spectra (A and B) collected from the buried nylon/MAHgEO interface at different temperatures in the amine N-H stretching frequency region. The SFG ssp spectrum collected from the nylon-air surface is also shown as a reference. The spectra were offset for clarification.

4.3.2 Nylon-air surface and buried nylon/MAHgEO (or EO) interface: Carbonyl C=O stretching region.

The carbonyl C=O stretching region of the SFG spectra can also give information on the interfacial chemical reaction between nylon NH_2 (and amide) groups and MAH functionalities at

the buried nylon/MAHgEO interface. SFG spectra of the nylon-air surface reveal a band at 1625 cm^{-1} in the ssp spectrum and at 1640 cm^{-1} in the ppp spectrum as shown in **Figure 4.6 (a)**, which were assigned to the amide C=O stretching mode of nylon.[44,62] It is worth mentioning that the nylon C=O stretching modes can generate slightly varied peak centers (separated by ~10 cm^{-1}) in IR and Raman spectra.[63,64] SFG spectra collected using ssp and ppp polarization combinations probe different IR transition dipole and Raman polarizability components, which peak centers can be affected by those in the IR and Raman spectra. In addition, the SFG instrument used to collect spectra has a spectral resolution of ~6 cm^{-1}, further influencing the nylon C=O stretching peak centers. These factors led to the varied peak positions observed in the SFG ssp and ppp spectra. The amide C=O stretching signal detected from the nylon film on prism is primarily generated from the nylon surface in air, not the buried interface between nylon and CaF_2, because after short (30 s) plasma treatment of the nylon film surface the SFG signal from the nylon film in the carbonyl stretching frequency region disappeared, similar to that in the amine N-H stretching region.

SFG spectra were collected from the buried interface of nylon with ungrafted EO polymer (nylon/EO) (**Figure 4.6 (b)**), which showed the nylon amide C=O stretching mode at 1625 cm^{-1} in the ssp spectrum and at 1640 cm^{-1} in the ppp spectrum. As expected, no amide C=O stretching signal was detected from the buried CaF_2/EO interface, and only the nylon C=O stretching peaks dominate the spectra collected from the buried nylon/EO interface in **Figure 4.6 (b)**. These spectra were similar to those collected from the nylon-air surface. However, nylon amide C=O stretching signal intensity ratios between the ssp and ppp spectra are different at the nylon surface (**Figure 4.6 (a)**) and at the buried nylon/EO interface (**Figure 4.6 (b)**), indicating that nylon C=O groups likely have different orientations in these two cases, and supports the observation described earlier in the amine N-H stretching region. The nylon carbonyl groups seem to lie more towards the plane

of the interface at the buried nylon/EO interface than that at the nylon-air surface. Quantitative investigations of the carbonyl bond orientations at the nylon surface and at the buried Nylon/EO interface have been reported elsewhere[65] using the existing methodology for data analysis.[66]

The SFG signals detected from the buried interface between nylon and MAHgEO (**Figure 4.6 (c)**) reveal a new band at 1725 cm^{-1}, which is assigned to imide groups and carboxylic acid present in the interfacial reaction product from MAH as shown in scheme 3.[67–69] The nylon C=O stretching signal at 1640 cm^{-1} was practically absent in the ssp spectrum and dramatically decreased in the ppp spectrum because some nylon amide groups participate in the interfacial reaction and the remaining nylon C=O groups change their interfacial orientations. This provides further confirmation that the nylon amide groups at the interface indeed indirectly react with MAH groups, following the second hydrolysis reaction mechanism mentioned above. However, weak SFG ppp signal at 1640 cm^{-1} was observed, indicating the amide groups were not totally consumed by MAH at the interface. The amine N-H stretching signals completely disappeared after reaction at the nylon/MAHgEO interface (**Figures 4.2 (b)** and **Figure 4.5**), which suggests that the remaining amide N-H groups (if any) probably lie in the plane of the buried interface or are randomly oriented, based on SFG theory,[28,70,71] leading to no detectable signal. Spectra collected from the nylon/EO interface are quite different in the carbonyl C=O stretching region than those from the buried nylon/MAHgEO interface (**Figure 4.6 (b) and (c)**). The chemical reaction occurring at the buried nylon/MAHgEO interface does not occur at the nylon/EO interface due to lack of MAH groups. The disappearance or substantial decrease of the nylon amide signal is due to consumption of amide groups during the interfacial chemical reaction by the hydrolysis mechanism as mentioned above. The increase in intensity of the band at 1725 cm^{-1} is a result of interfacial reaction products (carboxylic acid and imide groups) containing carbonyl moieties.

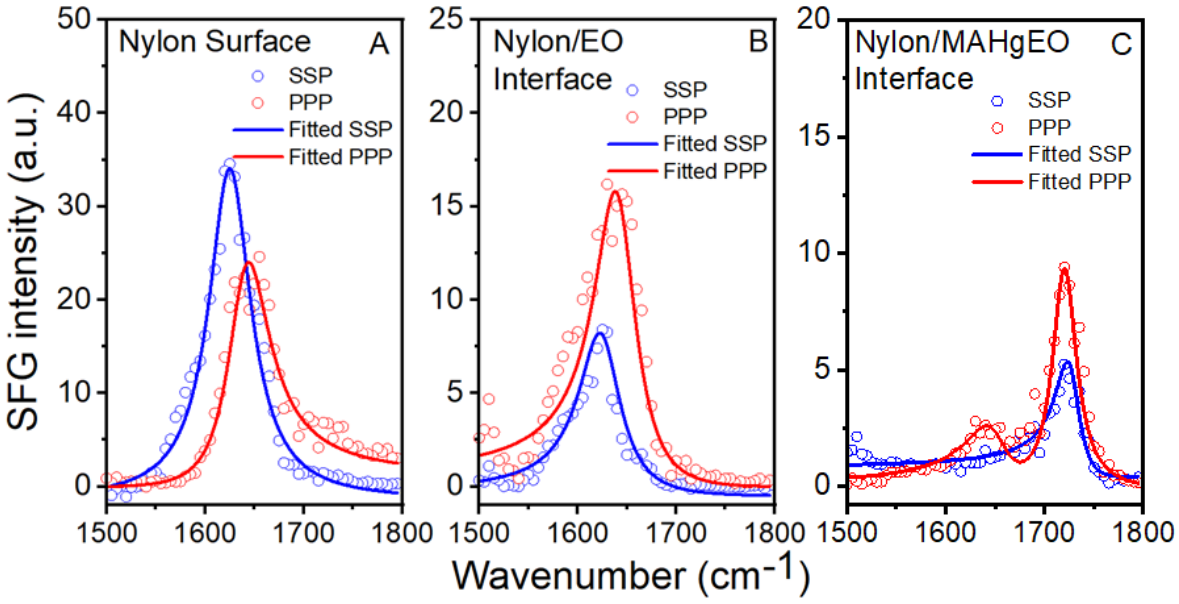

Figure 4.6 SFG ssp and ppp spectra collected in the carbonyl C=O stretching frequency region from (a) nylon-air surface, (b) buried nylon/EO interface, and (c) buried nylon/MAHgEO interface. The open circles and solid lines are experimental data and fitting curves, respectively.

Figure 4.6 (c) captures the final interfacial structure after the interfacial chemical reaction. To obtain a more detailed understanding of the interfacial chemical reaction and to complement the temperature-dependent changes in the amine N-H stretching frequency region, the spectra of buried nylon/MAHgEO interface were collected at different temperatures in the carbonyl stretching frequency region using SFG in situ (**Figure 4**.7). The SFG ssp spectrum collected from the nylon-air surface before contact with the MAHgEO sample at room temperature is also shown for comparison. Intensity of the nylon C=O stretching band at 1625 cm^{-1} begins to decrease at temperatures higher than 90 °C, and shows little change between 100 °C to 120 °C. At higher temperatures, this band almost disappears. Meanwhile, a new band at 1725 cm^{-1} appears in the SFG spectra at 90 °C, the intensity of this band increases with temperature, reaching a plateau at 120 °C. The temperature-dependent signal change in the carbonyl C=O stretching frequency region is consistent with that observed in the amine N-H stretching frequency region discussed

above, and again provides additional evidence of an interfacial chemical reaction which begins above 90 °C and accelerates at 120 °C. The consumption of reactants and the generation of products are observed simultaneously at the buried interface at the molecular level and in situ. It is worth pointing out that increase in the entropic effect due to increasing temperature is expected to randomize the interfacial functional group orientations and thus reduce the SFG intensity. However, SFG intensity at 1725 cm^{-1} increased. This clearly suggests that a chemical reaction occurs above 90 °C. At very high temperatures (e.g., 180 °C), the interfacial molecules can be more mobile and lose their orientational ordering at the buried nylon/MAHgEO interface or leave the interface by diffusing into bulk, leading to the disappearance of SFG signals (**Figure 4.7**). When the system was cooled down to room temperature, the interfacial C=O groups became ordered again, generating SFG signals (**Figure 4.6 (c)** and **Figure 4.7**). As shown in **Figure 4.4**, carboxylic acid groups and imide carbonyl groups can be generated from the interfacial reaction. The peak at 1725 cm^{-1} is assigned to the C=O stretching of the carboxylic acid groups and imide carbonyl groups in the reaction products.[66–68] Certainly, the hydrolysis of MAH at the interface can also produce carboxylic acid functionality. However, here we do not believe that the interfacial carboxylic acid observed comes from hydrolyzed MAH group in MAHgEO at the buried nylon/MAHgEO interface, because the peak at 1725 cm^{-1} was not initially observed. Furthermore, if this were the case, this peak should have continuously decreased as the temperature increased and behaved similar to the buried non-reactive EO/MAHgEO interface. In contrast, the peak at 1725 cm^{-1} from the buried nylon/MAHgEO interface increased, accompanied by the decrease of the nylon C=O peak at 1625 cm^{-1} with increasing temperature. This result further corroborates that the peak at 1725 cm^{-1} arises from the interfacial reaction products. More details about this peak assignment was reported in a recent publication.[65] In this study, the entire reaction process (reactant

consumption and product formation) was directly monitored at the buried nylon/MAHgEO interface at the molecular level and in situ using SFG.

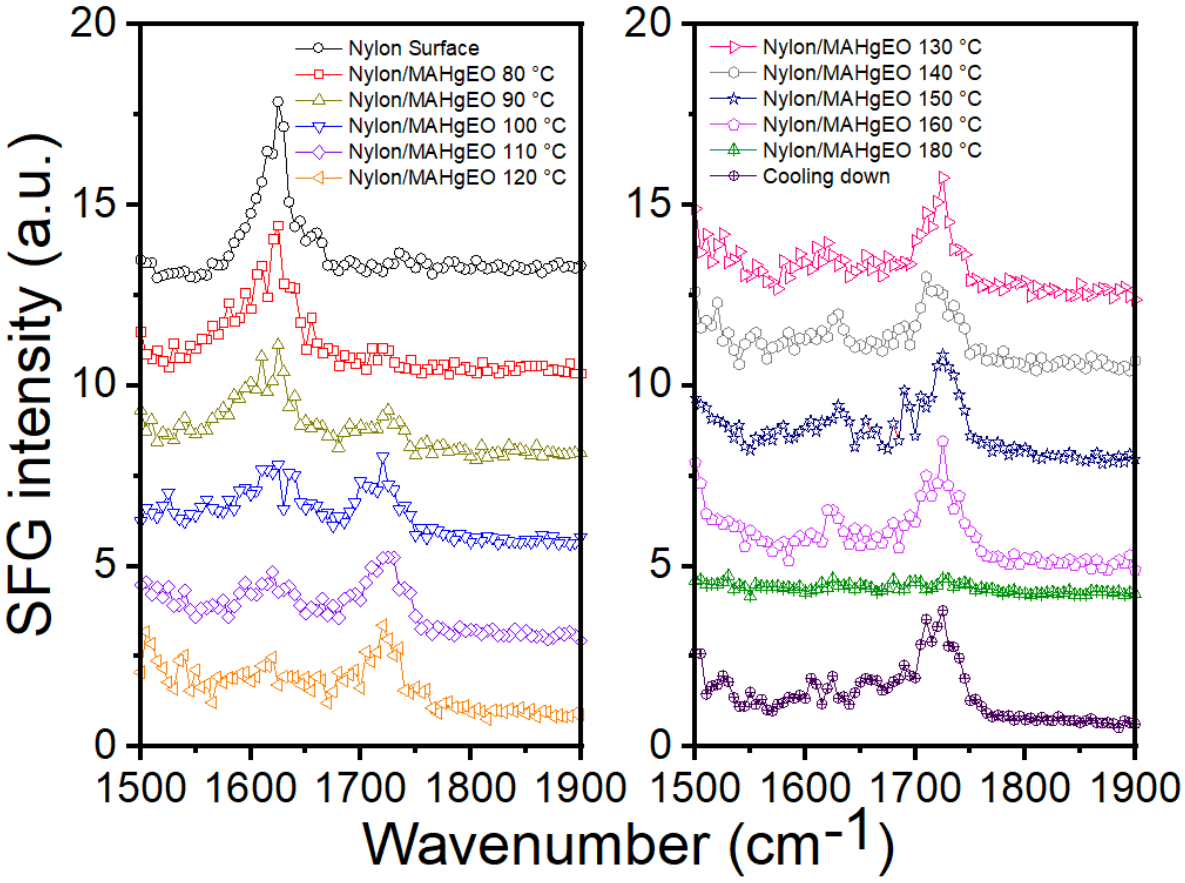

Figure 4.7 SFG ssp spectra collected from the buried interface between nylon and MAHgEO at different temperatures in the carbonyl C=O stretching frequency region. The SFG ssp spectrum obtained from the nylon-air surface is also shown as a reference. The spectra were offset for clarification. The spectrum collected from the nylon/MAHgEO interface at room temperature after heating to 180 ℃ was also shown (right panel, bottom spectrum) for comparison.

4.3.3 Kinetics of the buried interface reaction.

The reaction kinetics at the buried nylon/MAHgEO interface was evaluated by collection of the SFG intensity of the amine stretching mode as a function of time at three temperatures (110 ℃, 130 ℃, and 150 ℃). Since the intensity of an SFG band is proportional to the square of the interfacial molecular coverage,[72] the reaction kinetics can be deduced by plotting the square root of the SFG intensity as a function of time. The relationship between the square root of the

time-dependent SFG ssp signal intensities at 3300 cm^{-1} with time is shown in **Figure 4.8 (a)** for three temperatures. The same first order chemical reaction model was used to fit the reaction kinetics as proposed by Scott and Macosko and subsequently confirmed by Oyama and Inoue on a similar polymer-polymer system.[73,74] As shown in **Figure 4.8 (a)**, the data agree quite well over the entire time scale (early and later stages) to the first-order model. The Arrhenius activation energy for the overall reaction at the buried nylon/MAHgEO interface was calculated to be 33 kJ/mol (**Figure 4.8 (b)**). Schaefer et al. and Shin et al. studied reactions between MAH and NH_2 groups in a bilayer films (the bilayers consisted of styrene-maleic anhydride copolymer and amine-terminated butadiene-acrylonitrile copolymer or bis(amine) terminated poly(tetrahydrofuran)) using FTIR spectroscopy.[75,76] They found the Arrhenius activation energy to be about 52 kJ/mol. While this differs from the value reported here, there are few, if any, comparisons of reaction kinetics in the bulk versus those directly measured at an interface. In addition, the activation energy reported for the bulk reaction was determined for a different polymer system than MAHgEO, where MAH groups were on the backbone of the polymer. Side chain MAH groups have better mobility than anhydride groups on the backbone, which can possibly lower the activation energy necessary for the reaction to occur at the buried interface.

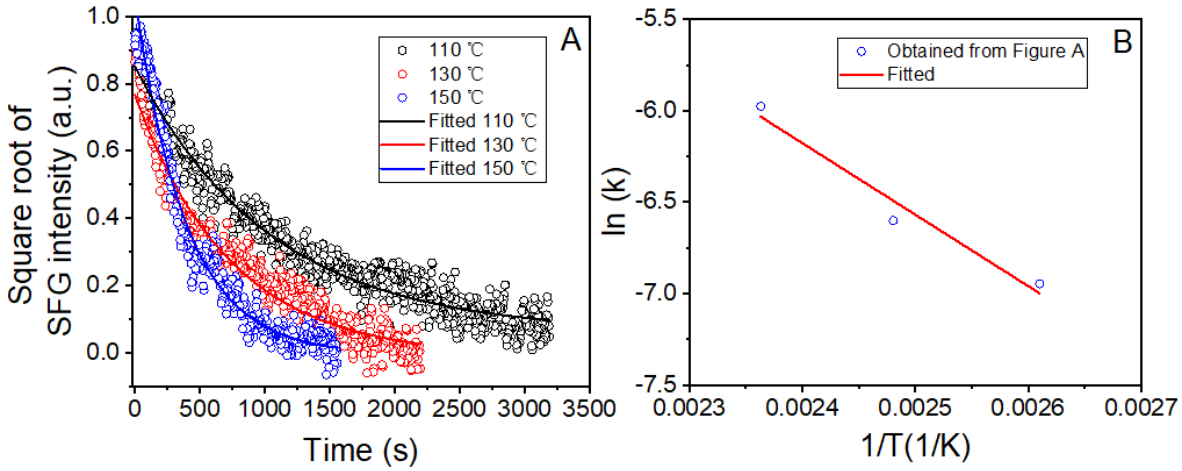

Figure 4.8 (a) Square root of time-dependent SFG ssp signal intensities collected from the buried

nylon/MAHgEO interface at three different temperatures (110 ℃, 130 ℃, and 150 ℃). Round circles are experimental points. Lines are fits based on the first order reaction model. (b) Arrhenius plot used to deduce the activation energy of the interfacial reaction.

The SFG results presented above demonstrate the interfacial chemical reaction at the buried nylon/MAHgEO interface, which is further corroborated by adhesion tests, comparable to the results shown in Chapter 3. The higher adhesion of the grafted polymer system was at least in part due to formation of covalent bonds between nylon and grafted MAH at the buried nylon/MAHgEO interface. In this study, not only was the interfacial reaction at a buried polymer/polymer interface revealed, but also the interfacial structure and adhesion properties of the buried interface are well correlated, as shown in **Figure 4.9**.

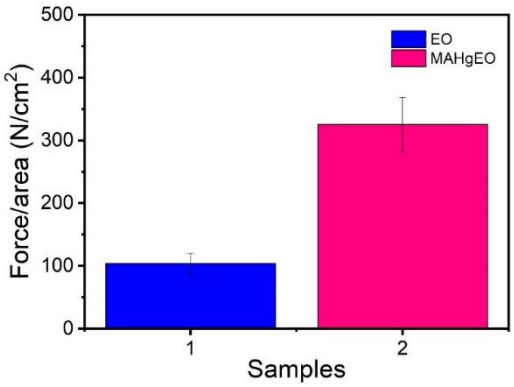

Figure 4.9. Adhesion strengths measured for nylon/EO and nylon/MAHgEO interfaces.

4.4 Conclusions

In this research, SFG was used for the first time to detect and monitor the interfacial chemical reaction between nylon and MAH-grafted EO, at the buried nylon/MAHgEO interface in real time and in situ. The chemical reaction was detected via the consumption of the reactants (NH_2 and amide groups of nylon) and formation of the products (imide and carboxylic acid groups). Nylon N-H stretching signals at ~3300 cm^{-1} disappeared in both SFG ssp and ppp spectra

after nylon reacted with grafted MAH groups in MAHgEO at the buried interface, while the nylon C=O stretching signal at ~1625 cm^{-1} disappeared in the ssp spectrum and dramatically decreased in the ppp spectrum after nylon reacted with grafted MAH groups in MAHgEO. A new peak at 1725 cm^{-1} appeared from the reaction products of carboxylic acid and imide groups. The temperature dependence of this reaction was investigated, and the activation energy was measured to be 33 kJ/mol. The interfacial adhesion was also evaluated and was enhanced by the formation of covalent bonds at buried nylon/MAHgEO interface. For the buried nylon/EO interface, the SFG spectra reveal totally different interfacial structures. To the best of our knowledge, this was the first direct detection (the consumption of reactants and the formation of products simultaneously) and quantification (the deduction of the reaction kinetics and activation energy) of a chemical reaction between two polymers, such as MAH-grafted EO and nylon, at buried polymer-polymer interfaces. Both the research reported in Chapters 3 and 4 demonstrated that SFG metrologies have great promise to probe interfacial reaction mechanisms, interfacial structures before and after interfacial reactions, and interfacial reaction kinetics. The characterization of chemical reactions at a polymer-polymer or other solid-solid buried interface at the molecular level in real time and in situ provides the basis to build a comprehensive fundamental understanding and manipulation of interfacial properties such as interlayer adhesion.

4.5 References

1. Li, J.; Huang, Y.; Ding, Y. Yang, Z.; Li, S.; Zhou, X.; Fan, F.; Zhang, W.; Zhou, Z.; Wu, D.; Ren, B.; Wang, Z.; Tian, Z. Shell-isolated Nanoparticle-enhanced Raman Spectroscopy. *Nature* **2010**, *464***,** 392−395.
2. Xu, M.; Ma, X.; Wei, T.; Lu, Z. X.; Ren, B. In Situ Imaging of Live-Cell Extracellular pH during Cell Apoptosis with Surface-Enhanced Raman Spectroscopy. *Anal. Chem.* **2018**, *90*, 13922−13928.
3. Wang, Y. H.; Wei, J.; Radjenovic, P.; Tian, Z. Q.; Li, J. F. In Situ Analysis of Surface Catalytic Reactions Using Shell-Isolated Nanoparticle-Enhanced Raman Spectroscopy. *Anal. Chem.* **2019**, *91*, 1675−1685.

4. Lynk, T, P.; Sit, C. S.; Brosseau, C. L. Electrochemical Surface-Enhanced Raman Spectroscopy as a Platform for Bacterial Detection and Identification. *Anal. Chem.* **2018**, *90*, 12639−12646
5. Huang, S. C.; Ye, J. Z.; Shen, X. R.; Zhao, Q. Q.; Zeng, Z. C. Li, M. H.; Wu, D. Y.; Wang, X.; Ren, B. Electrochemical Tip-Enhanced Raman Spectroscopy with Improved Sensitivity Enabled by a Water Immersion Objective. *Anal. Chem.* **2019**, *91*, 11092−11097.
6. Freitag, S.; Baumgartner, B.; Tauber, S.; Gasser, C.; Radel, S. Schwaighofer, A.; Lendl, B. An Acoustic Trap for Bead Injection Attenuated Total Reflection Infrared Spectroscopy. *Anal. Chem.* **2019**, *91*, 7672−7678.
7. Kasahara, S.; Ogose, T.; Ikemiya, N.; Yamamoto, T.; Natsui, K.; Yokota, Y.; Wong, R. A.; Iizuka, S.; Hoshi, N.; Tateyama, Y.; Kim, Y.; Nakamura, M.; Einaga, Y. In Situ Spectroscopic Study on the Surface Hydroxylation of Diamond Electrodes. *Anal. Chem.* **2019**, *91*, 4980−4986.
8. Zheng, B. Yang, X.; Li, J.; Shi, C. F.; Wang, Z. L.; Xia, X. H. Graphene Plasmon-Enhanced IR Biosensing for in Situ Detection of Aqueous-Phase Molecules with an Attenuated Total Reflection Mode. *Anal. Chem.* **2018**, *90*, 10786−10794.
9. Li, B.; Lu, X.; Ma, Y.; Chen, Z. Thermo- and pH-responsive Behaviors of Aqueous Poly(acrylic acid)/Poly(4-vinylpyridine) Complex Material Characterized by ATR-FTIR and UV–Vis Spectroscopy. *Eur. Polym. J.* **2014**, *60*, 255−261.
10. Zhang, C.; Hong, S.; Ji, N.; Wang, Y. P.; Wei, K. H.; Shen, Y. R. Sum-Frequency Vibrational Spectroscopic Study of Surface Glass Transition of Poly(vinyl alcohol). *Macromolecules* **2003**, *36*, 3303−3306.
11. Li, Q. F.; Hua, R.; Cheah, I. J.; Chou, K. C. Surface Structure Relaxation of Poly(methyl methacrylate). *J. Phys. Chem. B* **2008**, *112*, 694−697.
12. Tsuruta, H.; Fujii, Y.; Kai, N.; Kataoka, H.; Ishizone, T.; Doi, M.; Morita, H.; Tanaka, K. Local Conformation and Relaxation of Polystyrene at Substrate Interface. *Macromolecules* **2012**, *45*, 4643−4649.
13. Li, B.; Lu, X.; Ma, Y.; Han, X.; Chen, Z. Method to Probe Glass Transition Temperatures of Polymer Thin Films. *ACS Macro Lett.* **2015**, *4*, 548−551.
14. Xiao, M.; Mohler, C.; Tucker, C.; Walther, B.; Lu, X. Chen, Z. Structures and Adhesion Properties at Polyethylene/Silica and Polyethylene/Nylon Interfaces. *Langmuir* **2018**, *34*, 6194−6204.
15. Zuo, B.; Inutsuka, M.; Kawaguchi, D.; Wang, X.; Tanaka, K. Conformational Relaxation of Poly(styrene-co-butadiene) Chains at Substrate Interface in Spin-Coated and Solvent-Cast Films. *Macromolecules* **2018**, *51*, 2180−2186.
16. Zuo, B.; Xu, Q.; Jin, T.; Xing, H.; Shi, J.; Hao, Z.; Zhang, L.; Tanaka, K.; Wang, X. Suppressed Surface Reorganization in a High-Density Poly(methyl methacrylate) Brush. *Langmuir* **2019**, *35*, 14890−14895.
17. Inutsuka, M.; Haraguchi, M.; Ozawa, M.; Yamada, N. L.; Tanaka, K. Adhesion Control of Elastomer Sheet on the Basis of Interfacial Segregation of Hyperbranched Polymer. *ACS Macro Lett*. **2019**, *8*, 267−271.

18. Kaur, S.; Narayanan, A.; Dalvi, S.; Liu, Q.; Joy, A.; Dhinojwala, A. Direct Observation of the Interplay of Catechol Binding and Polymer Hydrophobicity in a Mussel-Inspired Elastomeric Adhesive. *ACS Cent. Sci.* **2018**, *4*, 1420−1429.
19. Chen, Z. Investigating Buried Polymer Interfaces Using Sum Frequency Generation Vibrational Spectroscopy. *Prog. Polym. Sci.* **2010**, *35*, 1376−1402.
20. Lu, X.; Zhang, C.; Ulrich, N.; Xiao, M.; Ma, Y. H.; Chen, Z. Studying Polymer Surfaces and Interfaces with Sum Frequency Generation Vibrational Spectroscopy. *Anal. Chem.* **2017**, *89*, 466−489.
21. Lu, X.; Shephard, N.; Han, J.; Xue, G.; Chen, Z. Probing Molecular Structures of Polymer/Metal Interfaces by Sum Frequency Generation Vibrational Spectroscopy. *Macromolecules* **2008**, *41*, 8770−8777.
22. Ulrich, N. W.; Andre, J.; Williamson, J.; Lee, K. W.; Chen, Z. Plasma Treatment Effect on Polymer Buried interfacial Structure and Property. *Phys. Chem. Chem. Phys*. **2017**, *19*, 12144−12155.
23. Chen, H.; McClelland, A. A.; Chen, Z.; Lahann, J. Solventless Adhesive Bonding Using Reactive Polymer Coatings. *Anal. Chem.* **2008**, *80*, 4119−4124.
24. He, Y.; Ren, H.; You, E. M.; Radjenovic, P, M.; Sun, S. G.; Tian, Z. Q, Li, J. F.; Wang, Z. Polarization- and Wavelength-Dependent Shell-Isolated-Nanoparticle-Enhanced Sum-Frequency Generation with High Sensitivity. *Phys. Rev. Lett.* **2020**, *125*, 047401.
25. Huang-Fu, Z. C.; Song, Q. T.; He, Y. H.; Liu, X. L.; Wang, J. J. Sun, S. G.; Wang, Z. Surface Configuration of CO Adsorbed on Nanostructured Pt Electrodes Probed Using Broadband Sum Frequency Generation Spectroscopy. *Chem. Commun*. **2020**, *56*, 9723−9726.
26. Sensui, K.; Tarui, T.; Miyamae, T.; Sato, C. Evidence of Chemical-bond Formation at the Interface Between an Epoxy Polymer and an Isocyanate Primer. *Chem. Commun.* **2019**, *55*, 14833−14836.
27. Van Duin, M.; Aussems, M.; Borggreve, R. J. Graft Formation and Chain Scission in Blends of Polyamide-6 and -6.6 with Maleic Anhydride Containing Polymers. *J. Polym. Sci. A Polym. Chem*. **1998**, *36*, 179−188.
28. Schmidt, U.; Zschoche, S.; Werner, C. Modification of Poly(octadecene-*alt*-maleic anhydride) Films by Reaction with Functional Amines. *J. Appl. Polym. Sci.* **2003**, *87*, 1255−1266.
29. Chen, Z.; Shen, Y. R.; Somorjai, G. A. Studies of Polymer Surfaces by Sum Frequency Generation Vibrational Spectroscopy. *Annu. Rev. Phys. Chem.* **2002**, *53*, 437−465.
30. Shen, Y. R. Basic Theory of Surface Sum-Frequency Generation. *J. Phys. Chem. B* **2012**, *116*, 15505−15509.
31. Elsa, C. Y. Y.; Li, F.; Wang, Z.; Liu, W. Biological Macromolecules at Interfaces Probed by Chiral Vibrational Sum Frequency Generation Spectroscopy. *Chem. Rev.* **2014**, *114*, 8471−8498.
32. Geiger, F. M. Second Harmonic Generation, Sum Frequency Generation, and $\chi^{(3)}$: Dissecting Environmental Interfaces with a Nonlinear Optical Swiss Army Knife. *Annu. Rev. Phys. Chem.* **2009**, *60*, 61−83.
33. Lin, L.; Husek, J.; Biswas, S.; Baumler, S. M.; Adel, T.; Ng, K. C.; Baker, L. R.; Allen, H. C. Iron(III) Speciation Observed at Aqueous and Glycerol Surfaces: Vibrational Sum Frequency and X-ray. *J. Am. Chem. Soc.* **2019,** *141*, 13525−13535.

34. Tan, J.; Zhang, B.; Luo, Y.; Ye, S. Ultrafast Vibrational Dynamics of Membrane-Bound Peptides at the Lipid Bilayer/Water Interface. *Angew. Chem. Int. Ed.* **2017**, *56*, 12977.
35. Richmond, G. L. Molecular Bonding and Interactions at Aqueous Surfaces as Probed by Vibrational Sum Frequency Spectroscopy. *Chem. Rev.* **2002**, *102*, 2693−2724.
36. Liu, J.; Conboy, J. C. Direct Measurement of the Transbilayer Movement of Phospholipids by Sum-Frequency Vibrational Spectroscopy. *J. Am. Chem. Soc.* **2004**, *126*, 8376−8377.
37. Chen, X.; Sagle, L. B.; Cremer, P. S. Urea Orientation at Protein Surfaces. *J. Am. Chem. Soc.* 2007, *129*,15104−15105.
38. Adhikari, N M.; Premadasa, U. I.; Cimatu, K. L. A. Sum Frequency Generation Vibrational Spectroscopy of Methacrylate-Based Functional Monomers at the Hydrophilic Solid–Liquid Interface. *Phys. Chem. Chem. Phys.* **2017**, *19*, 21818−21828.
39. Lovering, K. A.; Bertram, A. K.; Chou, K. C. Transient Phase of Ice Observed by Sum Frequency Generation at the Water/Mineral Interface During Freezing. *J. Phys. Chem. Lett.* **2017**, *8*, 871−875.
40. Tan, J.; Zhang, J.; Luo, Y.; Ye, S. Misfolding of a Human Islet Amyloid Polypeptide at the Lipid Membrane Populates through β-Sheet Conformers without Involving α-Helical Intermediates. *J. Am. Chem. Soc.* **2019**, *141*, 1941−1948.
41. Ding, B.; Jasensky, J.; Li, Y.; Chen, Z. Engineering and Characterization of Peptides and Proteins at Surfaces and Interfaces: A Case Study in Surface-Sensitive Vibrational Spectroscopy. *Acc. Chem. Res.* **2016**, *49*, 1149–1157.
42. Peng, Q.; Chen, J.; Ji, H.; Morita, A.; Ye, S. Origin of the Overpotential for the Oxygen Evolution Reaction on a Well-Defined Graphene Electrode Probed by in Situ Sum Frequency Generation Vibrational Spectroscopy. *J. Am. Chem. Soc.* **2018**, *140*, 15568−15571.
43. Enlow, E. M.; Kennedy, J. L.; Nieuwland, A. A.; Hendrix, J. E.; Morgan, S. L. Discrimination of Nylon Polymers Using Attenuated Total Reflection Mid-Infrared Spectra and Multivariate Statistical Techniques. *Appl. Spectrosc.* **2005**, *59*, 986–992.
44. Czarnecki, M. A.; Wu, P.; Siesler, H. W.; 2D FT-NIR and FT-IR Correlation Analysis of Temperature-Induced Changes of Nylon12. *Chem. Phys. Lett.* **1998**, *283*, 326−332.
45. Tong, Y.; Zhao, Y.; Li, N.; Ma, Y.; Osawa, M. Davies, P, B.; Ye, S. Interference Effects in the Sum Frequency Generation Spectra of Thin Organic Films. II: Applications to Different Thin-Film Systems. *J. Chem. Phys.* **2010**, *133*, 034705.
46. Ye, S.; Morita, S.; Li, G.; Noda, H.; Tanaka, M.; Uosaki, K.; Osawa, M. Structural Changes in Poly(2-methoxyethyl acrylate) Thin Films Induced by Absorption of Bisphenol A. An Infrared and Sum Frequency Generation (SFG) Study. *Macromolecules* **2003**, *36*, 5694−5703.
47. Zuo B.; Zhou, H.; Davis, M. J. B.; Wang, X.; Priestley, R. D. Effect of Local Chain Conformation in Adsorbed Nanolayers on Confined Polymer Molecular Mobility. *Phys. Rev. Lett.* **2019**, *122*, 217801.
48. Skrovanek, D. J.; Howe, S. E.; Painter, P. C.; Coleman, M. M. Hydrogen Bonding in Polymers: Infrared Temperature Studies of an Amorphous Polyamide. *Macromolecules* **1985**, *18*, 1676−1683.

49. Skrovanek, D. J.; Painter, P. C.; Coleman, M. M. Hydrogen Bonding in Polymers. 2. Infrared Temperature Studies of Nylon 11. *Macromolecules* **1986**, *19*, 699−705.
50. Fang, Y.; Li, B.; Yu, J.; Zhou, J.; Xu, X.; Shao, W.; Lu, X. Probing Surface and Interfacial Molecular Structures of a Rubbery Adhesion Promoter Using Sum Frequency Generation Vibrational Spectroscopy. *Surf. Sci.* **2013**, *615*, 26−32.
51. Joo, E.; Chang, Y.; Choi, I.; Lee, S. B.; Kim, D. H.; Choi, Y. J.; Yoon, C. S.; Han, J. Whey Protein-Coated High Oxygen Barrier Multilayer Films Using Surface Pretreated PET Substrate. *Food Hydrocoll.* **2018**, *80*, 1−7.
52. Kyu, T.; Chen, T. I.; Park, H. S.; White, J. L. Miscibility in Poly‐*p*‐Phenylene Terephthalamide/Nylon 6 and Nylon 66 Molecular Composites. *J. Appl. Polym. Sci.* **1989**, *37*, 201−213.
53. Triacca, V. J.; Ziaee, S.; Barlow, J. W.; Keskkula, H.; Paul, D. R. Reactive Compatibilization of Blends of Nylon 6 and ABS Materials. *Polymer* **1991**, *32*, 1401−1413.
54. Liu, H.; Cao, K.; Huang, Y.; Yao, Z.; Li, B.; Hu, G. Kinetics and Simulation of the Imidization of Poly(styrene‐co‐maleic anhydride) with Amines. *J. Appl. Polym. Sci.* **2006**, *100*, 2744−2749.
55. Kim, B. K.; Park, S. J. Reactive Melt Blends of Nylon with Poly(styrene‐*co*‐maleic anhydride). *J. Appl. Polym. Sci.* **1991**, *43*, 357−363.
56. Cho, K.; Seo, K. H.; Ahn, T. O.; Kim, J.; Kim, U, K. Enhancement of Interfacial Adhesion Between Polystyrene and Styrene Maleic Anhydride Random Copolymer via Reactive Reinforcement. *Polymer* **1997**, *38*, 4825−4830.
57. Kim, S.; Kim, D.; Cho, W.; Ha, C. Morphology and Properties of PBT/Nylon 6/EVA‐g‐MAH Ternary Blends Prepared by Reactive Extrusion. *Polym. Eng. Sci.* **2003**, *43*, 1298−1311.
58. Park, S. J.; Kim, B. K.; Jeong, H. M. Morphological, Thermal and Rheological Properties of the Blends Polypropylene/Nylon-6, Polypropylene/Nylon-6/(Maleic Anhydride-g-Polypropylene) and (Maleic Anhydride-g-Polypropylene)/Nylon-6. *Eur. Polym. J.* **1990**, *26*, 131−136.
59. Maréchal, P.; Coppens, G.; Legras, R.; Dekoninck, J. Amine/Anhydride Reaction Versus Amide/Anhydride Reaction in Polyamide/Anhydride Carriers. *J. Polym. Sci. A Polym. Chem.* **1995**, *33*, 757−766.
60. Eichhorn, K.; Lehmann, D.; Voigt, D. Characterization of Low Molecular Weight Carboxyl-Terminated Polyamides Obtained by Reactive Extrusion of Polyamide 6 with Trimellitic Anhydride. *J. Appl. Polym. Sci.* **1996**, *62*, 2053−2060.
61. Macosko, C. W.; Jeon, H. K.; Hoye, T. R. Reactions at Polymer–Polymer Interfaces for Blend Compatibilization. *Prog. Polym. Sci.* **2005**, *30*, 939−947.
62. Lee, K. H.; Kim, K. W.; Pesapane, A.; Kim, H. Y.; Rabolt, J. F. Polarized FT-IR Study of Macroscopically Oriented Electrospun Nylon-6 Nanofibers. *Macromolecules* **2008**, *41*, 1494−1498.

63. Enlow, E. M.; Kennedy, J. L.; Nieuwland, A. A.; Hendrix, J. E.; Morgan, S. L. Discrimination of Nylon Polymers Using Attenuated Total Reflection Mid-Infrared Spectra and Multivariate Statistical Techniques. *Appl. Spectrosc.* **2005**, *59*, 986–992.
64. Hendra, P. J.; Maddams, W. F.; Royaud, I. A. M.; Willis, H. A.; Zichy, V. The Application of Fourier Transform Raman Spectroscopy to the Identification and Characterization of Polyamides—I. Single Number Nylons. *Spectroc. Acta Pt. A: Molec. Spectr.* **1990**, *46*, 747–756.
65. Li, B.; Andre, J. S.; Chen, X.; Walther, B.; Paradkar, R.; Feng, C.; Tucker, C. J.; Mohler, C.; Chen, Z. Probing Molecular Behavior of Carbonyl Groups at Buried Nylon/Polyolefin Interfaces in Situ. *Langmuir* **2020**, DOI: 10.1021/acs.langmuir.0c02188
66. Avery, C.W.; Som, A.; Xu, Y.; Tew, G. N. Chen, Z. Dependence of Antimicrobial Selectivity and Potency on Oligomer Structure Investigated Using Substrate Supported Lipid Bilayers and Sum Frequency Generation Vibrational Spectroscopy. *Anal. Chem.* **2009**, *81*, 8365−8372.
67. Dreesen, L.; Sartenaer, Y.; Humbert, C.; Mani, A. A.; Lemaire, J. J.; Méthivier, C.; Pradier, C. M.; Thiry, P. A.; Peremans, A. Sum-Frequency Generation Spectroscopy Applied to Model Biosensors Systems. *Thin Solid Films*, **2004**, *464–465*, 373−378.
68. Wang, J.; Even, M. A.; Chen, X.; Alvin H. Schmaier, A. H.; Waite, J. H.; Chen, Z. Detection of Amide I Signals of Interfacial Proteins in Situ Using SFG. *J. Am. Chem. Soc.* **2003**, *125*, 9914−9915.
69. Sung J.; Kim, D.; Whang, C. N.; Oh-e, M.; Yokoyama, H. Sum-Frequency Vibrational Spectroscopic Study of Polyimide Surfaces Made by Spin Coating and Ionized Cluster Beam Deposition. *J. Phys. Chem. B* **2004**, *108*, 10991−10996.
70. Li, B.; Li, Xu.; Ma, Y. H.; Han, X. F.; Wu, F, G.; Guo, Z.; Chen, Z.; Lu, X. Sum Frequency Generation of Interfacial Lipid Monolayers Shows Polarization Dependence on Experimental Geometries. *Langmuir* **2016**, *32*, 7086–7095.
71. Li, B.; Wang, H. Y.; Feng, P.; Han, X.; Chen, Z.; Lu, X.; Wu, F. G. Qualitative and Quantitative Analyses of the Molecular-Level Interaction between Memantine and Model Cell Membranes. *J. Phys. Chem. C* **2015**, *119*, 17074–17083.
72. Wang, J.; Paszti, Z.; Even, M. A.; Chen, Z. Measuring Polymer Surface Ordering Differences in Air and Water by Sum Frequency Generation Vibrational Spectroscopy. *J. Am. Chem. Soc.* **2002**, *124*, 7016−7023.
73. Scott, C.; Macosko, C. Model Experiments for the Interfacial Reaction between Polymers During Reactive Polymer Blending. *J. Polym. Sci. B Polym. Phys.* **1994**, *32*, 205−213.
74. Oyama, H. T.; Inoue, T. Kinetics and Mechanism of Coupling of Functionalized Chains at the Immiscible Polymer−Polymer Interface. *Macromolecules* **2001**, *34*, 3331−3338.
75. Shin E. M.; Koenig, J. L. Study of the Interfacial Reaction of Styrene/Maleic Anhydride Copolymer and (Amine)-Terminated Butadiene-Acrylonitrile Copolymer Using FTIR Imaging Techniques. *J. Adhes.* **2002**, *78*, 877−894.
76. Ruediger Schaefer, R.; Kressler, J. Neuber, R.; Muelhaupt. R. FTIR Spectroscopy and Microscopy on the Interfacial Reaction and Interdiffusion of Styrene/Maleic Anhydride and Bis(amine)-Terminated Poly(tetrahydrofuran). *Macromolecules* **1995**, *28*, 5037−5042.

Chapter 5: Molecular Interactions between Amino Silane Adhesion Promoter and Acrylic Polymer Adhesive at Buried Silica Interfaces

5.1 Introduction

Acrylic polymers are widely used for textiles, paints, adhesives, and coating applications. In particular, waterborne coatings based on acrylic latexes are increasing in popularity since they are considered to be more environmentally friendly than solvent-based formulations and subsequently find use in a wide variety of applications. In order to achieve high performance of the final coating, various inorganic and organic additives are incorporated into the coating formulations to improve properties such as adhesion, opacity, color, flow, and durability.[1-2] Adhesion of acrylic polymer compositions with a variety of materials including glass or silica are important in many applications such as reflectivity modulation, paint formulations, and modifying properties of resin materials.[3-9] To improve adhesion, amino functionalized silanes are often added to acrylic polymer formulations.[8-12] It is generally known that waterborne acrylic polymer coatings with amino silane additives have better adhesive performance to glass than the polymer formulations without such an additive. However, the detailed molecular mechanisms of adhesion enhancement of amino silanes in acrylic polymer formulations have not been fully understood.

Acrylic latex polymers are prepared by emulsion polymerization with a variety of monomers that are selected based upon the intended end use of the materials. Methyl methacrylate

(MMA) and butyl acrylate (BA) are among the most common and lowest cost acrylic monomers and provide very different homopolymer glass transition temperatures. It is thus common to copolymerize BA and MMA in different ratios to target specific glass transition temperatures (film formation temperatures). Other monomers, such as acid functional monomers like methacrylic acid (MAA), are frequently included in the polymerizations at low levels to impart specific properties like colloidal stability of the latex and adhesion of the subsequently formed coating to substrates.

Waterborne acrylic polymer coatings can be applied to a substrate by methods such as rolling, brushing or spraying. After drying, the paint is transformed into a permanent solid coating film adhered to the substrate. The drying process of waterborne acrylic polymer coatings to form a film occurs in a step-wise fashion after the colloid is applied. A simple diagram of this process is shown in **Figure 5.1 (a)**. Drying begins with evaporation of water from the coating, moving the spherical polymer particles closer together. Many factors such as mixture composition can influence how fast evaporation occurs.[13] Defects can form in the film if evaporation is too fast or too slow. To optimize the evaporation rate additives such as surfactants, defoamers, and rheology modifiers are added to the emulsion formulation. Following the initial drying step, the polymer particles are densely packed and begin to deform and fill voids in the film left behind by water evaporation (second step in **Figure 5.1 (a)**. The deformation process is controlled by capillary forces and influenced by the minimum film formation temperature (MFFT); below this temperature a discontinuous film can form. MFFTs are typically close to or lower than the glass transition temperature (Tg) of the polymer. After the polymer particles have deformed in the film, forming a honey-comb like structure, coalescence occurs. Coalescence occurs when the water has mostly evaporated and the boundaries between polymer particles begin to disappear forming a

homogeneous structure, depicted in the last step of **Figure 5.1 (a)**. For this step the glass transition temperature is very important and environmental conditions must be above the MFFT to form a good film.[13] At this point the film is dry but polymer chain interdiffusion can still occur.

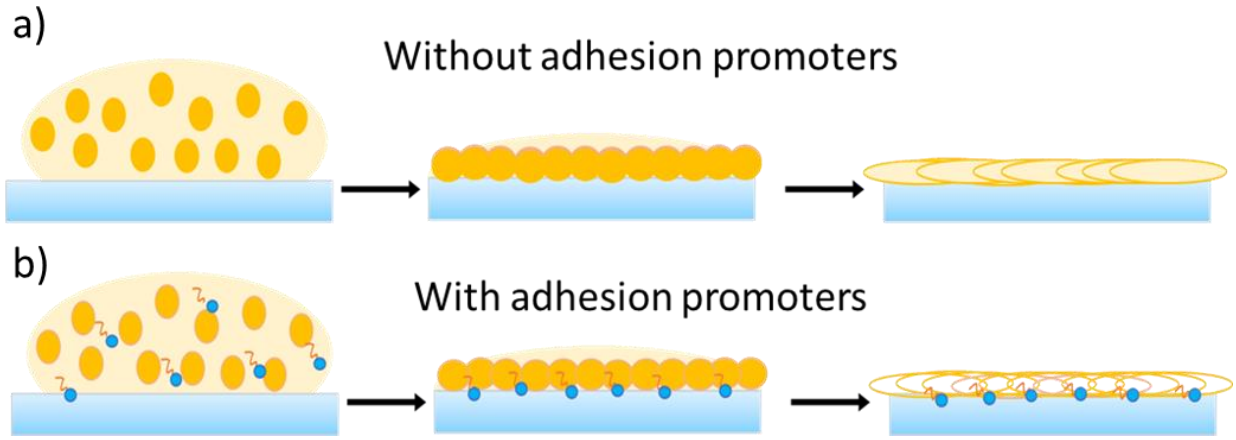

Figure 5.1 Schematics showing the drying processes after waterborne acrylic polymer emulsions without (a) and with (b) adhesion promoters are applied onto a substrate surface. The blue head and orange tail represent the silanol head group and amine tail group, respectively, of an amino silane additive.

It is believed that when an adhesion promoter is added to the polymer formulation, the interaction between the acrylic polymer coating film and substrate can be greatly altered, enhancing the adhesion between the coating and the substrate.[8] However, molecular level details regarding the interfacial behavior of adhesion promoters, the impact of their addition to the polymer formulation on the interfacial structure and interfacial interactions are not clear. This research aims to better understand the role of an amino silane adhesion promoter in acrylic polymer coatings to enhance the coating film interaction with the substrate. Such interactions occur at buried solid (coating film)/solid (substrate or filler) interfaces, which are difficult to study non-destructively using traditional surface/interface sensitive techniques, such as ATR-FTIR, XPS,

AFM, etc. Here we are using SFG to study the molecular structure of buried acrylic polymer coating film/fused silica interfaces *in-situ*, where fused silica is used as a model for glass.

SFG spectroscopy has been developed into a powerful analytical tool to noninvasively study buried polymer interfaces with a variety of substrates, including interfacial behavior of additives in polymer adhesive formulations.[14-34] Details about SFG are discussed in Chapter 1.

Here, we studied the adhesion mechanisms of a waterborne acrylic polymer formulation with added amino silane adhesion promoter to glass (using fused silica as a model for glass). SFG was used to probe the buried interface between acrylic copolymer formulations and silica *in-situ*. It has been shown that silanes can be used in polymer systems to enhance adhesion through a variety of mechanisms.[1] An amino silane was chosen in this study because of the potential for chemical reactions occurring between i) the polymer and the silane, and ii) the silane with the glass surface. A common role of a silane additives is to prevent water from reaching the interface (or displace it), which is especially important when the coating is waterborne.[1, 35-36] Another type of adhesion enhancement mechanism involves the formation of ionic or covalent bonds between the adhesion promoter and the acid groups of the polymer. In this study SFG was used to probe the buried interfaces to test both above possible mechanisms. Three different polymers were synthesized with varying levels of MAA in order to put particular focus on the spectral signals of the acid groups of the derived polymer in the presence of adhesion promoter. It was found that the interactions between adhesion promoters and the polymer molecules, and between adhesion promoters and the silica substrate play the dominating role in adhesion enhancement. The results obtained from the *in situ* buried interface study here demonstrate that the adhesion promoter acts as a bridge between materials to improve adhesion in this multicomponent formulation.

5.2 Materials and methods

5.2.1 Materials

Butyl acrylate, methyl methacrylate, methacrylic acid terpolymer latexes were provided by Dow Inc. and used as received. A simplified illustration of the molecular structure of the polymers (BAMMA) is shown in **Figure 5.2 (a)**. These polymers were prepared from ~50 wt% butyl acrylate (BA) /~50 wt% methyl methacrylate (MMA), with either 0.7 (0.7MAA), 1.4 (1.4MAA), or 1.8 (1.8MAA) wt% methacrylic acid (MAA). The BAMMA polymers were provided at ~50.5% solids in water at pH >9.5. A small amount of 1-dodecanethiol (nDDM) was used in the polymerization process to control the copolymer molecular weight.

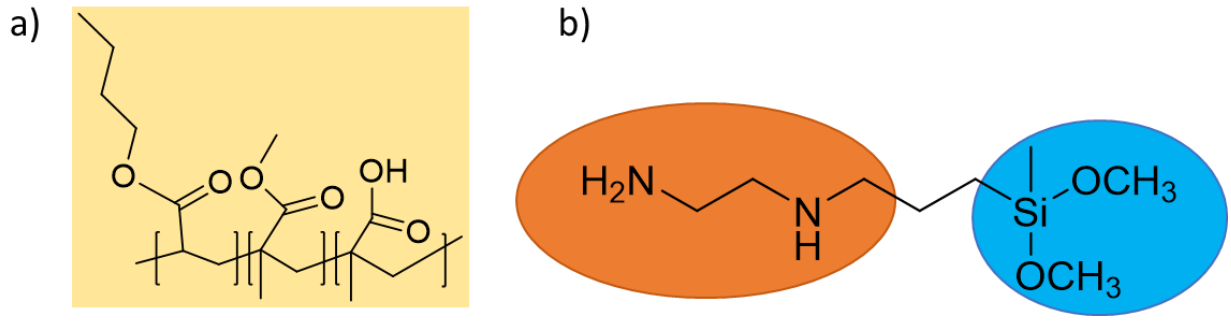

Figure 5.2 Illustrative molecular structures of (a) butyl acrylate/methyl methacrylate polymers (BAMMA) and (b) 3-(2-aminoethylamino)-propyldimethoxymethylsilane (AEAPS).

The amino silane studied here was 3-(2-aminoethylamino)-propyldimethoxymethylsilane (AEAPS, **Figure 5.2 (b)**) and was obtained from Momentive Performance Materials (Waterford, NY). Different amounts of AEAPS were added to an aqueous BAMMA emulsion at 0.0 wt%, 0.5 wt%, and 1.0 wt% concentrations, relative to the polymer solids.

Silica surfaces for SFG studies were prepared by depositing a 100 nm silica layer via PVD on calcium fluoride (CaF_2) right angle prisms (Altos Photonics, Bozeman MT), indicated in **Figure 5.3**. To make the buried silica/polymer interfaces, BAMMA polymers with 0.0 wt%, 0.5 wt%, and

1.0 wt% AEAPS were applied dropwise to the PVD silica surfaces. All samples were white and opaque in appearance. BAMMA polymers with and without AEAPS were allowed to dry in ambient conditions at room temperature for 48 hours or more before analysis. Upon drying, all of the films were clear and transparent. The polymer material on the substrate was about 2 mm thick.

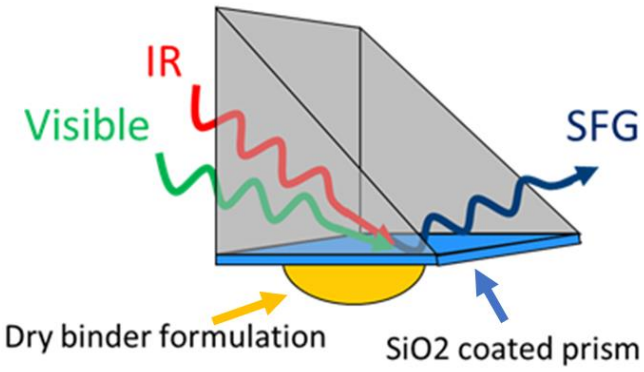

Figure 5.3 Schematic showing SFG sample geometry used in this study. Silica coating on the CaF_2 prism is indicated and the polymer material is also shown.

5.2.2 Methods

Details regarding SFG theory, equipment, and data analysis were covered in Chapter 1. Energies of the visible and IR beams at the sample were about 30 µJ for the visible beam and 120 µJ for the IR beam in the C-H and O-H stretching frequency region (2700-3800 cm^{-1}) and 30 µJ for the visible beam and 40 µJ for the IR beam in the carbonyl C=O stretching frequency region (1550-1900 cm^{-1}). SFG spectra were collected in the ssp (s-polarized output SFG, s-polarized input visible, p-polarized input IR) and ppp polarization combinations. The SFG sample geometry used in this study is shown in **Figure 5.3**.

5.3 Results and discussion

5.3.1 BAMMA latex containing 0.7 wt% MAA

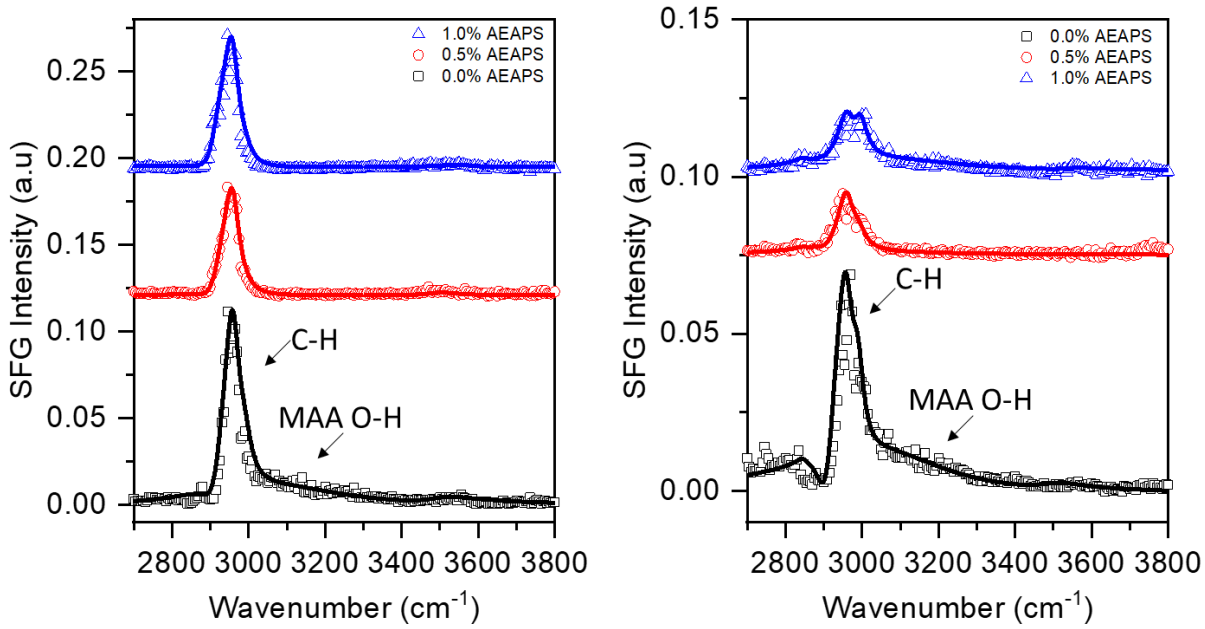

Figure 5.4 SFG ssp (left) and ppp (right) spectra collected from the interfaces between silica and BAMMA copolymer containing 0.7 wt% MAA and different amounts of AEAPS. The spectra are offset. Symbols are individual data points and the lines are fitting results. The fitting parameters of the spectra are listed in **Table 5.1**.

Here we first present the SFG results obtained from BAMMA containing 0.7% MAA (0.7MAA). **Figure 5.4** shows the ssp and ppp SFG spectra collected from the interfaces between silica and 0.7MAA with different amounts of aminosilane (0.0%, 0.5%, and 1.0%). For the SFG spectra collected from the silica interface with 0.7MAA (no added AEAPS, black curves in **Figure 5.4**), both the ssp and ppp spectra show a sharp peak between 2900 cm^{-1} and 3000 cm^{-1}, which is due to the aliphatic C-H stretching modes of the polymer. The broad peak that extends to about 3400 cm^{-1} is attributed to the O-H stretching mode, which becomes more pronounced at higher MAA amounts (shown later). This broad O-H peak extends to both sides of the C-H stretching

peaks, between 2900 and 3400 cm^{-1}, with a peak center located at around 3050 cm^{-1}. The typical water O-H stretching signals in SFG spectra are usually centered at about 3200 and 3400 cm^{-1}. The lower frequency of this O-H stretching mode suggests that it is due to interfacial acid (O-H stretching of the –COOH) from the polymer rather than water at the interface.[37]

Table 5.1 Fitting parameters of the SFG spectra collected from the interfaces between silica and BAMMA base polymers containing 0.7% MAA and different amounts of amino silane.

	0.0% AEAPS			0.5% AEAPS			1.0% AEAPS		
ppp Assignment	A	ω(cm^{-1})	Γ (cm^{-1})	A	ω(cm^{-1})	Γ (cm^{-1})	A	ω(cm^{-1})	Γ (cm^{-1})
Sym. Methyl	0.85	2880	30	0.25	2880	30	0.10	2880	15
Asym. Methyl/Sym. Ester Methyl	3.60	2960	25	2.75	2960	25	1.75	2960	25
Asym. Ester Methyl	1.50	2990	20	0.75	2990	22	1.3	2995	22
Sym. Methylene	0.25	2850	20	0.15	2850	20	0.25	2850	20
Asym. Methylene	-4.00	2915	30	-0.50	2915	30	-0.15	2915	30
Acid O-H 1	25.00	3050	225	5.00	3050	225	12.00	3050	225
Water O-H	1.50	3500	75	0.10	3500	50	0.50	3545	50
Water 1	x	x	x	x	x	x	x	x	x
Water 2	x	x	x	x	x	x	x	x	x
ssp Assignment	A	ω(cm^{-1})	Γ (cm^{-1})	A	ω(cm^{-1})	Γ (cm^{-1})	A	ω(cm^{-1})	Γ (cm^{-1})
Sym. Methyl	0.15	2880	30	0.10	2880	30	0.10	2880	30
Asym. Methyl/Sym. Ester Methyl	6.40	2960	25	6.70	2960	25	6.90	2960	25
Asym Ester Methyl	1.00	2990	20.35	0.20	2990	22	0.70	2990	22
Sym. Methylene	0.05	2850	20	0.10	2850	20	0.01	2850	20
Asym. Methylene	-3.00	2915	30	-3.50	2915	30	-4.00	2915	30
Acid O-H 1	21.00	3050	225	0.10	3050	225	0.10	3050	225
Water O-H	2.20	3500	75	2.00	3500	50	1.90	3545	50
Water 1	x	x	x	x	x	x	x	x	x
Water 2	x	x	x	x	x	x	x	x	x

The C-H stretching signals collected from the silica interface with 0.7MAA without added AEAPS (presented in black in **Figure 5.4**) contain contributions from methylene and methyl symmetric and asymmetric C-H stretching modes of the 0.7MAA polymer. The spectral fitting results and peak assignments are presented in the **Table 5.1**. The peaks at 2850 cm^{-1} and 2915 cm^{-1} are contributed by the symmetric stretching and asymmetric stretching of the CH_2 groups in 0.7MAA, respectively. The asymmetric CH_2 peak appears as a negative peak in the spectrum due to interference with the O-H mode discussed above. The symmetric methyl peak is at 2880 cm^{-1}. The peak at 2960 cm^{-1} could be generated from the asymmetric stretching of the regular methyl group (on butyl acrylate and/or methacrylate) and/or symmetric stretching of the ester methyl groups. The 2990 cm^{-1} peak is generated from the asymmetric stretch of ester methyl groups in the MMA component of 0.7MAA. The assignments are similar for samples containing AEAPS which will be discussed below since the CH_2 groups overlap with those of BAMMA. When AEAPS is added, the signal strength of the C-H modes decreases due to disordering or less interfacial coverage at the silica/polymer interface, but the peak centers and assignments remain the same.

To examine the effect of added AEAPS on interfacial structure and interfacial interaction at the 0.7MAA/silica interface, spectra were collected from the interface when 0.5% or 1.0% AEAPS was added to 0.7MAA, as shown in red or blue curves in **Figure 5.4**, respectively. After the introduction of AEAPS to the polymer system, the broad O-H peak between 2900 and at 3400 cm^{-1} almost disappeared in the ssp data and decreases significantly in the ppp spectrum. This result suggests that AEAPS influences the behavior of O-H groups at the silica/polymer interface. As mentioned above, this broad O-H peak could be assigned to OH stretching motions of the MAA (acid O-H) present in the polymer. It may also arise from strongly hydrogen bonded water left behind at the interface after the drying process. To determine what species the O-H band arises

from, BAMMA polymers with different MAA concentrations were studied systematically, the results of which will be discussed in later sections.

Besides the hydroxyl stretching signals, C-H stretching signals were also affected by the addition of the AEAPS. For 0.7MAA samples with 0.5% added AEAPS, the overall SFG signals from the C-H groups decrease (**Figure 5.4**). A decrease in the C-H signal, especially methyl C-H signals at interfaces involving polymers, has been shown to be a sign of improved adhesion at polymer/polymer and silica/polymer interfaces.[14, 38-40] This is believed to arise because methyl groups at an interface cannot generate strong interfacial interactions such as hydrogen bonding, ionic bonding, or covalent bonding. Addition of higher levels of AEAPS (1.0%, ~stoichiometric equivalent of nitrogen to acid groups) to the 0.7MAA sample did not cause a further decrease in the C-H or O-H signal and indicates that the influence of the AEAPS at the interface is similar at these two concentrations. The different spectra from the 0.7MAA without and with small amounts of AEAPS demonstrate that small amounts of added AEAPS could substantially impact the interfacial structure and therefore interactions between silica and 0.7MAA polymer samples, but interfacial structure does not appear to change after reaching a limiting level of AEAPS.

5.3.2 BAMMA latex containing 1.4 wt% MAA

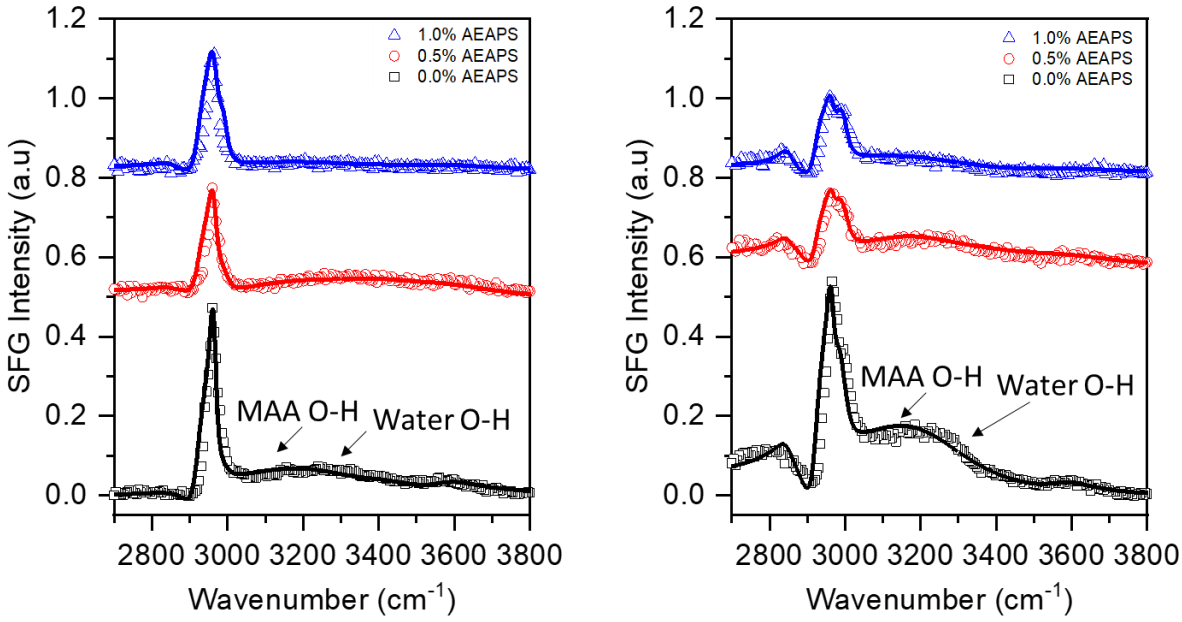

Figure 5.5 SFG ssp (left) and ppp (right) polarization combination spectra collected from interfaces between silica and BAMMA polymers containing 1.4% MAA and different amounts of AEAPS. The spectra are offset. Symbols are experimental data and the lines are fitting results. The fitting parameters of the spectra are listed in **Table 5.2**.

SFG spectra collected from interfaces between silica and BAMMA polymers containing 1.4% MAA (1.4MAA) without and with different amounts of AEAPS are displayed in **Figure 5.5**. The spectra of the 1.4MAA polymer with no adhesion promoter, have similar spectral features as the 0.7MAA polymer without AEAPS discussed above. Both SFG ssp and ppp spectra were dominated by sharp C-H stretching signals and broad O-H stretching signals. However, for the 1.4MAA polymer the O-H band extends to higher frequency than that for 0.7MAA polymer. Likely with a higher acid amount in polymer, more water was retained in the film which was then also manifested at the interface. The red and blue spectra shown in **Figure 5.5** were collected from the interfaces between silica and 1.4MAA with 0.5% and 1.0% adhesion promoter. Similar to the

0.7MAA the C-H group signals also decreased after adding AEAPS to the polymer samples in both the ssp and ppp spectra, indicating that the introduction of AEAPS to the BAMMA samples decreased SFG C-H stretching signals at the polymer/silica interface, regardless of the MAA amount in the BAMMA polymer (within the range studied).

Table 5.2 Fitting parameters of the SFG spectra collected from the interfaces between silica and BAMMA base polymers containing 1.4 % MAA and different amounts of amino silane.

	0.0% AEAPS			0.5% AEAPS			1.0% AEAPS		
ppp Assignment	A	ω(cm^{-1})	Γ (cm^{-1})	A	ω(cm^{-1})	Γ (cm^{-1})	A	ω(cm^{-1})	Γ (cm^{-1})
Sym. Methyl	1.20	2880	30	1.50	2880	30	0.50	2880	30
Asym. Methyl/Sym. Ester Methyl	2.30	2965	12	1.80	2965	15	2.00	2965	15
Asym. Ester Methyl	6.00	2990	25	3.00	2990	25	4.00	2995	20
Sym. Methylene	3.00	2850	30	1.75	2850	25	3.50	2850	25
Asym. Methylene	-9.25	2920	25	-5.00	2920	25	-9.00	2920	25
Acid O-H 1	30.00	3050	225	15.00	3050	245	28.00	3050	245
Water O-H	5.20	3580	75	15.00	3580	150	5.00	3580	120
Water 1	63.00	3200	200	42.00	3200	200	22.00	3200	200
Water 2	0.00	3400	100	1.50	3400	100	0.01	3400	200
ssp Assignment	A	ω(cm^{-1})	Γ (cm^{-1})	A	ω(cm^{-1})	Γ (cm^{-1})	A	ω(cm^{-1})	Γ (cm^{-1})
Sym. Methyl	1.20	2880	30	0.25	2880	30	0.50	2880	30
Asym. Methyl/Sym. Ester Methyl	5.50	2965	12	4.50	2965	15	7.30	2965	20
Asym Ester Methyl	1.50	2990	25	3.00	2990	25	2.50	2990	15
Sym. Methylene	0.25	2850	30	0.25	2850	25	0.80	2850	25
Asym. Methylene	-11.50	2920	25	-4.75	2920	25	-7.50	2920	25
Acid O-H 1	32.00	3050	245	5.00	3050	245	15.00	3050	245
Water O-H	4.75	3575	75	20.00	3580	150	6.00	3580	120
Water 1	34.00	3200	200	20.00	3200	200	15.00	3200	200
Water 2	3.50	3400	100	5.00	3400	100	10.00	3400	200

The O-H behavior detected from the interface between silica and 1.4MAA polymers with added AEAPS was different from the 0.7MAA samples. The addition of a small amount of AEAPS (0.5%) resulted in a decrease in intensity of the acid O-H stretching signals at 3050 cm^{-1} in both ppp and ssp spectra. As the concentration of AEAPS increased to 1.0%, the O-H signal continued to decrease but can still be detected in the ppp spectrum. This suggests the amount of acid functionality in BAMMA influences the O-H band present at the silica/polymer interface. Differences in the OH stretching region for these spectra could be due to a number of factors, one being the presence of more water at the interface as the MAA concentration increases. The presence of O-H signals in the 1.4MAA/AEAPS sample suggests the dominating O-H bands from 2900 to 3400 cm^{-1} likely come from interfacial MAA and water at the silica/BAMMA interface. For the interface of silica with 1.4MAA containing 0.5% added AEAPS, O-H spectra also contain high frequency O-H band beyond 3400 cm^{-1}, suggesting the presence of water at the interface due to the hydrophilicity of the remaining acid functionality at the interface. The interfacial AEAPS either causes the C-H and O-H groups from BAMMA to become less ordered or present in reduced levels at the buried interface, leading to the intensity decrease of the C-H and O-H signals. Another possible explanation is that the MAA carboxylic group reacts with the AEAPS amine group. Such a reaction forms either an ionic pair (negatively charged carboxylate/positively charged ammonium) or forms a covalent bond (amide), discussed later in the Further Discussion section.[41-42]

5.3.3 BAMMA latex containing 1.8 wt% MAA

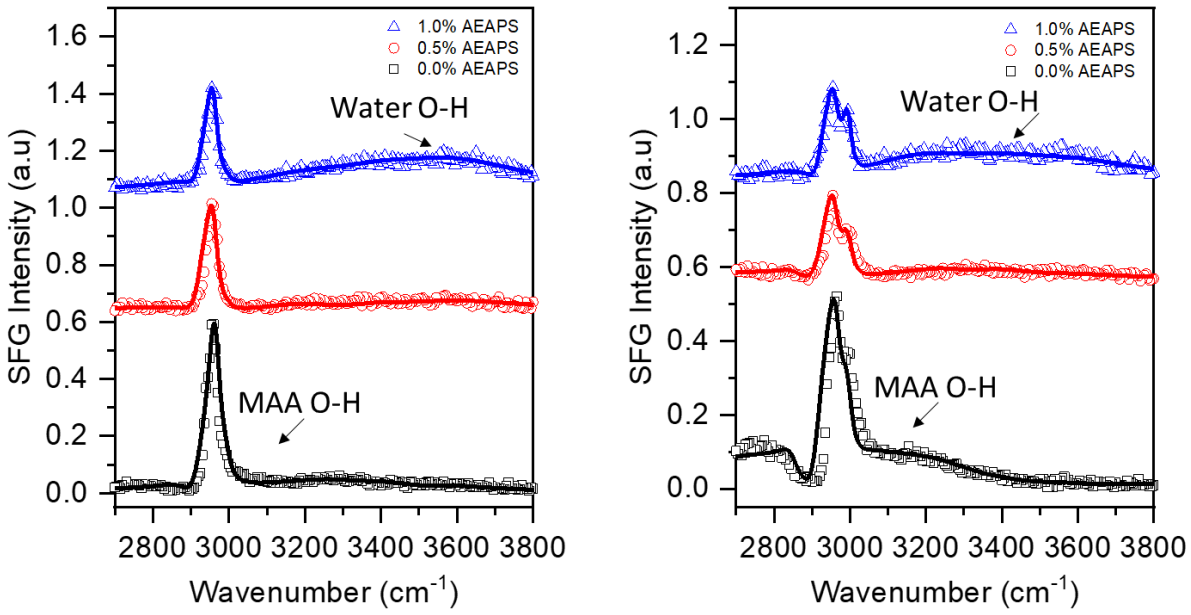

Figure 5.6 SFG ssp (left) and ppp (right) spectra collected from the interfaces between silica and BAMMA base polymers containing 1.8% MAA and different amounts of AEAPS. The spectra are offset. Individual symbols are experimental data and the lines are fitting results. The fitting parameters of the spectra are listed in **Table 5.3**.

The collected SFG spectra from the interfaces between silica and 1.8MAA with varying amounts of AEAPS are presented in **Figure 5.6**. Spectra for samples without AEAPS are dominated by sharp C-H stretching signals and broad O-H signals (dominated by the acid O-H contributions) as before. This observation for the 1.8MAA is similar to those from the BAMMAs containing 0.7% and 1.4% MAA (without added AEAPS). Perhaps for the 0% AEAPS 1.8MAA sample, more acid molecules are crowded onto the interface, thus less ordered. The 1.0% AEAPS 1.8MAA sample has more signal ascribed to interfacial water compared to 1.0% AEAPS 0.7MAA and 1.0% AEAPS 1.4MAA. This observation is consistent with our hypothesis of a correlation between interfacial water and acid concentration at the interface. The results from the 1.8MAA

system when AEAPS is added, (**Figure 5.6**), are much different than those obtained from the 0.7MAA and 1.4MAA polymer samples with AEAPS, with the OH bands shifted to higher frequency. Such O-H signals are signatures of interfacial water molecules, instead of acid O-H groups according to their peak positions. When the AEAPS level was increased to 1.0%, the water O-H peak (shown in blue) becomes more pronounced in both the ssp and ppp spectra, compared to those with 0.5% AEAPS (shown in red). Detection of water O-H signals is reasonable because the increased acid amount in the 1.8MAA polymer could lead to more acid functionalities segregating to the silica interface. The more hydrophilic groups at the interface can bind water more than the other systems, exhibiting detectable SFG O-H signals from water molecules. As with all polymers examined in this work there is very little O-H signal from the acid (the low frequency section of the O-H signals) after AEAPS is added (see the red and blue spectra in **Figure 5.6**), indicating that the vast majority of interfacial MAA molecules form strong interactions with AEAPS molecules as discussed above (through ionic interactions or covalent bonds). This result further supports that in the polymer samples containing 0.7% and 1.4% MAA, the low frequency part of the O-H SFG signal was due to carboxylic acid in MAA and that the decrease in signal intensity upon adhesion promoter addition is due to the carboxylic acid disappearing through disordering, dissociation or reaction with the amine group of the adhesion promoter.

Like the other BAMMA samples with lower MAA amounts discussed before, the SFG C-H stretching signals detected from 1.8MAA/silica interfaces decrease upon addition of AEAPS. Such signals did not further decrease substantially when the adhesion promoter concentration was increased (from 0.5% to 1.0%). As discussed above, the reduction of C-H signals may be correlated with stronger interfacial adhesion.[35, 39, 43] We did not detect distinguishable N-H stretching signals

from the adhesion promoter amine groups at the interface, but we see the impact of AEAPS on the interfacial structures in these data.

Table 5.3 Fitting parameters of the SFG spectra collected from the interfaces between silica and BAMMA base polymers containing 1.8 % MAA and different amounts of amino silane.

	0.0% AEAPS			0.5% AEAPS			1.0% AEAPS		
ppp Assignment	A	ω(cm^{-1})	Γ (cm^{-1})	A	ω(cm^{-1})	Γ (cm^{-1})	A	ω(cm^{-1})	Γ (cm^{-1})
Sym. Methyl	1.50	2880	30	1.50	2880	30	0.25	2880	30
Asym. Methyl/Sym. Ester Methyl	5.50	2965	20	5.75	2960	20	5.00	2960	20
Asym. Ester Methyl	4.50	2995	20	5.00	2995	20	3.50	2995	15
Sym. Methylene	2.30	2850	25	1.00	2850	25	0.25	2850	25
Asym. Methylene	-15.00	2915	35	-9.50	2920	35	-5.00	2920	25
Acid O-H 1	50.00	3050	250	10.00	3050	245	8.00	3050	245
Acid O-H 2	1.50	3580	75	15.00	3580	200	20.00	3580	200
Water 1	18.00	3250	150	7.00	3250	100	33.00	3200	200
Water 2	2.00	3400	100	7.50	3400	100	25.00	3400	200
ssp Assignment	A	ω(cm^{-1})	Γ (cm^{-1})	A	ω(cm^{-1})	Γ (cm^{-1})	A	ω(cm^{-1})	Γ (cm^{-1})
Sym. Methyl	1.50	2880	30	0.25	2880	30	0.15	2880	30
Asym. Methyl/Sym. Ester Methyl	12.75	2965	20	11.50	2960	20	9.00	2960	20
Asym Ester Methyl	1.25	2990	15	0.50	2995	15	0.50	2995	15
Sym. Methylene	0.25	2850	25	0.25	2850	25	0.15	2850	25
Asym. Methylene	-9.00	2915	35	-7.50	2920	25	-4.25	2920	25
Acid O-H 1	30.00	3050	245	0.50	3050	245	8.50	3050	245
Acid O-H 2	3.00	3580	75	30.00	3580	200	35.00	3580	200
Water 1	18.00	3250	150	8.50	3200	100	24.00	3200	200
Water 2	5.00	3400	100	5.50	3400	100	33.00	3400	200

5.3.4 C=O region

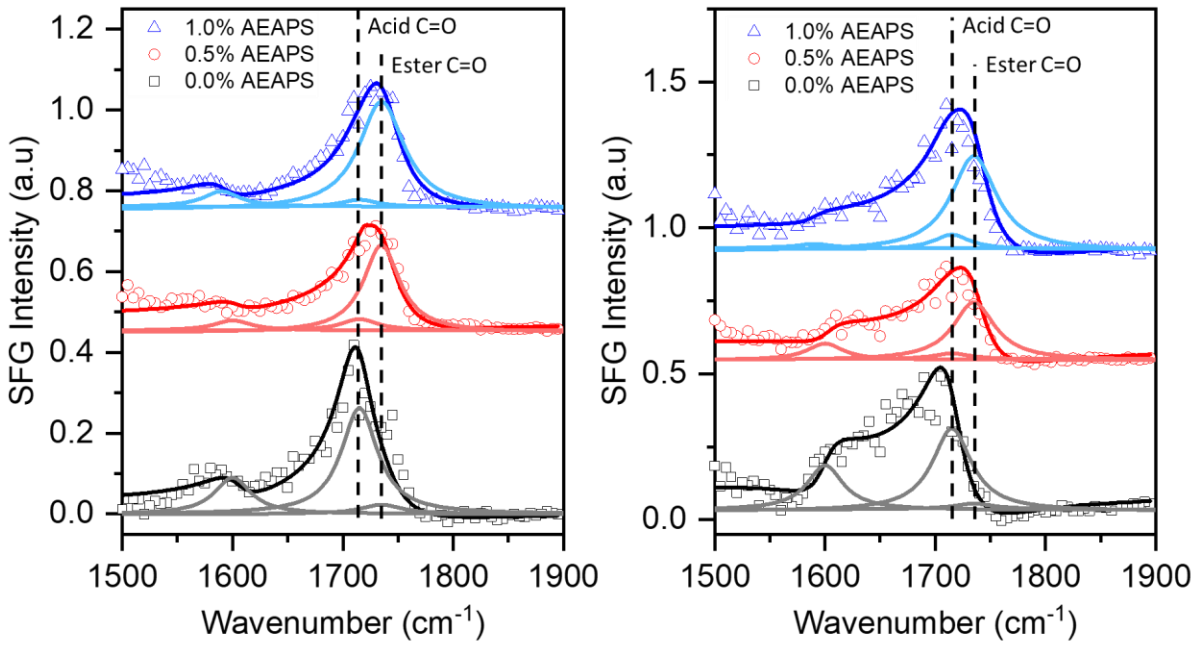

Figure 5.7 SFG ssp (left) and ppp (right) spectra collected from the interfaces between silica and BAMMA polymers containing 1.4% MAA and different amounts of AEAPS in the C=O stretching frequency region. Symbols represent experimental data points while lines represent fits to the data and underlying bands. Fitting parameters can be found in **Table 5.4**.

To further investigate the interfacial MAA acid behavior at the BAMMA/silica interfaces, SFG spectra were collected in the C=O stretching frequency region (**Figure 5.7**) to study interfacial carboxylic acid and ester groups. Here 1.4MAA polymer, the intermediate MAA concentration of the three samples studied, was examined. Without AEAPS, the SFG spectra collected from the 1.4MAA/silica interface, shown as black lines in **Figure 5.7**, contain two main peaks: a lower frequency peak centered at 1715 cm^{-1} assigned to the MAA carboxylic acid C=O stretching and another at 1735 cm^{-1} assigned to the C=O stretching of the ester groups of the MMA and BA components in BAMMA polymer. This was consistent with the presence of acid groups from the polymer at the interface and agrees with the previously presented results on SFG O-H stretching signals. After addition of the adhesion promoter AEAPS to the polymer, much weaker

signals from the MAA component are observed and similarly supports reduction of interfacial MAA acid groups at the silica/polymer interface by the adhesion promoter. The increased SFG signal intensity detected from the ester C=O stretching after the introduction of AEAPS indicates that more ester carbonyl groups move to the silica interface and/or they become more ordered. The observation of decreased interfacial C-H groups shown earlier and increased C=O ester groups shown here is consistent with increased interfacial adhesion.[43]

Table 5.4 Fitting parameters of SFG spectra collected from the interfaces between silica and BAMMA base polymers containing 1.4% MAA and different amounts of amino silane in the C=O stretching frequency region

	0.0% AEAPS			**0.5% AEAPS**			**1.0% AEAPS**		
ppp Assignment	A	ω(cm^{-1})	Γ (cm^{-1})	A	ω(cm^{-1})	Γ (cm^{-1})	A	ω(cm^{-1})	Γ (cm^{-1})
??	-3.50	1600	20	-1.50	1603	20	-0.750	1590	20
Acid	11.50	1715	21.64	0.89	1715	20	2.000	1715	20
Ester	1.01	1735	23	10.25	1735	23	14.250	1735	25
ssp Assignment	A	ω(cm^{-1})	Γ (cm^{-1})	A	ω(cm^{-1})	Γ (cm^{-1})	A	ω(cm^{-1})	Γ (cm^{-1})
??	1.90	1603	20	1.00	1603	20	1.750	1590	20
Acid	10.25	1715	20	0.15	1715	20	0.850	1715	20
Ester	3.50	1735	23	10.75	1735	23	12.940	1735	25

5.4 Discussion: Proposed adhesion mechanism of AEAPS at BAMMA/glass interface

In this study, three BAMMA latex polymers with different levels of MAA were investigated. The only difference between the three BAMMA polymers was the different MAA amount (i.e. the ratio of BA to MMA was held constant). The three BAMMA polymers contain 0.7 wt%, 1.4 wt%, and 1.8 wt% MAA respectively. A control sample with 0 wt% MAA was not included in the study because the absence of MAA would lead to an unstable emulsion. For each BAMMA polymer with different MAA content, three levels of added AEAPS was examined

(0.0%, 0.5%, and 1.0% based on polymer solids). Therefore, for the three BAMMA polymers, a total of nine different samples were studied.

Although AEAPS was added to the polymer emulsion by percent weight, the stoichiometry of the acid group and the amine group of AEAPS is important to consider. For the 0.7MAA samples spiked with AEAPS, there was an approximate stoichiometric equivalence of amine functionality to acid functionality available at 1.0% AEAPS; however, for 1.4MAA, there was always a stoichiometric deficiency of amine groups relative to acid groups from MAA. There was an even larger stoichiometric deficiency of amine groups from AEAPS relative to acid groups from MAA in the formulations of 1.8MAA. For example, at 0.5% AEAPS there was about 25% of what would be necessary for stoichiometric equivalence and at 1% AEAPS, there was about 50% of what would be needed. This deficiency in amine allows the influence of the acid at higher concentrations to be probed.

The SFG results in both C-H/O-H and C=O stretching frequency regions obtained with different amounts of copolymerized MAA and AEAPS adhesion promoter demonstrate that both the MAA content and AEAPS influence the interfacial structure at the glass interface. A number of different interactions between MAA and AEAPS could occur. One potential mechanism is a physical interaction only scenario (without any formation of chemical bonds) where the amino group of AEAPS causes the MAA acid groups of BAMMA to become disordered, leading to decreased SFG O-H and acid C=O stretching signals (**Figure 5.8 (a)**).[44-45] However, we believe that this physical interaction scenario is unlikely. Since the BAMMA system was applied as an aqueous emulsion onto silica and then dried, acid-base reactions are expected to easily occur. A possible interaction of MAA and AEAPS is through an ionic interaction where MAA is deprotonated and the amine is protonated, creating a carboxylate anion and ammonium cation that

form an ionic bond (**Figure 5.8 (b)**). Ionic bond formation is supported by the disappearance/reduction of the carboxylic acid SFG signal in both the O-H and C=O stretching frequency regions. The third possible mechanism is shown in **Figure 5.8 (c)**. Upon dehydration and under optimal reaction conditions, the ionic pair could react further to form an amide. An amide bond formation is also supported by the disappearance of the SFG O-H and carbonyl C=O stretching signals. However, if the amide bond formation occurred, an amide C=O stretching signal in the SFG spectra at around 1640 cm^{-1} should appear, which was not detected in our experiments. Certainly, the absence of detected amide C=O signals may be due to the disordering of the amide groups at the interface, but we believe that this is unlikely because the silica interface is hydrophilic. The hydrophilic amide C=O groups are expected to be ordered at the hydrophilic interface.[46-49] We therefore believe that the second mechanism described above is more reasonable. The ionic interaction between MAA acid and amine functionality from AEAPS at the interface is the most likely.

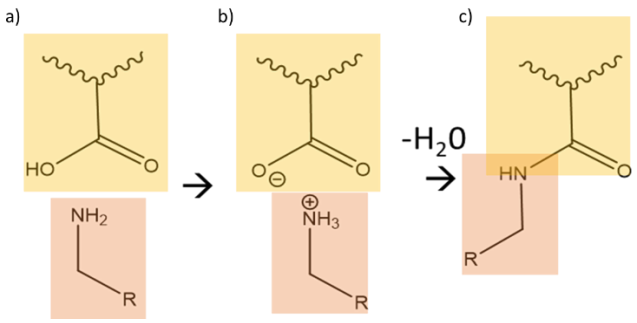

Figure 5.8 Three possible mechanisms of MAA – AEAPS interactions. Interaction a) indicates hydrogen bonding or weaker type of Van der Waals interaction, b) shows formation of an ionic bond between the acid and amine group, and c) depicts the formation of an amide bond by elimination of water.

It is well known that ordered self-assembled layers can be formed on glass or silica with silane molecules containing methoxy head groups.[50-53] Methoxy head groups are also easily hydrolyzed and can react with hydroxyl groups. Our previous SFG studies on silicone adhesives

with silane adhesion promoters containing methoxy head groups showed interfacial segregation and reaction of methoxy groups at buried interfaces.[54-58] In this study, methoxy groups were not observed at the interface because they have presumably already hydrolyzed before the drying process. While we could not directly observe the chemical reaction between AEAPS and silica substrate, earlier work suggests that AEAPS can react with silica and form a covalent interaction.

Extensive research has been performed to study preparation of thin films or SAMs using amino silanes on glass, silica, and other substrates. Such thin films can be prepared using silane vapor or silane solutions including organic solvent solutions and aqueous solutions.[9, 50-51, 54, 59-64] Since this study investigated a water-based acrylate coating, the interfacial behavior of amino silane in an aqueous environment is more relevant. It was reported that it is feasible to deposit amino silanes on silica substrate from aqueous solutions and generate a stable monolayer coating.[60] This publication also indicates that for aqueous solution deposition of amino silane, the silane head groups' (such as methoxy groups') chemical reactions with the surface OH groups are important, while the ionic interaction between NH_3^+ and the surface may also play a role.[64] It was also found that for a SAM deposited using amino silane in water, about 70% amino groups are still accessible, thus only about 30% amino groups interact with the surface or other parts of the silane molecule or other silane molecules, showing that the main interaction between the amino silane and surface should be the chemical reaction between the silane head groups and the surface, not interactions involving the amino groups.[59]

Our observations were consistent with the interaction of AEAPS adhesion promoter molecules with silica substrate through covalent bonding with the head groups and interaction with the MAA component in BAMMA through ionic interactions with the amine functional tails. At the same time, our SFG results showed that with the addition of adhesion promoter to BAMMA,

more ester C=O groups segregate and are ordered at the silica interface while the level of CH groups at the interface is either reduced or they are more disordered. These effects appear to further enhance the adhesion between BAMMA and silica. A schematic of the proposed mechanism is visualized in **Figure 5.9**.

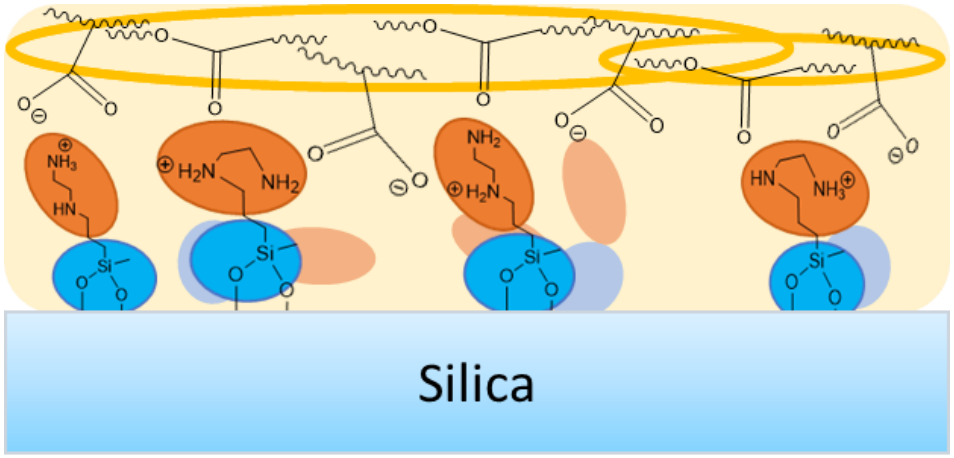

Figure 5.9 Depiction of the BAMMA interface with AEAPS present. Silane groups are bonded to the silica substrate through covalent bonds, and ammonium groups interact with carboxylate through ionic bonds.

It is worth mentioning that the presence of residual water molecules at the BAMMA/silica interface may reduce the interfacial adhesion. Our SFG studies showed that with higher MAA amount and higher AEAPS amount, interfacial water can be detected using SFG. An optimal concentration of MAA and AEPAS may be needed in BAMMA formulations to avoid interfacial water and maximize the interfacial adhesion.

5.5 Conclusions

In this study, SFG was used to investigate the influence of the adhesion promoter AEAPS on the structures of BAMMA/silica buried interfaces to understand the adhesion promoter mechanism at the molecular level. AEAPS addition resulted in reduced SFG hydroxyl and

carbonyl signals from MAA in BAMMA samples. The SFG signals from C-H groups of BAMMA also decreased upon addition of AEAPS. The reduction of these groups can be associated with various mechanisms that result in higher polymer adhesion to the silica substrate. The results suggest the most likely interaction mechanism between interfacial AEAPS and MAA functionality was the formation of ionic bonds through carboxylate groups and ammonium ions, leading to strong interactions between AEAPS bonded to the silica interface through siloxane linkages and the BAMMA polymer. As we discussed above, the amino silane molecules reacted with substrate surfaces via chemical reactions between silane head groups and surface OH groups. Therefore, the strong adhesion between BAMMA and silica was through the covalent interaction between silica and head groups of the adhesion promoter AEAPS and through ionic interaction between end group of AEAPS and the MAA component in BAMMA. The interfacially-segregated combination of AEAPS and polymer acid groups made the interface more hydrophilic, leading to increased amount and/or ordering of ester C=O groups and reduced level and/or disordering of C-H groups, further enhancing the interfacial adhesion between silica and BAMMA. Further increasing the MAA content in BAMMA in the presence of the same amount of adhesion promoter, AEAPS, may lead to an even more hydrophilic silica interface, resulting in the presence of interface water which could reduce adhesion.

The two amine groups in AEAPS (primary and secondary) may form varied intramolecular or intermolecular interactions, which could not be determined in this study. A model system with silane solution (without BAMMA polymer) interacting with silica can be studied with SFG in combination with computer simulation to further reveal the detailed amino silane – silica interaction in the future, which is beyond the scope of this research. Nevertheless, new information has been gained on the change in interfacial structure of select acrylic-based copolymers at silica

substrate in the presence of a common aminosilane adhesion promoter. These changes in interfacial structure give insight into the mechanism of adhesion enhancement that aminosilanes such as AEAPS provide for acrylic copolymers at glass substrates and can be extended to explore mechanisms for other aminosilane-based adhesion promoters and acrylic polymers.

5.6 References

1. Ulrich, N. W.; Myers, J. N.; Chen, Z., Characterization of polymer/epoxy buried interfaces with silane adhesion promoters before and after hygrothermal aging for the elucidation of molecular level details relevant to adhesion. *RSC Advances* **2015,** *5* (128), 105622-105631.
2. Fang, Y.; Li, B.; Yu, J.; Zhou, J.; Xu, X.; Shao, W.; Lu, X., Probing surface and interfacial molecular structures of a rubbery adhesion promoter using sum frequency generation vibrational spectroscopy. *Surface Science* **2013,** *615*, 26-32.
3. Zhang, X.; Carter, M. C. D.; Belowich, M. E.; Wan, G.; Crimmins, M.; Laughlin, K. B.; Even, R. C.; Kalantar, T. H., Catechol-Functionalized Latex Polymers Display Improved Adhesion to Low-Surface-Energy Thermoplastic Polyolefin Substrates. *ACS Applied Polymer Materials* **2019,** *1* (6), 1317-1325.
4. Gong, L.; Xiang, L.; Zhang, J.; Chen, J.; Zeng, H., Fundamentals and advances in the adhesion of polymer surfaces and thin films. *Langmuir* **2019,** *35* (48), 15914-15936.
5. *Multicomponent Polymeric Materials*. Springer: 2016; Vol. 223.
6. Chevallier, P.; Turgeon, S.; Sarra-Bournet, C.; Turcotte, R.; Laroche, G., Characterization of multilayer anti-fog coatings. *ACS Appl Mater Interfaces* **2011,** *3* (3), 750-8.
7. Song, Y.-W.; Do, H.-S.; Joo, H.-S.; Lim, D.-H.; Kim, S.; Kim, H.-J., Effect of grafting of acrylic acid onto PET film surfaces by UV irradiation on the adhesion of PSAs. *Journal of Adhesion Science and Technology* **2006,** *20* (12), 1357-1365.
8. Jo, H.; Blum, F. D., Characterization of the Interface in Polymer-Silica Composites Containing an Acrylic Silane Coupling Agent. *Chem Mater* **1999,** *11* (9), 2548-2553.
9. Giraud, L.; Nadarajah, R.; Matar, Y.; Bazin, G.; Sun, J.; Zhu, X. X.; Giasson, S., Amino-functionalized monolayers covalently grafted to silica-based substrates as a robust primer anchorage in aqueous media. *Applied Surface Science* **2016,** *370*, 476-485.
10. Aboudzadeh, M. A.; Mirabedini, S. M.; Atai, M., Effect of silane-based treatment on the adhesion strength of acrylic lacquers on the PP surfaces. *International Journal of Adhesion and Adhesives* **2007,** *27* (7), 519-526.
11. Plueddemann, E. P., Adhesion Through Silane Coupling Agents. *The Journal of Adhesion* **2008,** *2* (3), 184-201.
12. Sonnenschein, M. F.; Webb, S. P.; Wendt, B. L., Poly(acrylate/siloxane) hybrid adhesives for polymers with low surface energy. *International Journal of Adhesion and Adhesives* **2008,** *28* (3), 126-134.
13. Steward, P. A.; Hearna, J.; Wilkinsonb, M. C., An overview of polymer latex film formation and properties. *Advances in Colloid and Interface Science* **2000,** *86*, 195-267.
14. Andre, J. S.; Ulrich, N.; Ji, K.; Chen, Z., Interfacial behavior of flux residues and its impact on copper/underfill adhesion in microelectronic packaging. *J. Electron. Packag.* **2021,** *143*, 011004.

15. Myers, J. N.; Zhang, X.; Xiu, Y.; Wei, Y.; Williamson, J. M.; Lee, K.-W.; Chen, Z., Nondestructive characterization of molecular structures at buried copper/epoxy interfaces and their relationship to locus of failure analysis. *IEEE Trans. Adv. Packag.* **2015,** *5* (10), 1432-1440.
16. Xiao, M.; Lu, T.; Lin, T.; Andre, J. S.; Chen, Z., Understanding Molecular Structures of Buried Interfaces in Halide Perovskite Photovoltaic Devices Nondestructively with Sub-Monolayer Sensitivity Using Sum Frequency Generation Vibrational Spectroscopy. *Advanced Energy Materials* **2019,** *10* (26), 1903053.
17. Andre, J. S.; Li, B.; Chen, X.; Paradkar, R.; Walther, B.; Feng, C.; Tucker, C.; Mohler, C.; Chen, Z., Interfacial reaction of a maleic anhydride grafted polyolefin with ethylene vinyl alcohol copolymer at the buried solid/solid interface. *Polymer* **2021,** *212*, 123141.
18. Li, B.; Andre, J. S.; Chen, X.; Walther, B.; Paradkar, R.; Feng, C.; Tucker, C.; Mohler, C.; Chen, Z., Observing a chemical reaction at a buried solid/solid interface in situ. *Anal. Chem.* **2020,** *92* (20), 14145-14152.
19. Zhang, S.; Andre, J. S.; Hsu, L.; Toolis, A.; Esarey, S. L.; Li, B.; Chen, Z., Nondestructive in situ detection of chemical reactions at the buried interface between polyurethane and isocyanate-based primer. *Macromolecules* **2020,** *53* (22), 10189-10197.
20. Yamamoto, S.; Kuwahara, R.; Aoki, M.; Shundo, A.; Tanaka, K., Molecular events for an epoxy–amine system at a copper interface. *ACS Appl. Polym. Mater.* **2020,** *2* (4), 1474-1481.
21. Hong, Y.; Bao, S.; Xiang, X.; Wang, X., Concentration-Dominated Orientation of Phenyl Groups at the Polystyrene/Graphene Interface. *ACS Macro Letters* **2020,** *9* (6), 889-894.
22. Zuo, B.; Zhou, H.; Davis, M. J. B.; Wang, X.; Priestley, R. D., Effect of Local Chain Conformation in Adsorbed Nanolayers on Confined Polymer Molecular Mobility. *Physical Review Letters* **2019,** *122* (21).
23. Aoki, M.; Shundo, A.; Okamoto, K.; Ganbe, T.; Tanaka, K., Segregation of an amine component in a model epoxy resin at a copper interface. *Polymer Journal* **2018,** *51* (3), 359-363.
24. Xiao, M.; Joglekar, S.; Zhang, X.; Jasensky, J.; Ma, J.; Cui, Q.; Guo, L. J.; Chen, Z., Effect of Interfacial Molecular Orientation on Power Conversion Efficiency of Perovskite Solar Cells. *J Am Chem Soc* **2017,** *139* (9), 3378-3386.
25. Sugimoto, S.; Inutsuka, M.; Kawaguchi, D.; Tanaka, K., Reorientation Kinetics of Local Conformation of Polyisoprene at Substrate Interface. *ACS Macro Letters* **2017,** *7* (1), 85-89.
26. Guo, W.; Xu, S.; Reichart, T. M.; Xiao, M.; Lu, T.; Mello, C.; Chen, Z., Probing Molecular Interactions between Surface-Immobilized Antimicrobial Peptides and Lipopolysaccharides In Situ. *Langmuir* **2020,** *36* (41), 12383-12393.
27. Alamdari, S.; Roeters, S. J.; Golbek, T. W.; Schmuser, L.; Weidner, T.; Pfaendtner, J., Orientation and Conformation of Proteins at the Air-Water Interface Determined from Integrative Molecular Dynamics Simulations and Sum Frequency Generation Spectroscopy. *Langmuir* **2020,** *36* (40), 11855-11865.
28. Golbek, T. W.; Schmuser, L.; Rasmussen, M. H.; Poulsen, T. B.; Weidner, T., Lasalocid Acid Antibiotic at a Membrane Surface Probed by Sum Frequency Generation Spectroscopy. *Langmuir* **2020,** *36* (12), 3184-3192.
29. Weidner, T.; Apte, J. S.; Gamble, L. J.; Castner, D. G., Probing the orientation and conformation of alpha-helix and beta-strand model peptides on self-assembled monolayers

using sum frequency generation and NEXAFS spectroscopy. *Langmuir* **2010,** *26* (5), 3433-3440.
30. Lin, T.; Guo, W.; Guo, R.; Chen, Z., Probing Biological Molecule Orientation and Polymer Surface Structure at the Polymer/Solution Interface In Situ. *Langmuir* **2020,** *36* (26), 7681-7690.
31. Li, X.; Li, B.; Zhang, X.; Li, C.; Guo, Z.; Zhou, D.; Lu, X., Detecting Surface Hydration of Poly(2-hydroxyethyl methacrylate) in Solution in situ. *Macromolecules* **2016,** *49* (8), 3116-3125.
32. Zhang, J.; Tan, J.; Pei, R.; Ye, S., Acidic Environment Significantly Alters Aggregation Pathway of Human Islet Amyloid Polypeptide at Negative Lipid Membrane. *Langmuir* **2020,** *36* (6), 1530-1537.
33. Wang, W.; Tan, J.; Ye, S., Unsaturated Lipid Accelerates Formation of Oligomeric beta-Sheet Structure of GP41 Fusion Peptide in Model Cell Membrane. *J Phys Chem B* **2020,** *124* (25), 5169-5176.
34. Perry, A.; Neipert, C.; Space, B.; Moore, P. B., Theoretical modeling of interface specific vibrational spectroscopy: Methods and applications to aqueous interfaces. *Chem. Rev.* **2006,** *106*, 1234−1258.
35. Lu, X.; Zhang, C.; Ulrich, N.; Xiao, M.; Ma, Y. H.; Chen, Z., Studying polymer surfaces and interfaces with sum frequency generation vibrational spectroscopy. *Anal. Chem.* **2017,** *89* (1), 466-489.
36. Ji, W.-G.; Hu, J.-M.; Zhang, J.-Q.; Cao, C.-N., Reducing the water absorption in epoxy coatings by silane monomer incorporation. *Corrosion Science* **2006,** *48* (11), 3731-3739.
37. Lin-Vien, D.; Colthup, N. B.; Fateley, W. G.; Grasselli, J. G., *The handbook of infrared and Raman characteristic frequencies of organic molecules*. Elsevier: 1991.
38. Ulrich, N. W.; Andre, J. S.; Khanna, K.; Wei, Y.; Xiu, Y.; Chen, Z., Nondestructive analysis of buried interfacial behaviors of flux residue and their impact on interfacial mechanical property. *IEEE Trans. Compon. Packag. Manuf. Technol.* **2018,** *8* (6), 982-990.
39. Ulrich, N. W.; Andre, J.; Williamson, J.; Lee, K. W.; Chen, Z., Plasma treatment effect on polymer buried interfacial structure and property. *Phys. Chem. Chem. Phys.* **2017,** *19* (19), 12144-12155.
40. Inutsuka, M.; Haraguchi, M.; Ozawa, M.; Yamada, N. L.; Tanaka, K., Adhesion Control of Elastomer Sheet on the Basis of Interfacial Segregation of Hyperbranched Polymer. *ACS Macro Letters* **2019,** *8* (3), 267-271.
41. Haynes, D. A.; Pietersen, L. K., Hydrogen bonding networks in ammonium carboxylate salts : the crystal structures of phenylethylammonium fumarate-fumaric acid, phenylethylammonium succinate-succinic acid and anilinium fumarate-fumaric acid. *CrystEngComm* **2008,** *10* (5).
42. Sada, K.; Tani, T.; Shinkai, S., Organic Ammonium Carboxylates as Supramolecular Building Blocks: The Role of Ionic Hydrogen Bonding. *Synlett* **2006,** *2006* (15), 2364-2374.
43. Myers, J. N.; Chen, Z., Polymer molecular behaviors at buried polymer/metal and polymer/polymer interfaces and their relations to adhesion in packaging. *J. Adhes.* **2016,** *93* (13), 1081-1103.
44. Zhao, H.; Tang, S.; Xu, X.; Du, L., Hydrogen Bonding Interaction between Atmospheric Gaseous Amides and Methanol. *Int J Mol Sci* **2016,** *18* (1).

45. Scheiner, S.; Kar, T.; Pattanayak, J., Comparison of Various Types of Hydrogen Bonds Involving Aromatic Amino Acids. *J Am Chem Soc* **2002,** *124*, 13257-13264.
46. Zou, X.; Wei, S.; Badieyan, S.; Schroeder, M.; Jasensky, J.; Brooks, C. L.; Marsh, E. N. G.; Chen, Z., Investigating the Effect of Two-point Surface Attachment on Enzyme Stability and Activity. *J Am Chem Soc* **2018**.
47. Xiao, M.; Wei, S.; Li, Y.; Jasensky, J.; Chen, J.; Brooks, C. L., 3rd; Chen, Z., Molecular interactions between single layered MoS2 and biological molecules. *Chem Sci* **2018,** *9* (7), 1769-1773.
48. Jasensky, J.; Ferguson, K.; Baria, M.; Zou, X.; McGinnis, R.; Kaneshiro, A.; Badieyan, S.; Wei, S.; Marsh, E. N. G.; Chen, Z., Simultaneous observation of the orientation and activity of surface-immobilized enzymes. *Langmuir* **2018,** *34* (31), 9133-9140.
49. Zhang, C.; Myers, J.; Chen, Z., Elucidation of molecular structures at buried polymer interfaces and biological interfaces using sum frequency generation vibrational spectroscopy. *Soft Matter* **2013,** *9*, 4738-4761.
50. Knorr Jr, D. B.; Williams, K. S.; Baril, N. F.; Weiland, C.; Andzelm, J. W.; Lenhart, J. L.; Woicik, J. C.; Fischer, D. A.; Tidrow, M. Z.; Bandara, S. V.; Henry, N. C., Use of 3-aminopropyltriethoxysilane deposited from aqueous solution for surface modification of III-V materials. *Applied Surface Science* **2014,** *320*, 414-428.
51. King, M. D.; Kihara, M. T.; Lott, G. A.; Hill, M. W.; Scatena, L. F., Surface Structures of Amine-Bearing Siloxane Self-Assembled Monolayers: Influence of Conformation on Methylene Vibrational Frequencies. *The Journal of Physical Chemistry C* **2014,** *118* (29), 15804-15815.
52. Jakša, G.; Štefane, B.; Kovač, J., XPS and AFM characterization of aminosilanes with different numbers of bonding sites on a silicon wafer. *Surface and Interface Analysis* **2013,** *45* (11-12), 1709-1713.
53. Kristalyn, C. B.; Watt, S.; Spanninga, S. A.; Barnard, R. A.; Nguyen, K.; Chen, Z., Investigation of sub-monolayer, monolayer, and multilayer self-assembled semifluorinated alkylsilane films. *J Colloid Interface Sci* **2011,** *353* (1), 322-30.
54. Lin, T.; Wu, Y.; Santos, E.; Chen, X.; Ahn, D.; Mohler, C.; Chen, Z., Molecular insights into adhesion at a buried silica-filled silicone/polyethylene terephthalate interface. *Langmuir* **2020,** *36* (49), 15128-15140.
55. Zhang, C.; Chen, Z., Quantitative molecular level understanding of ethoxysilane at poly(dimethylsiloxane)/polymer interfaces. *Langmuir* **2013,** *29* (2), 610-619.
56. Liu, Y.; Leng, C.; Chisholm, B.; Stafslien, S.; Majumdar, P.; Chen, Z., Surface structures of PDMS incorporated with quaternary ammonium salts designed for antibiofouling and fouling release applications. *Langmuir* **2013,** *29* (9), 2897-905.
57. Vazquez, A. V.; Shephard, N. E.; Steinecker, C. L.; Ahn, D.; Spanninga, S.; Chen, Z., Understanding molecular structures of silanes at buried polymer interfaces using sum frequency generation vibrational spectroscopy and relating interfacial structures to polymer adhesion. *J. Colloid. Interface Sci.* **2009,** *331* (2), 408-16.
58. Loch, C. L.; Ahn, D.; Chen, Z., Sum frequency generation vibrational spectroscopic studies on a silane adhesion-promoting mixture at a polymer interface. *J. Phys. Chem. B* **2006,** *110*, 914-918.
59. Bauer, F.; Czihal, S.; Bertmer, M.; Decker, U.; Naumov, S.; Wassersleben, S.; Enke, D., Water-based functionalization of mesoporous siliceous materials, Part 1: Morphology and

stability of grafted 3-aminopropyltriethoxysilane. *Microporous and Mesoporous Materials* **2017,** *250*, 221-231.
60. Yadav, A. R.; Sriram, R.; Carter, J. A.; Miller, B. L., Comparative study of solution-phase and vapor-phase deposition of aminosilanes on silicon dioxide surfaces. *Mater Sci Eng C Mater Biol Appl* **2014,** *35*, 283-90.
61. Zhu, M.; Lerum, M. Z.; Chen, W., How to prepare reproducible, homogeneous, and hydrolytically stable aminosilane-derived layers on silica. *Langmuir* **2012,** *28* (1), 416-23.
62. Cuoq, F.; Masion, A.; Labille, J.; Rose, J.; Ziarelli, F.; Prelot, B.; Bottero, J.-Y., Preparation of amino-functionalized silica in aqueous conditions. *Applied Surface Science* **2013,** *266*, 155-160.
63. Smith, E. A.; Chen, W., How to prevent the loss of surface functionality derived from aminosilanes. *Langmuir* **2008,** *24* (21), 12405-9.
64. Sun, Y.; Yanagisawa, M.; Kunimoto, M.; Nakamura, M.; Homma, T., Depth profiling of APTES self-assembled monolayers using surface-enhanced confocal Raman microspectroscopy. *Spectrochim Acta A Mol Biomol Spectrosc* **2017,** *184*, 1-6.

Chapter 6: UV Sensitive Debonding Self-Assembled Monolayer for Reversible Adhesive Applications

6.1 Introduction

Debonding adhesive interfaces selectively is a desirable feature for many adhesive applications, achieving this end would greatly enhance the ability to recycle many polymer-based products and to recover valuable materials from a variety of applications. Typically, research and new applications in polymer adhesion are aimed at enhancing adhesion between the polymer and substrate, much work has been done in this regard in the electronics and food packaging industry.[1-5] Many types of substrates are of interest when studying polymer adhesion such as semiconductors, metals, dissimilar polymers, and similar polymers where adhesion has been greatly enhanced.[6-20] This enhanced adhesion becomes an issue once the interface in the application is no longer in use; breaking these interfaces is difficult and as a result a large amount of waste is generated. At the end-of-life stage for many of the polymer products containing adhesive interfaces, a method to break the interface selectively would be valuable.[21] Work has been done on this problem at various scales and with different approaches. For example, biomimicry is a pathway to breaking adhesive interfaces: Materials can be developed to mimic the function of a gecko's foot to achieve adhesion and break adhesion selectively.[1, 22-28] This gain or loss of adhesion is reliant on special types of polymers that can disrupt the overall function of the polymer adhesive structure, relying on

nanoscale structures to change at an interface, thus the biomimicry approach is not due to molecular interactions at the interface but due to mechanical and structural properties of the polymers. Devising a method that is general for debonding polymers typically used in industry continues to be elusive.

Here, a method for breaking adhesive interfaces is proposed, which relies on the ability of one of the materials at the adhesive interface to be functionalized with small molecule self-assembled monolayers (SAMs) that contain a cleavable covalent bond.[29-31] SAMs have been used at a variety of interfaces for a number of different applications, such as surface reaction modifiers, chemical probes, electronics insulators, and adhesion promoters.[32-36] The method developed here depends on a chemical change in the system rather than a mechanical change to achieve debonding. Specifically, this research explores the ability of a silane-based SAM on silica to debond polymer adhesives from the silica surface. Silica serves as a model for glass. Different polymer adhesives, an epoxy adhesive and a silicone adhesive, were chosen to show the general applicability of the debonding SAM application in this study.

SAMs with similar structure to the one studied here have been shown to have light sensitive bonds are used in a variety of applications[37], notably in drug delivery applications.[30, 38-40] The steps to form the debonding SAM are shown in **Figure 6.1**, in which the complete SAM and the assumed structure in air after UV treatment is shown. The debonding mechanism relies on the cleavage of a thioester bond with UV light (365 nm), and is used to reduce adhesion at polymer interfaces here.[30, 41] The mechanism of action is the nitro group on the benzene ring which acts as a withdrawing/oxidizing group, allowing the ether and thioether bonds to be more UV sensitive.[41-44] Because this chemistry is documented, the SAM presented was chose as the proof-of-principle system to study. The steps to make the SAM will be discussed further in the methods section.

To better understand how the debonding SAM behaves at an adhesive interface, sum frequency generation (SFG) vibrational spectroscopy was employed. As presented in the previous chapters in this thesis, SFG has been used to study adhesive interfaces related to many applications, notably in the electronics industry and blown film polyolefin-based packaging.[6-7, 10, 13, 45-47] SFG is a key tool to reveal molecular structures, chemical interactions, and functional group orientations at surfaces and buried interfaces specifically.[48-60] Traditionally, an interface can be studied by breaking the interface and analyzing the resulting surfaces with methods such as XRD, FTIR, Raman scattering, and many others, with the assumption that the exposed surfaces serve as good models of the buried interface. However, breaking an interface destroys the interfacial interactions, which very likely leads to studying surfaces that are not representative of the original buried interface. Recently SFG has been employed to study polymer adhesive interfaces and was used to elucidate chemical reactions occurring at the buried polymer/polymer interface in situ in real time.[7-8, 10] SFG has also been widely used to explore hard/soft interfaces between silica and a variety of polymer materials in situ nondestructively.[61-68] Details on SFG theory and experiments were discussed in the previous chapters.

In this study, along with SFG, the SAM structure was characterized with x-ray photoelectron spectroscopy (XPS). These results were important for determining the completion of the SAM on the silica surface as well as provide insight into the functionality that does not show up in the SFG spectra due to various reasons. To support the SFG and XPS data, water contact angle measurements were carried out for each SAM preparation step. Lap shear adhesion testing was also performed to determine the effectiveness of the debonding SAM. In addition, control experiments were performed to show that the adhesive polymers were not affected by the UV light treatment and that the adhesion loss was due to the SAM being cleaved at the buried interface. It

is worth mentioning that we have not proved that the thin silane coating layer in this study is indeed an ordered single monolayer. Here "SAM" means the thin silane coating layer and we used "SAM" for simplicity.

6.2 Materials and methods

6.2.1 Materials

IR grade fused silica (IRFS) prisms or windows (Altos Photonics, Bozeman MT) were used in all the spectroscopy experiments. For lap shear experiments, glass microscope slides (Fisher Scientific, Hampton NH) were used. All chemicals used in this research were purchased from Sigma Aldrich, St. Louis MO unless stated otherwise. Anhydrous toluene and N, N-dimethylformamide (DMF) were used as solvents in reactions involving the SAM. The SAM is constructed from (3-aminopropyl) triethoxysilane (APTES), 4-bromomethyl-3-nitrobenzoic acid (BNBA) coupled with N, N′-dicyclohexylcarbodiimide (DCC), and 6-mecpro-1-hexanol (mercaptohexanol). One of the adhesives studied consists of poly (dimethyl siloxane) (PDMS, Sylgard 184 silicone elastomer, The Dow Chemical Company, Midland MI) with 1% wt/wt (3-glycidyloxypropyl) trimethoxysilane (γ-GPS) added as an adhesion promoter. The other adhesive, an epoxy adhesive consisting of bisphenol A diglycidyl ether (BADGE) cured with 4,4'-diaminodiphenylmethane (DDM) (Tokyo Chemical Industry Co., Tokyo Japan) was also studied. The epoxy materials were solid at room temperature and needed to be melted at a slightly elevated temperature with a heat gun to make a liquid epoxy solution. The reaction for making the SAM and the bonding adhesives can be found in **Figure 6.1**.

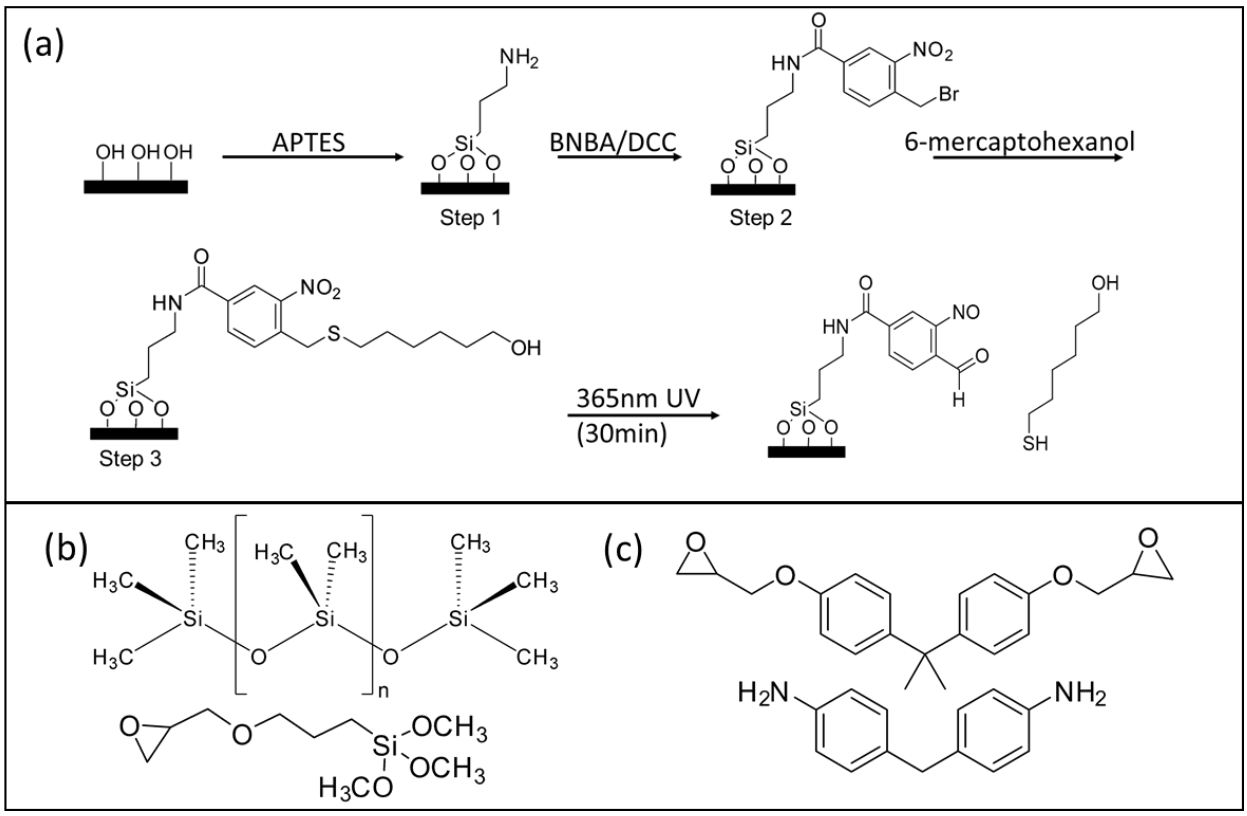

Figure 6.1: Structures of the debonding SAM (a) and adhesives (b and c) utilized in this study. Bottom of (a) shows the complete SAM and the proposed SAM after UV treatment in air. PDMS with γ-GPS adhesion promoter (b) and BADGE and the DDM curing agent (c).

6.2.2 Sample preparation

The debonding SAM was prepared in three steps on clean IRFS prisms for SFG. IRFS prisms were cleaned in a solution of potassium dichromate in sulfuric acid for at least 24 hours, followed by rising with water, drying with a nitrogen stream, and finally treated with air plasma (PE-50, Plasma Etch Inc., Carson City NV) for 5 minutes. Clean IRFS prisms were again treated with air plasma for 3 minutes, to ensure the silica surface was functionalized with hydroxyl groups for reaction with silane groups on APTES. After the second plasma treatment IRFS prisms were immediately transferred to clean glass containers containing a 2% (wt/wt) solution of APTES in anhydrous toluene and sealed. The APTES solution with IRFS prisms were kept at 70 °C for 24

hours in dark conditions. After the 24-hour period, the prisms/windows with the SAM were rinsed with toluene, ethanol and finally water, and then dried with nitrogen. To anneal the APTES on the silica surface, the prisms/windows were placed in an oven set to 110 °C for 15 minutes. After the substrates cooled, they were rinsed again with toluene, ethanol, and water. They were then dried with nitrogen and ready for further SAM functionalization or for analysis. The top-left in **Figure 6.1 (a)** shows the structure of the APTES SAM on silica.

After the APTES SAM was formed on the IRFS surface the substrates were ready for coupling of BNBA via a DCC coupling reaction to the terminal amine of the APTES SAM. Equal molar solutions of 4 mM DCC and BMNA in DMF were prepared, then mixed 1:1 by volume and the substrates were placed in the solution. The reaction was kept at 70 °C for 48 hours in dark conditions. Substrates were removed from the solution then rinsed with toluene, ethanol, and water. The structure of the SAM after the DCC coupling step is shown in the top-right of **Figure 6.1 (a)**. Substrates were ready for analysis or further functionalization.

Finally, to form the light sensitive sulfide bond and complete the debonding SAM, a solution of 4 mM mercaptohexanol was prepared in DMF. A drop of 0.5 M sodium hydroxide was added to the solution to help accelerate the reaction. Substrates were placed in the solution and kept in the dark. The reaction was performed at room temperature for 24 hours. Once complete the substrates were removed from the mercaptohexanol solution and rinsed with toluene, ethanol, and water then dried under nitrogen. The complete deboning SAM is shown in **Figure 6.1 (a)**. The substrates were then ready for analysis and contact with adhesive materials. The UV degradation of the sulfide bond shown in **Figure 6.1 (a)** is consistent with lituratre.[30, 43-44, 69]

To cleave the mercapto group from the surface the SAM, a UV lamp (Spectroline ENF-240C) at 365 nm was used. For surface characterization the UV light was held about 2.5 cm above

the SAM surface. For adhesion studies the UV light was held 2.5 cm above the microscope slide and the SAM was exposed to UV irradiation after it was passed through the substrate. UV exposure time for all samples was 30 minutes. The UV light intensity was ~300 μW/cm^2.

The PDMS adhesive was prepared by mixing 10 parts base resin to 1 part curing agent by weight. 1% (wt/wt) γ-GPS was added to the PDMS mixture to act as an adhesion promoter, then was mixed well. The mixture was applied to the SAM surface and then cured at 100 °C for 4 hours. The PDMS and γ-GPS structures are shown in **Figure 6.1 (b)**. According to the manufacturer's technical data sheet, the glass transition temperature (Tg) of PDMS is -60 °C, and the operation temperatures are -45 to 200 °C. Therefore, PDMS can be cured at room temperature or at elevated temperatures according to the manufacturer's specification.

The BADGE epoxy adhesive was prepared by melting a 2:1 mol ratio of BADGE and DDM, then mixing vigorously. The epoxy was applied to the SAM and cured for 1 hour at 50 °C, 1 hour at 75 °C, and 1 hour at 110 °C. **Figure 6.1 (c)** shows the structures of the BADGE epoxy and the DDM curing agent. The T_g of BADGE cured with DDM was reported to be between 178 °C and 189 °C, depending on the curing conditions.[70] The BADGE sample in this study falls within these limits as the curing conditions are similar to that reported in the literature.[6, 46]

Two types of samples were prepared: (1) The SAM was prepared on IRFS prisms for SFG spectroscopy measurements, and on IRFS windows for XPS analysis. (2) The SAM sample was prepared on glass microscope slides for mechanical adhesion testing. SFG samples had the SAM and adhesive applied to the base of the prism, **Figure 6.2** shows all sample geometries for data collection used in this study. For SFG studies the adhesive polymer layer was at least 4 mm thick, for adhesion studies the adhesive polymer layer was much thinner (<1 mm).

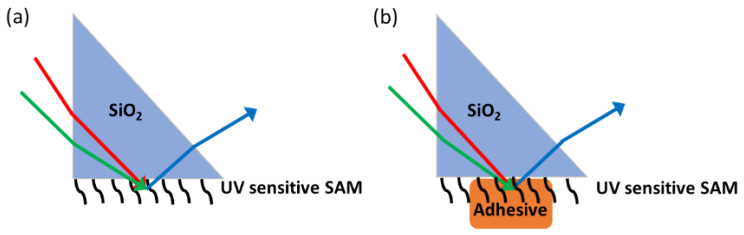

Figure 6.1: Experimental sample geometries used to study the SAM and buried interface. For SFG, prism geometry was used to study the debonding SAM surface (a), and the buried debonding SAM/adhesive interfaces (b).

6.2.3 Instrumentation

SFG experimental background, instrumentation, and data analysis were covered in the previous chapters and will not be covered further here.

XPS measurements were made using a Kratos Axis Ultra XPS (Kyoto Japan) to confirm that we successfully prepared the SAM on the silica substrate. Elemental analysis of bromine at the second step of the reaction and sulfur at the third step of the reaction was performed. To generate the x-ray, an 8 mA emission current and 14 kV high voltage were used. For the survey scan, 160 eV pass energy was used, while 20 eV pass energy was used for the core scan on bromine and sulfur. Collection time for bromine was 15 minutes, and 45 minutes for sulfur.

Mechanical adhesion tests were performed using a lap shear geometry following the ASTM D3163 standard method. Samples had on average a half-centimeter overlap on the microscope slides used. The test was performed at room temperature with an Instron 5544 mechanical testing device (Instron Co., Norwood MA). When the lap shear samples broke at the interface, a sudden drop in shear force was observed and recorded. Four types of samples were prepared for adhesion testing: (1) adhesive on silica with neither debonding SAM or UV light treatment, (2) adhesive on silica with no debonding SAM but with UV light treatment, (3) adhesive on silica with debonding

SAM but no UV light treatment, and (4) adhesive on silica with both debonding SAM after UV light treatment. All the results presented are an average of the data tested for 10 or more samples.

A CAM 100 optical contact angle goniometer (KSV Instruments, Finland) was used to measure static water contact angles on the silica/SAM surface after each step of the reaction, which can be a metric to characterize the surface modification at each step. Samples used for contact angle measurements were prepared in the same fashion as the lap shear samples, on microscope slides.

6.3 Results and discussion

6.3.1 Characterizing the debonding SAM surface

To confirm that the debonding SAM was successfully synthesized on silica surfaces, SFG, XPS, and contact angel measurements were utilized. **Figure 6.3** shows the SFG spectra collected after each step of the SAM formation. In panel (a) there is a clear peak from the APTES amine group at 3300 cm^{-1}, contributed by the N-H stretching mode, indicating the formation of APTES SAM, terminated by the NH_2 group, as expected. This peak is a result of ordered amine groups of the APTES SAM on the silica surface. Other peaks in this spectrum are contributions from the methylene (CH_2) groups. The broad peak centered at ~3120 cm^{-1} is likely contributed by adsorbed water on the surface which has strong hydrogen bonding. The APTES SAM has substantial surface coverage of NH_2 groups, which can strongly interact with water molecules, leading to strongly hydrogen bonded water molecules on the surface.

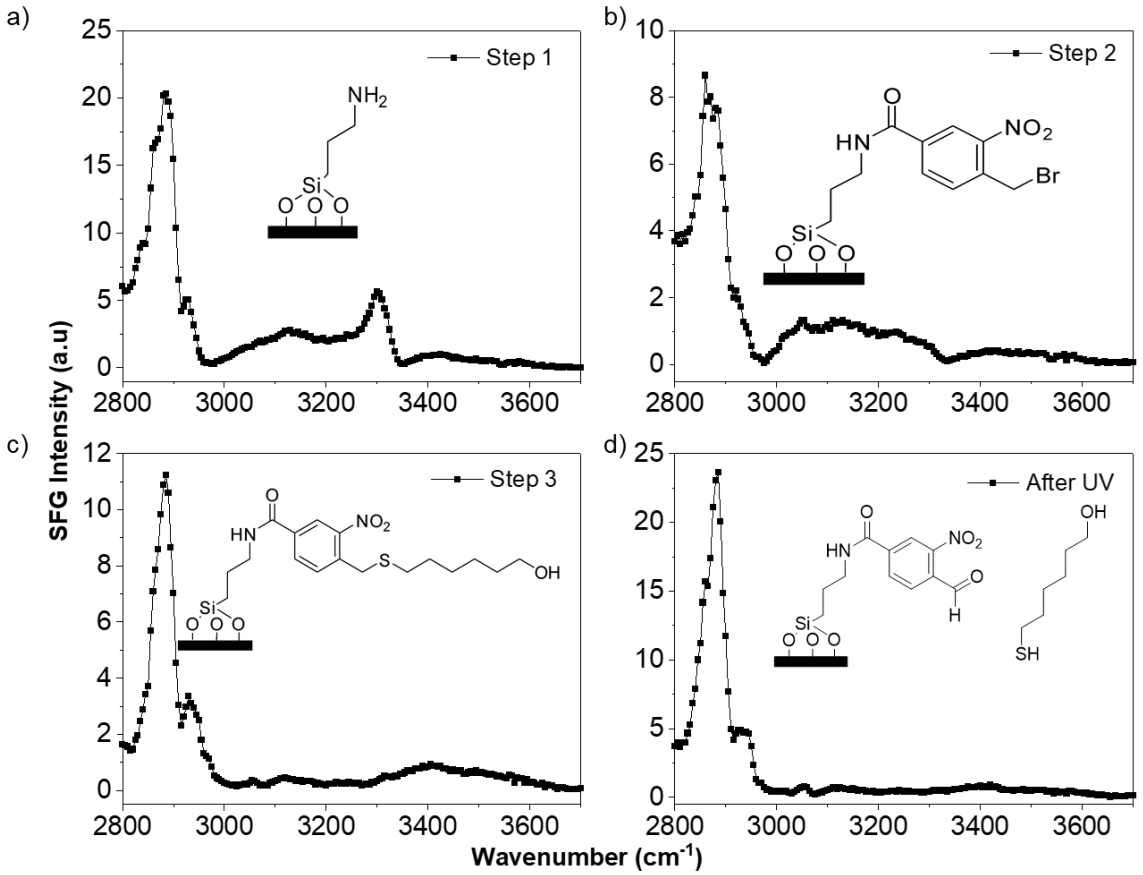

Figure 6.3: SFG spectra of the debonding SAM surface at each step. Panel (a) shows SFG spectra of the APTES SAM, (b) shows SFG result from the coupling of BNBA to the APTES amine group, and (c) shows after addition of the mercaptohexanol the debonding SAM. Panel (d) is the SFG spectrum of the SAM surface after 365 nm UV treatment.

In **Figure 6.3 (b)**, SFG features contributed from the methylene groups are observed as before, but the strong amine peak at about 3300 cm^{-1} disappeared, and a small peak from aromatic C-H stretching around 3050 cm^{-1} was found. This result shows that the amine end group of the previously formed APTES SAM was reacted as desired, and the BNBA functionality was coupled to the SAM successfully, as shown in the schematic in **Figure 6.3 (b)**. This also indicated that the phenyl groups on the SAM have some ordering on the silica surface. The broad OH stretching centered at ~3120 cm^{-1} contributed by the adsorbed water was still observed, along with a small

negative peak at 3310 cm^{-1}, likely generated by the amide N-H stretching. After this second step of SAM preparation, the surface should have –NH, -CO, -NO_2, and –Br groups, which can strongly interact with water molecules, leading to the presence of strongly hydrogen bonded water molecules on the surface.

Panel (c) in **Figure 6.3** shows the distinguishing hydroxyl vibrational feature centered at 3400 cm^{-1} of the last step in the SAM functionalization reaction. This peak can be contributed by the hydroxyl group from step 3 of the SAM functionalization and/or some adsorbed weakly hydrogen bonded water. We believe that more likely this broad peak is a contribution from both the adsorbed water and SAM hydroxyl group. Adsorbed water with strong hydrogen bonds which contributed to the ~3120 cm^{-1} peak was not observed here anymore. This step of SAM preparation introduced substantial amount of methylene groups to the surface, which may weakly interact with water molecules, leading to the absence of the strongly hydrogen bonded water O-H stretching signal.

The above three SFG spectra collected from the SAM surface after each preparation step clearly demonstrated successful surface functionalization and SAM formation on the silica substrate. For the SFG spectrum taken after the 365 nm UV treatment (panel (d) in **Figure 6.3**), the hydroxyl peak observed in panel (c) of **Figure 6.3** disappears. The loss of OH was due to removal or disordering of the hydroxyl group mercaptohexanol segment or loss of weakly hydrogen bonded water on the SAM the surface. Any water that remained absorbed to the substrate was disordered and does not appear in the SFG spectrum. The CH_2 groups were still ordered at the prism/air interface. To further support the conclusion which we obtained from the SFG study, we also applied XPS to examine the above SAM formation process. XPS provided elemental composition of the key steps in the SAM formation.

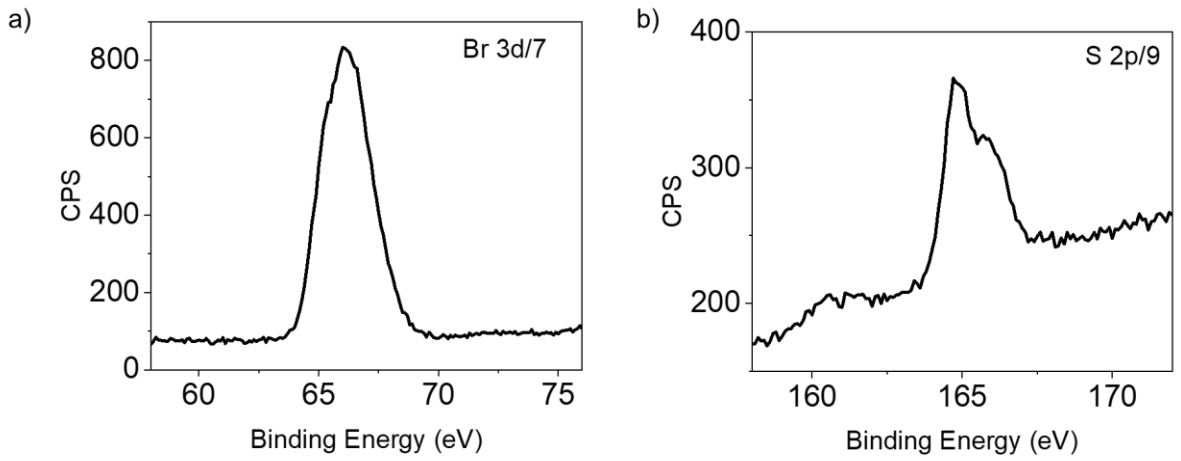

Figure 6.4: XPS results form a) the debonding SAM at step 2 showed the characteristic peak for bromine, and b) at step 3 showed the characteristic peak for sulfur.

An XPS spectrum was collected from the SAM after the BMNA coupling step, shown in **Figure 6.4 (a)**, where a 3d/7 peak with a binding energy of 65 eV was detected. This indicated that bromine from BNMB was present on the SAM and that this step (step 2 of the SAM preparation) was successful. After this BMNA reaction step, the mercaptohexanol was added to the SAM in step 3 and the XPS data were collected, shown in **Figure 6.4 (b)**. The XPS spectrum from step 3 of the SAM clearly had sulfur signal with a 2p/9 peak having a binding energy of about 166 eV, indicated the success of step 3 of the reaction. The above reported XPS elemental analysis confirms that the SAM was formed on the silica substrate, further supporting the SFG results.

In addition to SFG and XPS measurements, contact angle measurements were made on the SAM surface after each step. Before SAM deposition, water drops spread on the silica surface easily because the silica surface is very hydrophilic. Therefore, we believe that the water contact angle on the silica surface is nearly zero. **Figure 6.5** shows the contact angle measured after each step of SAM deposition. For APTES, the contact angle was measured to be 14.1°, indicating that the surface was slightly more hydrophobic than pure silica but still very hydrophilic. This result is reasonable since the APTES has an amine end group, which is hydrophilic. The backbone of

APTES is a hydrocarbon chain, which can occupy part of the surface to make the surface more hydrophobic than silica. After BNBA was coupled to the SAM the contact angle increased to 59.3°, an increase of the angle was expected because of the amount of the organic functionality such as phenyl group would make the surface more hydrophobic. After the addition of mercaptohexanol to the SAM surface the contact angle decreased to 47.3°, this could be due to the mercaptohexanol hydroxyl end group of the SAM making the surface more hydrophilic.

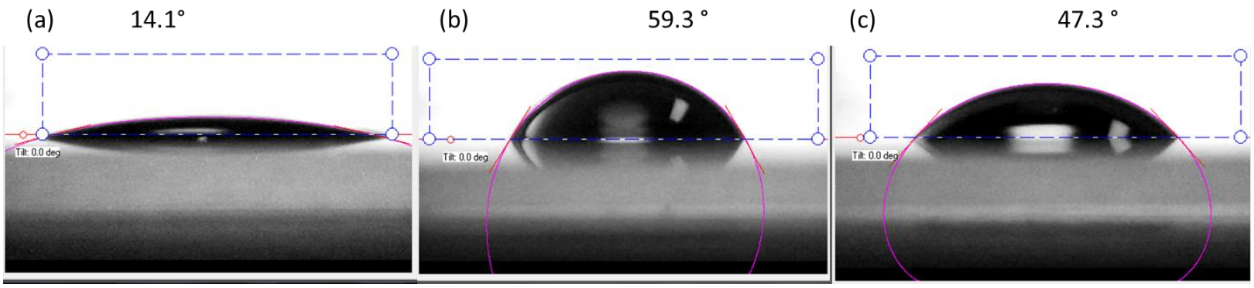

Figure 6.5: Contact angle results for (a) APTES, (b) coupling of BMNB to APTES, (c) addition of MH to BMNB. Contact angles for APTES was found to be 14.1°, BMNB was 59.3°, and MH was 47.3°.

It is clear that we were successful in preparing the debonding SAM on silica based on the data from SFG, XPS, and contact angle measurements. The surface of the debonding SAM was studied with SFG after exposure to 365nm UV light as well. No substantial CH spectral feature changes were observed with SFG, likely showing that the debonded products stay on the substrate. The loss of the O-H stretching signals in SFG can be explained by the loss or disordering of product hydroxyl groups on the surface or loss of water from the surface. To confirm the debonding reaction after the UV irradiation, we performed the adhesion tests which will be presented below.

6.3.2 Debonding SAM/PDMS interface: SFG

After characterizing the SAM surface with SFG, XPS, and water contact angle, buried interfaces between the debonding SAM and different adhesives were studied using SFG, along

with the adhesion testing experiments. Two types of adhesives were used, a PDMS elastomer with 1% γ-GPS adhesion promoter, and a BADGE epoxy. The role of UV treatment on the buried interfacial structure was studied with SFG and correlated to adhesion strength with lap shear adhesion testing. First, the PDMS system was studied. It is worth mentioning that we have extensively studied PDMS at varied interfaces including silica interface using SFG to elucidate their interfacial behavior and/or molecular adhesion mechanisms of silicone adhesives.[65, 71-78]

SFG spectra collected from the buried PDMS/debonding SAM (on silica) interface before and after UV treatment are shown in **Figure 6.6 (a)**. For comparison purposes, SFG spectra collected from PDMS (without SAM)/silica interfaces before and after UV irradiation, as well as SFG spectra collected from the SAM before and after UV treatment in the C-H stretching frequency region are also displayed in **Figure 6.7 (a)**. For the PDMS/silica interface, SFG spectra are dominated by contributions from the methoxy group of γ-GPS (2840 cm^{-1}), and asymmetric stretching of the PDMS Si-CH_3 group as well as the methoxy group at 2960 cm^{-1}. The 2865 cm^{-1} signal generated by the Si-CH_2 groups in PDMS was also detected. The SFG spectra collected from the PDMS/SAM (on silica) interface are dominated by the 2840 cm^{-1} adhesion promoter peak, and the 2915 cm^{-1} and 2960 cm^{-1} signals contributed by the symmetric and asymmetric stretching of the Si-CH_3 group, which are very different from those detected from the SAM surface, indicating that the PDMS/SAM (on silica) interface was dominated by PDMS and the adhesion promoter. There may be some overlap in the signal from methylene groups of the debonding SAM at 2865 cm^{-1} (can also be Si-CH_2 groups of PDMS) and 2940 cm^{-1}. The strong SFG signal indicated that the adhesion promoter and the elastomer were ordered at the PDMS/debonding SAM (on silica) interface.

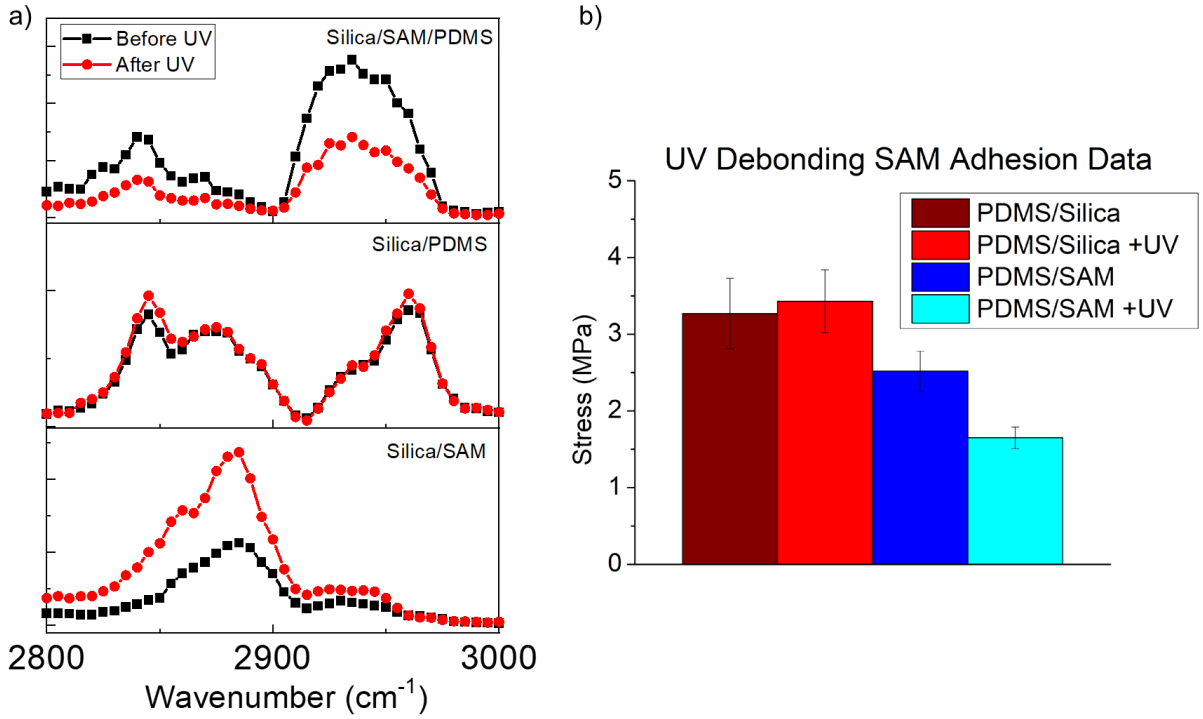

Figure 6.6: In panel (a) the SFG results for the PDMS system are shown. The bottom of panel (a) shows the SAM surface before and after UV treatment. The middle panel shows the silica/PDMS interface before and after UV treatment. The top panel shows the silica/SAM/PDMS interface before and after UV treatment. Lap shear adhesion data from the PDMS/debonding SAM system shown in (b). PDMS control tests, in red, only on silica substrates. The blue bars are samples with PDMS on the debonding SAM coated substrates.

The SFG spectra collected from the PDMS/debonding SAM (on silica) interface were also different from those detected from the PDMS/silica interface, showing that SAM impacts the interfacial PDMS structure. As we have shown previously, good adhesion of silicone to a surface needs to meet two requirements: (1) Ordered methoxy groups of the adhesion promoter segregate to the interface before curing (evidenced by strong SFG methoxy signal).[14, 76-79] (2) Interfacial methoxy groups react during the curing process (evidenced by SFG signal reduction after curing).[71, 76-77] In our previous work, we observed that for some cases SFG signals from γ-GPS could be detected from the cured PDMS interfaces, indicating that not all the interfacial methoxy

groups reacted after curing. The top spectrum in **Figure 6.6 (a)** shows that methoxy groups were present at the PDMS/debonding SAM (on silica) interface before and after the UV treatment. After UV treatment, the SFG intensity from the interface decreased. This change in signal could be due to PDMS changing orientation or ordering after UV treatment degrading the SAM. PDMS has a low glass transition temperature, therefore at the room temperature the interfacial PDMS molecules can be quite flexible. UV treatment changes the SAM, leading to changes at the PDMS interface, resulting in SFG spectral intensity change. Such a change was not detected from the SFG spectra collected from the PDMS/silica interface. Without the presence of the SAM, the silica substrate would not change after the UV irradiation, leading to no change for the PDMS/silica interface, resulting in no SFG signal change.

6.3.3 Debonding SAM/PDMS interface: Adhesion

Adhesion strengths were tested for different sample interfaces discussed above, namely PDMS/silica, PDMS/silica + UV, PDMS/debonding SAM, PDMS/debonding SAM + UV interfaces. The measured results are presented in **Figure 6.6(b)**. The first two samples above with PDMS on bare silica served as control samples to test whether UV light exposure affects PDMS adhesion strength without the debonding SAM. The results indicate that the adhesion strength of the PDMS adhesive alone on silica without the SAM was not affected by UV treatment. When the debonding SAM was present on silica, the adhesion strength decreased compared to the control samples of PDMS on silica. After UV exposure, the adhesion of PDMS to the debonding SAM surface decreased further, to about half the adhesion strength of the control samples and one-third less than PDMS on the debonding SAM without UV treatment. Therefore, the debonding SAM successfully reduced the interfacial adhesion of PDMS after UV light exposure, which can be important for creating reversible adhesives with silicone-based materials.

6.3.4 Debonding SAM/epoxy interface: SFG

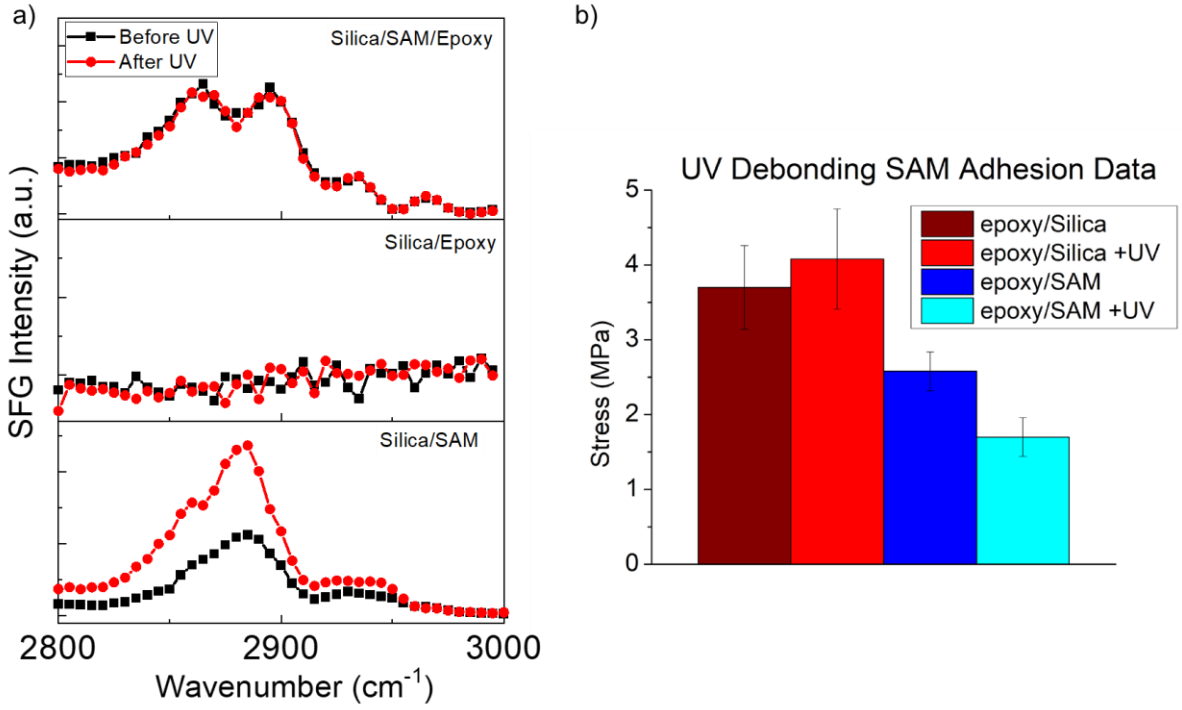

Figure 6.7: In panel (a) the SFG results for the BADGE epoxy system are shown. The bottom of panel (a) again shows the SAM surface before and after UV treatment (same spectra as the bottom spectra in **Figure 6.6(a)**). The middle panel shows the silica/epoxy interface before and after UV treatment. The top panel show the silica/SAM/epoxy interface before and after UV treatment. Lap shear adhesion data for the BADGE epoxy/debonding SAM system shown in (b). A similar trend was observed for the BADGE system as the PDMS system.

In addition to the silicone adhesive, we also studied a model epoxy adhesive, BADGE. SFG spectra were collected from the BADGE/debonding SAM interface, shown in the top spectrum of **Figure 6.7 (a)**. For comparison purposes, SFG spectra collected from epoxy (without SAM)/silica interfaces before and after UV irradiation, as well as SFG spectra collected from the SAM before and after UV treatment in the C-H stretching frequency region are also displayed in **Figure 6.7 (a)**. For the epoxy/silica interface, no SFG spectra were detected, as we reported previously[46], showing that there was no ordering of CH groups at the epoxy/silica interface. Both

SFG spectra collected from the BADGE/debonding SAM interface before and after UV exposure have four peaks. The peak centered at ~2850 cm^{-1} is due to the methylene symmetric stretch of the SAM and epoxy. The signal at ~2880 cm^{-1} is likely due to the methyl symmetric stretch of the epoxy, while the 2940 cm^{-1} peak is likely a methyl Fermi resonance. A small peak centered around 2970 cm^{-1} is assigned to methyl asymmetric stretching of the epoxy. SFG signals from the BADGE/debonding SAM interface were different from the SAM surfaces, showing that epoxy molecules were ordered at the interface. The SFG spectrum did not decrease after the sample's exposure to UV light for 30 minutes. Very similar SFG spectra before and after UV treatment were collected from the epoxy/SAM interface, showing no noticeable structural changes observed at the interface. The T_g of the BADGE-DDM epoxy system is above room temperature (43 °C), meaning that there is little chain mobility in the epoxy resin. This is much different from the PDMS case which has a T_g lower than room temperature. The effect of T_g of the epoxy resin vs PDMS could explain the different SFG results for the SAM/adhesive interfaces, where the SFG signals change significantly for PDMS and do not change in the epoxy case. Although chemical bonds in the SAM could be broken after the UV treatment, the chemical products could stay on the substrates as discussed above. Because the epoxy is rigid at room temperature, such a change could not induce observable changes of epoxy/SAM interface, resulting in no change in the SFG spectrum.

6.3.5 Debonding SAM/epoxy interface: Adhesion

The adhesion strengths of the epoxy on silica and on debonding SAM/epoxy interface before and after exposure to UV light were measured, as shown in **Figure 6.7 (b)**. A similar trend in the adhesion strengths to that measured from the PDMS adhesive system was observed, as presented above, where after UV exposure of the debonding SAM/PDMS interface the adhesion strength drops by about 33%. This result shows the successful reduction of the adhesion of epoxy

by using the debonding SAM and UV irradiation. Combining the results from silicone and epoxy, we believe that the debonding SAM approach is generally applicable to effectively reduce interfacial adhesion, helping to develop reversible adhesives.

6.3.6 Debonding SAM/adhesive discussion

At the debonding SAM/PDMS interface the SFG results showed similar peaks after UV treatment but much lower signal intensity after treatment. The adhesion results showed a decrease of about 33% vs the non-UV treated sample. Since the control sample (silica/PDMS) SFG and adhesion results did not seem to change with UV treatment and the debond SAM/PDMS samples show significant change, we believe that the SFG results and adhesion results are correlated. PDMS has a T_g much lower than room temperature, therefore there is substantial chain mobility of the elastomer at room temperature. After the SAM molecules were degraded by the UV light, the SAM structure may change at the flexible PDMS interface, which will further alter the interfacial flexible PDMS structure. Therefore, the structure at the SAM/flexible PDMS interface can change after UV irradiation. The low glass transition temperature plays a role in the change in the interfacial structures observed for this system.

The SFG results from the debonding SAM/epoxy interface did not show any change after UV treatment. This can be rationalized when the higher T_g is considered. The BADGE-DDM epoxy resin has a T_g greater than room temperature, thus the polymer has lower or no chain mobility at room temperature. The cleaving of the UV sensitive bond in the SAM does not influence the interfacial structure because of the low polymer chain mobility – the interface is rigid.

It is worth mentioning that the SFG spectra collected from buried interfaces displayed in **Figure 6.6 (a)** and **6.7 (a)** were shown between 2800 and 3000 cm^{-1} in the C-H stretching

frequency region. We collected SFG spectra in the higher frequency region, but no SFG signal was detected, showing hydroxyl groups are disordered at these interfaces. We therefore did not present the O-H signals from the buried interfaces.

6.4 Conclusions

This research shows the feasibility of reducing polymer adhesion using a UV degradable SAM. The SAM can be prepared via three steps. Each the SAM preparation step was carefully characterized using a variety of analytical tools including SFG, XPS, and contact angle goniometry. Two polymer adhesives, PDMS and epoxy, were investigated on the prepared SAMs before and after UV irradiation. It was found by the adhesion testing experiments that because of the UV degradation of the SAM, polymer adhesion can be reduced by more than 30% on silica. SFG was applied to study buried polymer adhesive/SAM interfaces before and after UV treatment. SFG showed a decrease in PDMS signal after UV treatment and no change for the epoxy interface, which was a peculiar result. Nevertheless, UV degradation of SAM reduced adhesion at both interfaces.

This result is important as it shows the promise of selectively debonding materials that can be generalized to a variety of adhesive or other materials. The future improvement on the chemistry of photodegradable SAMs, SAM deposition procedures, and UV irradiation conditions could increase the effectiveness of the interfacial debonding to further reduce adhesion after UV treatment. The application of this methodology to the packaging and polymer materials could solve some of the problems related to recycling plastics and recovering expensive materials in the future. This can also help to optimize the use of debonding motifs in temporary wafer bonding during the productions of microelectronics.

6.5 References

1. Niklaus, F.; Stemme, G.; Lu, J. Q.; Gutmann, R. J., Adhesive wafer bonding. *J. Appl. Phys.* **2006,** *99* (3), 031101.
2. Gong, L.; Xiang, L.; Zhang, J.; Chen, J.; Zeng, H., Fundamentals and advances in the adhesion of polymer surfaces and thin films. *Langmuir* **2019,** *35* (48), 15914-15936.
3. Bouhamed, A.; Kia, A. M.; Naifar, S.; Dzhagan, V.; Müller, C.; Zahn, D. R. T.; Choura, S.; Kanoun, O., Tuning the adhesion between polyimide substrate and MWCNTs/epoxy nanocomposite by surface treatment. *Appl. Surf. Sci.* **2017,** *422*, 420-429.
4. Hong, S. I.; Kim, K. B.; Lee, Y.; Cho, S. Y.; Ko, J. A.; Hong, S. K.; Park, H. J., Surface modification of ethylene-vinyl alcohol copolymer treated with plasma source ion implantation. *J. Appl. Polym. Sci.* **2009,** *113* (5), 2988-2996.
5. Ge, C.; Fortuna, C.; Lei, K.; Lu, L.-X., Neat EVOH and EVOH/LDPE blend centered three-layer co-extruded blown film without tie layers. *Food Packaging and Shelf Life* **2016,** *8*, 33-40.
6. Andre, J. S.; Ulrich, N.; Ji, K.; Chen, Z., Interfacial behavior of flux residues and its impact on copper/underfill adhesion in microelectronic packaging. *J. Electron. Packag.* **2021,** *143*, 011004.
7. Andre, J. S.; Li, B.; Chen, X.; Paradkar, R.; Walther, B.; Feng, C.; Tucker, C.; Mohler, C.; Chen, Z., Interfacial reaction of a maleic anhydride grafted polyolefin with ethylene vinyl alcohol copolymer at the buried solid/solid interface. *Polymer* **2021,** *212*, 123141.
8. Zhang, S.; Andre, J. S.; Hsu, L.; Toolis, A.; Esarey, S. L.; Li, B.; Chen, Z., Nondestructive in situ detection of chemical reactions at the buried interface between polyurethane and isocyanate-based primer. *Macromolecules* **2020,** *53* (22), 10189-10197.
9. Yamamoto, S.; Kuwahara, R.; Aoki, M.; Shundo, A.; Tanaka, K., Molecular events for an epoxy–amine system at a copper interface. *ACS Appl. Polym. Mater.* **2020,** *2* (4), 1474-1481.
10. Li, B.; Andre, J. S.; Chen, X.; Walther, B.; Paradkar, R.; Feng, C.; Tucker, C.; Mohler, C.; Chen, Z., Observing a chemical reaction at a buried solid/solid interface in situ. *Anal. Chem.* **2020,** *92* (20), 14145-14152.
11. Tardio, S.; Abel, M.-L.; Carr, R. H.; Watts, J. F., The interfacial interaction between isocyanate and stainless steel. *Int. J. Adhes. Adhes.* **2019,** *88*, 1-10.
12. Bhati, M.; Senftle, T. P., Identifying adhesion properties at Si/polymer interfaces with ReaxFF. *J. Phys. Chem. C* **2019,** *123* (44), 27036-27047.
13. Xiao, M.; Mohler, C.; Tucker, C.; Walther, B.; Lu, X.; Chen, Z., Structures and adhesion properties at polyethylene/silica and polyethylene/nylon interfaces. *Langmuir* **2018,** *34* (21), 6194-6204.
14. Ulrich, N. W.; Myers, J. N.; Chen, Z., Characterization of polymer/epoxy buried interfaces with silane adhesion promoters before and after hygrothermal aging for the elucidation of molecular level details relevant to adhesion. *RSC Advances* **2015,** *5* (128), 105622-105631.
15. Villani, M.; Scheerder, J.; van Benthem, R. A. T. M.; de With, G., Interfacial interactions of poly(urethane–urea) based primers with polypropylene. *Eur. Polym. J.* **2014,** *56*, 118-130.
16. Myers, J. N.; Zhang, C.; Lee, K. W.; Williamson, J.; Chen, Z., Hygrothermal aging effects on buried molecular structures at epoxy interfaces. *Langmuir* **2014,** *30* (1), 165-71.

17. Zhang, C.; Hankett, J.; Chen, Z., Molecular level understanding of adhesion mechanisms at the epoxy/polymer interfaces. *ACS Appl. Mater. Interfaces* **2012,** *4* (7), 3730-7.
18. Nies, C.; Wehlack, C.; Ehbing, H.; Dijkstra, D. J.; Possart, W., Adhesive interactions of polyurethane monomers with native metal surfaces. *J. Adhes.* **2012,** *88* (8), 665-683.
19. Shimizu, K.; Abel, M.-L.; Phanopoulos, C.; Holvoet, S.; Watts, J. F., The characterisation of the interfacial chemistry of adhesion of rigid polyurethane foam to aluminium. *J. Mater. Sci.* **2011,** *47* (2), 902-918.
20. Tse, M. F.; Hu, W.; Yeganeh, M. S.; Zhang, D., Adhesion between dissimilar polymers. II. Effects of bonding temperature and crosslinking agent. *J. Appl. Polym. Sci.* **2004,** *93* (1), 323-335.
21. Kaiser, K.; Schmid, M.; Schlummer, M., Recycling of polymer-based multilayer packaging: A review. *Recycling* **2017,** *3* (1), 1-26.
22. Oh, Y.; Park, J.; Park, J.-J.; Jeong, S.; Kim, H., Dual cross-linked, polymer thermosets: Modular design, reversible transformation, and triggered debonding. *Chem. Mater.* **2020,** *32* (15), 6384-6391.
23. Bandl, C.; Kern, W.; Schlögl, S., Adhesives for "debonding-on-demand": Triggered release mechanisms and typical applications. *Int. J. Adhes. Adhes.* **2020,** *99*, 102585.
24. Mutlu, H.; Geiselhart, C. M.; Barner-Kowollik, C., Untapped potential for debonding on demand: the wonderful world of azo-compounds. *Mater. Horiz.* **2018,** *5* (2), 162-183.
25. Phommahaxay, A.; Jourdain, A.; Potoms, G.; Verbinnen, G.; Sleeckx, E.; Beyer, G.; Beyne, E.; Guerrero, A.; Bai, D.; Yess, K.; Arnold, K., Advances in thin wafer debonding and ultrathin 28-nm FinFET substrate transfer. In *2017 IEEE 67th Electronic Components and Technology Conference*, 2017; pp 740-745.
26. Ayer, M. A.; Simon, Y. C.; Weder, C., Azo-containing polymers with degradation on-demand feature. *Macromolecules* **2016,** *49* (8), 2917-2927.
27. Kim, H.; Mohapatra, H.; Phillips, S. T., Rapid, on-command debonding of stimuli-responsive cross-linked adhesives by continuous, sequential quinone methide elimination reactions. *Angew Chem. Int. Ed. Engl.* **2015,** *54* (44), 13063-7.
28. Heinzmann, C.; Coulibaly, S.; Roulin, A.; Fiore, G. L.; Weder, C., Light-induced bonding and debonding with supramolecular adhesives. *ACS Appl. Mater. Interfaces* **2014,** *6* (7), 4713-9.
29. Lee, S.-H.; Lin, W.-C.; Kuo, C.-H.; Karakachian, M.; Lin, Y.-C.; Yu, B.-Y.; Shyue, J.-J., Photooxidation of Amine-Terminated Self-Assembled Monolayers on Gold. *J. Phys. Chem. C* **2010,** *114*, 10512–10519.
30. Cheng, N.; Cao, X., Photoactive SAM surface for control of cell attachment. *J. Colloid. Interface Sci.* **2010,** *348* (1), 71-9.
31. Ye, T.; McArthur, E. A.; Borguet, E., Mechanism of UV photoreactivity of alkylsiloxane self-assembled monolayers. *J. Phys. Chem. B* **2005,** *109* (20), 9927-38.
32. Tian, L.; Song, X.; Yu, X.; Hu, W., Modulated rectification of carboxylate-terminated self-assembled monolayer junction by humidity and alkali metal ions: The coupling and asymmetric factor matter. *J. Phys. Chem. C* **2021,** *125* (39), 21614-21623.
33. Asyuda, A.; Das, S.; Zharnikov, M., Thermal stability of alkanethiolate and aromatic thiolate self-assembled monolayers on Au(111): An x-ray photoelectron spectroscopy study. *J. Phys. Chem. C* **2021,** *125* (39), 21754-21763.

34. Elinski, M. B.; Menard, B. D.; Liu, Z.; Batteas, J. D., Adhesion and friction at graphene/self-assembled monolayer interfaces investigated by atomic force microscopy. *J. Phys. Chem. C* **2017,** *121* (10), 5635-5641.
35. Hunt, L. A.; Rodrigues, R. R.; Foell, K.; Nugegoda, D.; Cheema, H.; Hammer, N. I.; Delcamp, J. H., Preferential direction of electron transfers at a dye–metal oxide interface with an insulating fluorinated self-assembled monolayer and MgO. *J. phys. Chem. C* **2021,** *125* (46), 25410–25421.
36. Parhizkar, N.; Ramezanzadeh, B.; Shahrabi, T., Corrosion protection and adhesion properties of the epoxy coating applied on the steel substrate pre-treated by a sol-gel based silane coating filled with amino and isocyanate silane functionalized graphene oxide nanosheets. *Appl. Surf. Sci.* **2018,** *439*, 45-59.
37. Wu, C.; Chen, C.; Lai, J.; Chen, J.; Mu, X.; Zheng, J.; Zhao, Y., Molecule-scale controlled-release system based on light-responsive silica nanoparticles. *Chem. Commun.* **2008,** (23), 2662-2664.
38. Ma, Y.; Shi, L.; Liu, F.; Zhang, Y.; Pang, Y.; Shen, X., Self-assembled thixotropic silver cluster hydrogel for anticancer drug release. *Chem. Eng. J.* **2019,** *362*, 650-657.
39. Motealleh, A.; Dorri, P.; Kehr, N. S., Self-assembled monolayers of chiral periodic mesoporous organosilica as a stimuli responsive local drug delivery system. *J. Mater. Chem. B* **2019,** *7* (14), 2362-2371.
40. Blass, J.; Albrecht, M.; Wenz, G.; Guerra, R.; Urbakh, M.; Bennewitz, R., Multivalent adhesion and friction dynamics depend on attachment flexibility. *J. Phys. Chem. C* **2017,** *121* (29), 15888-15896.
41. Worrell, B. T.; McBride, M. K.; Lyon, G. B.; Cox, L. M.; Wang, C.; Mavila, S.; Lim, C. H.; Coley, H. M.; Musgrave, C. B.; Ding, Y.; Bowman, C. N., Bistable and photoswitchable states of matter. *Nat. Commun.* **2018,** *9* (1), 2804.
42. Jung, N.; Diehl, F.; Jonas, U., Thiol-substituted poly(2-oxazoline)s with photolabile protecting groups-tandem network formation by light. *Polymers* **2020,** *12* (8).
43. Gorner, H., Effects of 4,5-dimethoxy groups on the time-resolved photoconversion of 2-nitrobenzyl alcohols and 2-nitrobenzaldehyde into nitroso derivatives. *Photochem. Photobiol. Sci.* **2005,** *4* (10), 822-8.
44. Gaplovsky, M.; Il'ichev, Y. V.; Kamdzhilov, Y.; Kombarova, S. V.; Mac, M.; Schworer, M. A.; Wirz, J., Photochemical reaction mechanisms of 2-nitrobenzyl compounds: 2-nitrobenzyl alcohols form 2-nitroso hydrates by dual proton transfer. *Photochem. Photobiol. Sci.* **2005,** *4* (1), 33-42.
45. Ulrich, N. W.; Xiao, M.; Zou, X.; Williamson, J.; Chen, Z., Probing molecular structures of buried interfaces in thick multilayered microelectronic packages. *IEEE Trans. Compon. Packag. Manuf. Technol.* **2018,** *8* (7), 1213-1224.
46. Ulrich, N. W.; Andre, J. S.; Khanna, K.; Wei, Y.; Xiu, Y.; Chen, Z., Nondestructive analysis of buried interfacial behaviors of flux residue and their impact on interfacial mechanical property. *IEEE Trans. Compon. Packag. Manuf. Technol.* **2018,** *8* (6), 982-990.
47. Li, B.; Andre, J. S.; Chen, X.; Walther, B.; Paradkar, R.; Feng, C.; Tucker, C.; Mohler, C.; Chen, Z., Probing molecular behavior of carbonyl groups at buried nylon/polyolefin interfaces in situ. *Langmuir* **2020,** *36* (38), 11349-11357.

48. Sheth, N.; Ngo, D.; Banerjee, J.; Zhou, Y.; Pantano, C. G.; Kim, S. H., Probing hydrogen-bonding interactions of water molecules adsorbed on silica, sodium calcium silicate, and calcium aluminosilicate glasses. *J. Phys. Chem. C* **2018,** *122* (31), 17792-17801.
49. Li, H.; Baldelli, S., Influence of microcrystallinity on the CO/Pt(poly) electrode surface using sum frequency generation microscopy combined with electrochemistry. *J. Phys. Chem. C* **2021,** *125* (24), 13560-13571.
50. Cai, C.; Azam, M. S.; Hore, D., Temperature-dependent chemical functional group reorientation at silicone surfaces. *J. Phys. Chem. C* **2021,** *125* (40), 22214-22222.
51. Nojima, Y.; Yamaguchi, S., Heterodyne-detected sum frequency generation spectroscopic study of weakly hydrogen-bonded water at charged lipid interfaces, revisited. *J. Phys. Chem. C* **2021,** *125* (42), 23483-23489.
52. Luo, T.; Zhang, R.; Zeng, W.-W.; Zhou, C.; Yang, X.; Ren, Z., Alkoxylation reaction of alcohol on silica surfaces studied by sum frequency vibrational spectroscopy. *J. Phys. Chem. C* **2021,** *125* (16), 8638-8646.
53. Wilson, M. C.; Singla, S.; Stefin, A. J.; Kaur, S.; Brown, J. V.; Dhinojwala, A., Characterization of acid–base interactions using interface-sensitive sum frequency generation spectroscopy. *J. Phys. Chem. C* **2019,** *123* (30), 18495-18501.
54. Seki, T.; Yu, X.; Zhang, P.; Yu, C.-C.; Liu, K.; Gunkel, L.; Dong, R.; Nagata, Y.; Feng, X.; Bonn, M., Real-time study of on-water chemistry: Surfactant monolayer-assisted growth of a crystalline quasi-2D polymer. *Chem* **2021,** *7* (10), 2758-2770.
55. Peng, Q.; Chen, J.; Ji, H.; Morita, A.; Ye, S., Origin of the overpotential for the oxygen evolution reaction on a well-defined graphene electrode probed by in situ sum frequency generation vibrational spectroscopy. *J. Am. Chem. Soc.* **2018,** *140* (46), 15568-15571.
56. Saito, K.; Peng, Q.; Qiao, L.; Wang, L.; Joutsuka, T.; Ishiyama, T.; Ye, S.; Morita, A., Theoretical and experimental examination of SFG polarization analysis at acetonitrile-water solution surfaces. *Phys. Chem. Chem. Phys.* **2017,** *19* (13), 8941-8961.
57. Cimatu, K. A.; Chan, S. C.; Jang, J. H.; Hafer, K., Preferential Organization of Methacrylate Monomers and Polymer Thin Films at the Air Interface Using Femtosecond Sum Frequency Generation Spectroscopy. *J. Phys. Chem. C* **2015,** *119* (45), 25327-25339.
58. Adhikari, N. M.; Premadasa, U. I.; Rudy, Z. J.; Cimatu, K. L. A., Orientational analysis of monolayers at low surface concentrations due to an increased signal-to-noise Ratio (S/N) using broadband sum frequency generation vibrational spectroscopy. *Appl. Spectrosc.* **2019,** *73* (10), 1146-1159.
59. Kawaguchi, D.; Yamamoto, K.; Abe, T.; Jiang, N.; Koga, T.; Yamamoto, S.; Tanaka, K., Local orientation of chains at crystal/amorphous interfaces buried in isotactic polypropylene thin films. *Phys. Chem. Chem. Phys.* **2021,** *23* (41), 23466-23472.
60. Cimatu, K. L. A.; Premadasa, U. I.; Ambagaspitiya, T. D.; Adhikari, N. M.; Jang, J. H., Evident phase separation and surface segregation of hydrophobic moieties at the copolymer surface using atomic force microscopy and SFG spectroscopy. *J. Colloid Interface. Sci.* **2020,** *580*, 645-659.
61. Li, X.; Lu, X., Interfacial irreversibly and loosely adsorbed layers abide by different evolution dynamics. *ACS Macro Lett.* **2019,** *8* (11), 1426-1431.
62. Li, B.; Zhang, S.; Andre, J. S.; Chen, Z., Relaxation behavior of polymer thin films: Effects of free surface, buried interface, and geometrical confinement. *Prog. Polym. Sci.* **2021,** *120*.

63. Ulrich, N. W.; Andre, J.; Williamson, J.; Lee, K. W.; Chen, Z., Plasma treatment effect on polymer buried interfacial structure and property. *Phys. Chem. Chem. Phys.* **2017,** *19* (19), 12144-12155.
64. Myers, J. N.; Zhang, X.; Huang, H.; Shobha, H.; Grill, A.; Chen, Z., SFG analysis of the molecular structures at the surfaces and buried interfaces of PECVD ultralow-dielectric constant pSiCOH: Reactive ion etching and dielectric recovery. *Appl. Phys. Lett.* **2017,** *110* (18).
65. Lu, X.; Zhang, C.; Ulrich, N.; Xiao, M.; Ma, Y. H.; Chen, Z., Studying polymer surfaces and interfaces with sum frequency generation vibrational spectroscopy. *Anal. Chem.* **2017,** *89* (1), 466-489.
66. Hong, Y.; Li, Y.; Wang, F.; Zuo, B.; Wang, X.; Zhang, L.; Kawaguchi, D.; Tanaka, K., Enhanced thermal stability of polystyrene by interfacial noncovalent interactions. *Macromolecules* **2018,** *51* (15), 5620-5627.
67. Liu, Y.; Chase, H. M.; Geiger, F. M., Partially (resp. fully) reversible adsorption of monoterpenes (resp. alkanes and cycloalkanes) to fused silica. *J. Chem. Phys.* **2019,** *150* (7), 074701.
68. Ge, A.; Qiao, L.; Seo, J. H.; Yui, N.; Ye, S., Surface-restructuring differences between polyrotaxanes and random copolymers in aqueous environment. *Langmuir* **2018,** *34* (41), 12463-12470.
69. Klan, P.; Solomek, T.; Bochet, C. G.; Blanc, A.; Givens, R.; Rubina, M.; Popik, V.; Kostikov, A.; Wirz, J., Photoremovable protecting groups in chemistry and biology: reaction mechanisms and efficacy. *Chem. Rev.* **2013,** *113* (1), 119-91.
70. Ellis, B.; Found, M. S.; Bell, J. R., Effects of cure treatment on glass transition temperatures for a BADGE-DDM epoxy resin. *J. Appl. Polym. Sci.* **1996,** *59*, 1493-1505.
71. Lin, T.; Wu, Y.; Santos, E.; Chen, X.; Ahn, D.; Mohler, C.; Chen, Z., Molecular insights into adhesion at a buried silica-filled silicone/polyethylene terephthalate interface. *Langmuir* **2020,** *36* (49), 15128-15140.
72. Zhang, C.; Chen, Z., Probing molecular structures of poly(dimethylsiloxane) at buried interfaces in situ. *J. Phys. Chem. C* **2013,** *117* (8), 3903-3914.
73. Zhang, C.; Chen, Z., Quantitative molecular level understanding of ethoxysilane at poly(dimethylsiloxane)/polymer interfaces. *Langmuir* **2013,** *29* (2), 610-619.
74. Liu, Y.; Leng, C.; Chisholm, B.; Stafslien, S.; Majumdar, P.; Chen, Z., Surface structures of PDMS incorporated with quaternary ammonium salts designed for antibiofouling and fouling release applications. *Langmuir* **2013,** *29* (9), 2897-905.
75. Chen, Z., Investigating buried polymer interfaces using sum frequency generation vibrational spectroscopy. *Prog. Polym. Sci.* **2010,** *35* (11), 1376-1402.
76. Vazquez, A. V.; Shephard, N. E.; Steinecker, C. L.; Ahn, D.; Spanninga, S.; Chen, Z., Understanding molecular structures of silanes at buried polymer interfaces using sum frequency generation vibrational spectroscopy and relating interfacial structures to polymer adhesion. *J. Colloid. Interface Sci.* **2009,** *331* (2), 408-16.
77. Vázquez, A. V.; Boughton, A. P.; Shephard, N. E.; Rhodes, S. M.; Chen, Z., Molecular structures of the buried interfaces between silicone elastomer and silane adhesion promoters probed by sum frequency generation vibrational spectroscopy and molecular dynamics simulations. *ACS Appl. Mater. Interfaces* **2009,** *2* (1), 96-103.

78. Loch, C. L.; Ahn, D.; Chen, Z., Sum frequency generation vibrational spectroscopic studies on a silane adhesion-promoting mixture at a polymer interface. *J. Phys. Chem. B* **2006,** *110*, 914-918.
79. Myers, J. N.; Chen, Z., Polymer molecular behaviors at buried polymer/metal and polymer/polymer interfaces and their relations to adhesion in packaging. *J. Adhes.* **2016,** *93* (13), 1081-1103.

Chapter 7: Conclusions and Outlook

7.1 Introduction

SFG is an advanced nonlinear optical spectroscopic method. Most of the work conducted in SFG research/application fields have been focused on simple model systems. The goal of the research presented in this thesis was to demonstrate that SFG is a powerful and unique tool to probe adhesive interfaces of complex and multicomponent materials, including commercially available "real world" samples. The results and knowledge gained from the studies presented are important for fundamental science and practical application, providing better understanding of molecular mechanisms of adhesion as well as leading to improved understanding of complex commercial materials used in everyday industrial applications where adhesion is a key factor for quality and durability. Edwin Plueddemann predicted in the early 1990s that "…it should be possible to observe structures and reactions that have been inferred in the past from indirect evidence of composite performance. It should then be possible to design total composites with consistently good performance."[1] I believe that this thesis work is an important step in realizing his statement and SFG will continue to be a valuable tool for industry and academic research alike. The techniques used here show that insight can be gained from multicomponent materials used in real industry application and those insights have important scientific implications on understanding of adhesion through interfacial molecular interactions, chemical reactions, and bonding.

Specifically in this thesis the impacts of surface treatments, chemical reactions, and additives on interfacial molecular structures and molecular interactions were studied at buried interfaces in situ, and their relations to interfacial properties such as adhesion were elucidated.

7.2 Conclusion of the thesis study

In Chapter 2, two model flux materials were first characterized on calcium fluoride and copper substrates to identify the characteristic peaks in an SFG spectrum. Copper surfaces were also characterized after rinsing with water showing that the flux materials can be removed or disordered. Following characterization of the model fluxes on surfaces, buried interfaces between copper with and without flux treatment and an epoxy-based polymer were studied with SFG and adhesion tests. Buried interfaces of the rinsed copper surfaces and the epoxy polymer were prepared and SFG results showed loss of resonant signals from the flux or polymer at the interface that were correlated with adhesion studies. After studying the two model fluxes, a real flux material used in microelectronics was also studied at the copper/epoxy polymer interface. Instead of washing to remove the material, this flux was heat treated as close to the manufacturer's specification as possible. SFG results showed a similar trend at the buried interfaces for the model and real flux materials where the heating surface treatment resulted in loss of resonate signals from the flux or epoxy polymer. The adhesion after the heating surface treatment was also enhanced due to oxide removal and the resulting disordered polymer at the interface. Gaining this general knowledge about surface treatments and the role of flux materials at buried interfaces related to adhesion of polymers to metals specifically is important to the electronics industry.

Chapters 3 and 4 show that chemical reactions at buried interfaces to enhance adhesion between two polymer materials commonly used in food packaging can be probed with analytical techniques. The interfacial reaction between EVOH and MAHgEO and the resulting adhesion

enhancement between these materials compared to a non-grafted EO were studied in Chapter 3. In this work, SFG spectral changes in the -OH and C=O stretching regions were consistent with a chemical reaction between EVOH hydroxyl groups and maleic anhydride grafted to a polyethylene. The SFG signals detected in the OH stretching frequency region showed a sharp decrease at the EVOH/MAHgEO interface and a new peak corresponding to a weakly hydrogen bound carboxylic acid group. In the C=O stretching frequency region the carboxylic acid reaction product was also present in the SFG spectrum as well as the ester reaction product. Unreacted MAH signal was also observed in the C=O region spectrum. At the EVOH/EO interface these reaction products did not appear as no reaction between the two materials was feasible without MAH. The adhesion strength between EVOH and EO was found to be much weaker than the adhesion between EVOH and MAHgEO, further supporting that adhesion can be enhanced through interfacial molecular bonding. This result is significant which provides guidance for the design of multilayer film materials where adhesion between layers is important – ensuring interfacial chemical reactions.

In Chapter 4, SFG was used to detect and monitor another interfacial reaction important to multilayer films used as packaging materials. The same MAHgEO and EO polymers were used as those in Chapter 3 but the interfacial reaction with nylon was studied in more detail. Nylon was an ideal material to study with MAHgEO using SFG because the SFG signals of nylon amide bonds appearing in the C=O stretching frequency region, the signals of the nylon amine terminal group appearing at higher N-H stretching frequencies, and the reaction product SFG peaks expected to appear in the C=O stretching frequency region but with differ peak centers compared to those from the nylon amide bonds. This allowed for characterization of the interfacial reaction in the two important frequency regions, C=O stretching and N-H stretching regions. It was found that after

reaction with MAHgEO, the nylon amine peak at 3300 cm^{-1} disappeared and the nylon amide peak around 1625 cm^{-1} decreased, meanwhile a peak appeared at 1725 cm^{-1} in the SFG spectra related to the reaction products. Furthermore, the activation energy of the interfacial chemical reaction was able to be determined by following the reaction kinetics with the nylon SFG signals collected at different temperatures. This study further demonstrates that SFG can be used to characterize interfacial reactions between solid materials and to provide quantitative parameters such as temperature dependent kinetics and activation energy of interfacial chemical reactions.

Chapter 5 demonstrates that SFG can be used to probe the influence of adhesion promoter additives on interfacial structures of emulsion polymer formulations after drying. It is important to understand the role of an adhesion promoter at the molecular level in order to choose the best material for the application. This research showed that the amino silane used here influenced the polymer acid groups present at the silica/polymer interface. The results in this study showed that the most likely interaction between the amino silane and the acid groups was the formation of ionic bonds between amino silane ammonium ions and polymer carboxylate ions. Ionic bonds enhanced adhesion because they are stronger than the hydrogen bonds that would form between the silica and polymer without the addition of the adhesion promoter. The decrease in acid groups at the interface and the presence of other groups appearing at the interface supported this conclusion from the SFG results. In order to probe and characterize the influence of the amino silane further and the role of hydrophilic groups in this system, the acid content on the polymer was changed. When the acid concentration was high, more water remained at the interface. The amino silane chosen had two amine groups that could influence the interfacial interaction, leaving many possible orientations for the adhesion promoter therefore the adhesion promoter orientation was not detected at the interface.

Above the research explored methods to enhance adhesion at buried interfaces through molecular bonding and interactions at various interfaces that are scientifically and industrially important. Chapter 6 shows the feasibility of a SAM containing a UV degradable bond that can debond at a buried polymer interface leading to the reduction of adhesion strength. To study the SAM on a glass surface SFG, XPS, and contact angle were utilized. Following characterization of the SAM, buried interfaces with two polymeric materials were studied with SFG and the adhesion was characterized with lap shear adhesion tests. Lap shear tests showed that after UV treating the SAM/polymer interface the adhesion strength decreased about 30%. A peculiar result was that the buried SAM/polymer buried interface showed little change before and after the UV treatment. Nevertheless, the adhesion study and characterization of the SAM shows the promise of selectively debonding materials where the bulk polymer does not have to be modified but a monolayer on a substrate surface can be utilized. This application has great utility for recycling plastics and recovery of materials in many industries.

In summary, one important achievement of this thesis research is that it successfully realized the research goal to demonstrate that SFG is a powerful technique which can be applied to study complex buried interfaces with real world materials at the molecular level. These real-world materials include the commercial no-wash flux sample studied in Chapter 2, polymer materials studied in Chapters 3 and 4 such as EVOH, nylon, and MAHgEO which are used in multi-layer packaging films, as well as polyacrylates and amino silanes investigated in Chapter 5. Another achievement of this research was to reveal important structure – function relations of buried polymer interfaces to elucidate the molecular mechanisms of adhesion at various interfaces, providing important knowledge on how to improve the adhesion of various interfaces. In addition, this thesis research investigated a method to debond polymer adhesives, relevant to sustainability.

Such research provides a new method to reduced interfacial adhesion of polymer materials at the end of use life, helping the material recycling and saving our environment.

7.3 Outlook

It is worth mentioning that each of the projects presented in various chapters can be further studied in the future. The work in Chapter 2 generalized a method to study polymer/metal interfaces with surface treatments of flux, and one commercial flux materials was investigated. There are many different types of commercial fluxes are being used, which can be studied and compared with SFG to understand their interfacial structure-function relations and their performance. Using the similar approach, SFG can be applied to study other surface treatments beyond flux for a number of applications where treatments may disrupt adhesion of a coating or packaging material. Although in the system shown here the flux disrupted adhesion, it would be interesting to study a system where the small molecules enhance adhesion and their removal decreases adhesion such as that with SAM present on a substrate before applying the adhesive. Furthermore, more detailed characterization of metal surfaces after surface treatments, including techniques beyond SFG, would be important to the scientific and industrial communities.

Chapters 3 and 4 provide methodology and detail reaction products that can form at a buried interface. Such an approach can be used to study many different chemical reactions between polymers. SFG can be sued to study many different types of polyethylenes and many kinds of polymer materials with reactive groups beyond grafted polyethylenes.

Although three different amounts of a single amino silane were studied in Chapter 5, higher concentrations in the polymer formulation could lead to detection of the amino silane at the buried interface with SFG. Using another amino silane with only one amine group could also simplify the interfacial structures and still provide insight into the role of this type of adhesion promoter as an

additive to emulsion polymer formulations. Another possible study from Chapter 5 would be to make an amino silane SAM on the silica surface before applying the polymer coating and studying the resulting interface. Changing the polymer coating monomer composition, such as adding aromatic groups is also a possibility as there are a number of different acrylic polymers used in practice. The results from this study act as a first step in studying acrylic formulations and interfaces with different substrates using SFG at the primary analytical tool.

Chapter 6 showed in principle that a surface coating can decrease adhesion where decreasing adhesion further would be a key goal of further studies. Studying the same SAM quantitatively would also be interesting with a focus on optimizing the surface coverage in hopes to decrease adhesion more than what was presented. Further characterization of the UV mechanism could be performed and other debonding mechanisms occurring at an interface could be explored. The debonding SAM in Chapter 6 takes many steps to produce and is not general for any substrate, these two points would be interesting to explore further. It is also necessary to study the general applicability of this method to debonding adhesives from other substrates such as metals.

In summary, this thesis research built a foundation to apply SFG to study complex interfaces of "real world" materials to understand adhesion and developed a UV irradiation method to debond polymer adhesives from substrates. The methodologies presented above can be widely applied to study polymer interfaces in situ nondestructively, making contributions to many applications such as polymer packing, microelectronics, water-borne adhesives, polymer recycling, etc.

7.4 References

1. Plueddemann, E. P., *Silane Coupling Agents*. 2 ed.; Springer US: New York, 1991.